Aus der Medizinischen Universitätsklinik und Poliklinik Tübingen

Abteilung Innere Medizin VIII, Medizinische Onkologie und Pneumologie

A novel treatment strategy for colorectal cancer: Measles vaccine virus-induced oncolysis in combination with immune checkpoint inhibitors and NK cells / peripheral blood mononuclear cells

Inaugural-Dissertation

zur Erlangung des Doktorgrades

der Medizin

der Medizinischen Fakultät

der Eberhard Karls Universität

zu Tübingen

vorgelegt von

Gehring, Svenja

2019

Dekan:	Professor Dr. I. B. Autenrieth
1. Berichterstatter:	Professor Dr. U. M. Lauer
2. Berichterstatter:	Professor Dr. F. Stubenrauch
Tag der Disputation:	09.12.2019

Widmung

Für meine Oma Elisabeth.

Outline

1. INTRODUCTION 17

1.1. COLORECTAL CANCER AS A MAJOR HEALTH PROBLEM 17

1.1.1. Epidemiology of colorectal carcinoma 17

1.1.2. Colorectal cancer - an overview of pathology and clinical presentation 19

1.1.3. Existing therapeutic possibilities and problems in treatment of colorectal cancer 20

1.2. VIROTHERAPY AS AN ANTI-CANCER TREATMENT APPROACH 21

1.2.1. Principles of virotherapy - how an infectious virus becomes anti-cancer therapy. 21

1.2.2. History of virotherapy - from historical approaches to new generations of genetically engineered oncolytic viruses 24

1.2.3. Oncolytic virus in clinical usage - from bench to bedside 26

1.3. MEASLES VIRUS - BOON OR BANE IN MODERN MEDICINE? 28

1.3.1. Morphology and classification of measles virus 28

1.3.2. Measles virus as an infectious pathogen - epidemiology and clinical appearance. 31

1.3.3. Measles vaccine virus as a virotherapeutic agent 31

1.4. IMMUNOTHERAPY AS AN ANTI-CANCER TREATMENT APPROACH 33

1.4.1. Principles of immunotherapy - how to activate the body's defences against cancer 33

1.4.2. Immune checkpoint inhibitors entering the stage of clinical trials as anti-cancer drugs 35

1.4.3. Immunotherapy and colorectal cancer - a way of treatment worthy to go? 36

1.5. COMBINATION OF VIRUS AND IMMUNE CHECKPOINT INHIBITORS IN CANCER THERAPY 37

1.6. AIM OF THIS DISSERTATION 40

2. MATERIALS AND METHODS 42

2.1. CELL CULTURE OF TUMOR CELLS 42

2.1.1. Materials and devices for cell culture 42

2.1.2. Used cell lines 43

2.1.3. Cell culture 44

2.1.4. Counting of cells via Neubauer haemocytometer ... *45*
2.1.5. Cryopreservation of cells ... *45*
2.1.6. Thawing of cells for recultivation ... *46*
2.1.7. Seeding of cells ... *46*
2.1.8. Treatment of cells with immune checkpoint inhibitors ... *47*
2.2. CELL CULTURE OF VIRUS-INFECTED CELLS ... 47
2.2.1. Used virus strains ... *47*
2.2.2. Infection of cells ... *47*
2.2.3. Control of tumor cell infection with MeV-GFP using fluorescence microscopy ... *48*
2.3. CELL CULTURE OF NK CELLS AND PERIPHERAL BLOOD MONONUCLEAR CELLS ... 49
2.3.1. Cultivation of immune cells ... *49*
2.3.2. Thawing of NK cells ... *50*
2.3.3. Cocultivation of tumor cells with immune cells ... *50*
2.4. QUANTIFICATION OF PD-L1 EXPRESSION ON TUMOR CELL LINES VIA FACS ANALYSIS ... 51
2.4.1. Materials and devices for FACS analysis ... *51*
2.4.2. Staining antibodies for FACS analysis with their corresponding isotypes ... *51*
2.4.3. Staining for FACS analysis ... *52*
2.4.4. Procedure of FACS analysis ... *53*
2.5. FACS ANALYSIS OF PD-1 EXPRESSION ON NK CELL POPULATIONS FROM DIFFERENT HEALTHY DONORS ... 53
2.5.1. Staining for CD279 (PD-1) expression ... *53*
2.5.2. Analysis of CD279 expression via flow cytometry ... *54*
2.6. INVESTIGATION OF ANTI-TUMOR EFFECTS VIA SULFORHODAMINE B CYTOTOXICITY ASSAY ... 54
2.6.1. Materials and devices for SRB assay ... *55*
2.6.2. Procedure of SRB assay ... *55*
2.7. XCELLIGENCE REAL-TIME CELL PROLIFERATION ASSAY ... 56
2.7.1. Materials and devices for xCELLigence analysis ... *57*
2.7.2. Seeding tumor cells for xCELLigence analysis ... *57*
2.7.3. Infection of tumor cells for xCELLigence analysis with MeV-GFP at different MOIs ... *59*
2.7.4. Coincubation with peripheral blood mononuclear cells or NK cells at different effector : target ratios and treatment with immune checkpoint inhibitors ... *59*
2.7.5. Evaluation of xCELLigence analysis ... *60*
2.8. VIRAL GROWTH CURVES OF MEV-GFP ON HT29 AND HCT-15 TUMOR CELLS ... 60

2.8.1. Viral infection of HT29 and HCT-15 cells for preparation of virus growth curves. ... 60

2.8.2. Titration for virus growth curves ... 61

2.8.3. Analysis of viral growth curves ... 62

2.9. DETERMINATION OF VIRAL TITERS ON HT-29 AND HCT-15 TUMOR CELLS AFTER COCULTURE WITH NK CELLS OR PBMC AND TREATMENT WITH ATEZOLIZUMAB OR NIVOLUMAB ... 62

3. RESULTS ... 64

3.1. QUANTIFICATION OF ANTI-TUMOR EFFECTS OF MONOTHERAPEUTIC TREATMENT WITH MEASLES VIROTHERAPEUTIC OR IMMUNE CHECKPOINT BLOCKADE IN COLORECTAL CARCINOMA ... 65

3.1.1. Measurement of cytotoxicity under MeV-GFP-infection in human colorectal carcinoma cell lines HCT-15, HT29 and SW-620 ... 65

3.1.2. Examination of cytotoxicity after treatment with immune checkpoint inhibitors nivolumab or atezolizumab in human colorectal carcinoma cell lines HCT-15 and HT29 ... 68

3.2. ANALYSIS OF PD-L1 EXPRESSION ON DIFFERENT HUMAN COLORECTAL CARCINOMA CELL LINES UNDER THE INFLUENCE OF MEASLES-INDUCED ONCOLYSIS ... 69

3.2.1. Basal PD-L1 expression in human colorectal carcinoma cell lines HT29, HCT-15 and SW-620 under the influence of different culturing conditions ... 70

3.2.2. PD-L1 expression in human colorectal carcinoma cell lines HT29, HCT-15 and SW-620 after infection with MeV-GFP ... 72

3.2.3. PD-L1 expression in human colorectal carcinoma cell lines HCT-15, HT29 and SW620 after infection with MeV-SCD ... 78

3.3. FACS ANALYSIS OF PD-1 EXPRESSION ON NK CELL POPULATIONS FROM DIFFERENT HEALTHY DONORS ... 84

3.4. IN VITRO THERAPEUTIC EFFECTS OF COMBINING MEV-GFP WITH IMMUNE CHECKPOINT INHIBITORS AND IMMUNE CELL COCULTURE IN HUMAN COLORECTAL CARCINOMA CELL LINES ... 86

3.4.1. xCELLigence real-time cell proliferation assay for analysis of HT29 / HCT-15 growth and viability under the influence of MeV-GFP-infection together with nivolumab and / or atezolizumab treatment ... 87

3.4.2. xCELLigence real-time cell proliferation assay for analysis of HT29 / HCT-15 growth and viability under the influence of MeV-GFP-infection, treatment with nivolumab and / or atezolizumab and PBMC or NK cell coculture ... 89

3.5. QUANTIFICATION OF ANTIVIRAL EFFECTS OF IMMUNE CHECKPOINT INHIBITORS ON THE REPLICATION OF MEV-GFP IN HUMAN COLORECTAL CARCINOMA CELL LINES ... 105

3.5.1. Quantification of antiviral effects of immune checkpoint inhibitors in a viral growth curve model on MeV-GFP-infected HT29 and HCT-15 tumor cells 105

3.5.2. Quantification of antiviral effects of immune checkpoint inhibitors in MeV-GFP-infected HT29 and HCT-15 tumor cells after immune cell cocultivation 107

4. DISCUSSION 110

5. SUMMARY 125

6. REFERENCES 129

7. ERKLÄRUNG ZUM EIGENANTEIL DER DISSERTATIONSSCHRIFT 143

Abbreviations

5-FC	5-fluorocytosine
FdUMP	5-fluorodeoxyuridine monophosphate
5-FU	5-fluorouracil
ADCC	antibody-dependent cellular cytotoxicity
APC	adenomatous polyposis coli
APC	antigen-presenting cell
APME	acute postinfectious measles encephalitis
BiTE	bispecific T-cell engagers
CD16	cluster of differentiation 16 receptor, Fc receptor expressed on NK cells
CD20	cluster of differentiation 20 receptor, expressed by B-cell Non-Hodgkin lymphoma
CD28	cluster of differentiation 28 receptor, costimulatory T-cell receptor
CD46 / MCP	membrane cofactor protein, plays a role in host cell entrance of measles vaccine virus
CD56	cluster of differentiation 56, expressed on NK cells
CD80 / B7.1	cluster of differentiation 80, ligand of CD28 receptor
CD86 / B7.2	cluster of differentiation 86, ligand of CD28 receptor
CD107 / LAMP-1	cluster of differentiation 107 / lysosomal-associated membrane protein-1, marker of NK cell activity
CD150 / SLAM	cluster of differentiation 150 / signaling lymphocytic

	activation molecule
CD152 / CTLA-4	cluster of differentiation 152 / cytotoxic T-lymphocyte-associated antigen-4
CD273 / PD-L2 / B7-DC	cluster of differentiation 273 / programmed cell death 2 ligand
CD274 / PD-L1 / B7-H1	cluster of differentiation 274 / programmed cell death 1 ligand
CD279 / PD-1	cluster of differentiation 279 / programmed cell death 1 receptor
CEA	carcinoembryonic antigen
CI	cell index
CI	confidence interval
CPE	cytopathic effect
CR	complete response
CRC	colorectal carcinoma
CTL	cytotoxic T-lymphocyte
DAMP	danger-associated molecular pattern
DC	dendritic cell
DLT	dose limiting toxicity
DMEM	Dulbecco's modified Eagle medium
DMSO	dimethylsulfoxide
dpi	days post infection

EDTA	ethylenediaminetetraacetic acid
EGFR	epidermal growth factor receptor
E : T ratio	effector : target cell ratio
FACS	fluorescence-activated cell sorting
FAP	familial adenomatous polyposis
FBS / FCS	fetal bovine serum / fetal calf serum
FITC	fluorescein isothiocyanate
GBM	glioblastoma
GFP	green fluorescent protein
GM-CSF	granulocyte-macrophage colony-stimulating factor
GMP	good manufacturing practice
HCG	human chorionic gonadotropin
HNPCC	hereditary non-polyposis colon cancer
hpi	hours post infection
HSV-1	human herpes simplex virus type 1
IBD	inflammatory bowel disease
ICD	immunogenic cell death
ICI	immune checkpoint inhibitor
IFIT	interferon-induced protein with tetratricopeptide repeats
IFN	interferon

IgSF	immunoglobulin superfamily
mAb	monoclonal antibody
MCP	membrane cofactor protein (also CD46)
MeV	measles vaccine virus
MHC	major histocompatibility complex
MIBE	measles inclusion body encephalitis
MOI	multiplicity of infection
MSI	microsatellite instability
MSS	microsatellite stability
NCI	National Cancer Institute
NDV	Newcastle disease virus
NIS	sodium iodide symporter
NOD / SCID	non-obese diabetic / severe combined immunodeficiency
ORR	objective response rate
OS	overall survival
OV	oncolytic virus
PAMP	pathogen-associated molecular pattern
PBS	phosphate buffered saline
PE	phycoerythrin
PET	positron emission tomography

PFS	progression-free survival
PR	partial response
PRR	pattern recognition receptor
rpm	revolutions per minute
RECIST	Response Evaluation Criteria in Solid Tumors
rrVSV	recombinant replicating vesicular stomatitis virus
RT	room temperature
SCD	super-cytosine deaminase
SD	stable disease
SD	standard deviation
SEM	standard error of the mean
SLAM	signaling lymphocytic activation molecule (also CD150)
SPECT	single photon emission computed tomography
SSPE	subacute sclerosing panencephalitis
TAA	tumor-associated antigen
TCR	T-cell receptor
TH1 cell	T helper cell type 1
TIL	tumor-infiltrating lymphocyte
T-VEC	Talimogene laherparepvec
VEGF	vascular endothelial growth factor

VSV	vesicular stomatitis virus
wt	wildtype

List of figures

FIGURE 1, A - B: CANCER INCIDENCE AND MORTALITY IN 2012. 18
FIGURE 2: VIROTHERAPY AS HIGHLY IMMUNOGENIC STIMULUS 22
FIGURE 3: PRINCIPLES OF TUMOR-SPECIFIC VIRAL ONCOLYSIS 23
FIGURE 4, A - B: SCHEMATIC STRUCTURE OF THE MEASLES VIRUS PARTICLE (A) AND ITS RESPECTIVE GENOME (B) 29
FIGURE 5: SCHEMATIC STRUCTURE OF THE GENETICALLY ENGINEERED MEASLES VIRUS GENOME 30
FIGURE 6: PRINCIPLE OF COMBINING ONCOLYTIC VIRUS (MEV) WITH IMMUNE CHECKPOINT BLOCKADE (*ATEZOLIZUMAB, NIVOLUMAB*) 38
FIGURE 7: SCHEMATIC ILLUSTRATION OF NK CELL CULTIVATION 49
FIGURE 8: PRINCIPLE OF IMMUNHISTOCHEMICAL STAINING FOR FLOW CYTOMETRY 52
FIGURE 9: 96-WELL ELECTRONIC MICROTITER PLATE 56
FIGURE 10: PROCEDURE OF XCELLIGENCE ANALYSIS 57
FIGURE 11: 96-WELL PLATE OF DILUTION SERIES FOR MEV-GFP VIRUS GROWTH CURVES 61
FIGURE 12: WORKFLOW OF VIRUS TITER DETERMINATION AFTER COINCUBATION WITH NK CELLS / PBMC AND TREATMENT WITH ICI 63
FIGURE 13: SRB CYTOTOXICITY ASSAYS OF THE MEV-GFP-INFECTED HUMAN CRC CELL LINE HT29 65
FIGURE 14: SRB CYTOTOXICITY ASSAYS OF THE MEV-GFP-INFECTED HUMAN CRC CELL LINE HCT-15 66
FIGURE 15: SRB CYTOTOXICITY ASSAYS OF THE MEV-GFP-INFECTED HUMAN CRC CELL LINE SW-620 67
FIGURE 16: SRB CYTOTOXICITY ASSAYS OF HT29 TUMOR CELLS AFTER TREATMENT WITH IMMUNE CHECKPOINT INHIBITORS *ATEZOLIZUMAB* OR *NIVOLUMAB* 68
FIGURE 17: SRB CYTOTOXICITY ASSAYS OF HCT-15 AFTER TREATMENT WITH IMMUNE CHECKPOINT INHIBITORS *ATEZOLIZUMAB* OR *NIVOLUMAB* 69
FIGURE 18: FACS ANALYSIS OF THE BASAL PD-L1 EXPRESSION ON HUMAN COLORECTAL CARCINOMA CELL LINES HT29, HCT-15 AND SW-620 UNDER DIFFERENT CULTURING CONDITIONS 70
FIGURE 19: FACS ANALYSIS OF GFP EXPRESSION ON MOCK- OR MEV-GFP-INFECTED HUMAN COLORECTAL CARCINOMA CELL LINES HT29, HCT-15 AND SW-620 73
FIGURE 20, A - C: FACS ANALYSIS OF PD-L1 EXPRESSION ON MEV-GFP-INFECTED IN COMPARISON TO MOCK-INFECTED HUMAN COLORECTAL CANCER CELL LINES HT29, HCT-15 AND SW-620 76

FIGURE 21, A - C: FACS ANALYSIS OF PD-L1 EXPRESSION ON MEV-SCD-INFECTED IN COMPARISON TO MOCK-INFECTED HUMAN COLORECTAL CANCER CELL LINES HT29, HCT-15 AND SW-620 82
FIGURE 22 A - B: XCELLIGENCE REAL-TIME ASSAY OF HT29 AND HCT-15 GROWTH AND VIABILITY UNDER TREATMENT WITH MEV-GFP AND / OR IMMUNE CHECKPOINT INHIBITORS 88
FIGURE 23, A - G: XCELLIGENCE REAL-TIME ASSAY OF HT29 GROWTH AND VIABILITY UNDER TREATMENT WITH MEV-GFP, IMMUNE CHECKPOINT INHIBITORS AND PBMC / NK CELLS 93
FIGURE 24, A - G: XCELLIGENCE REAL-TIME CELL PROLIFERATION ASSAY OF HCT-15 GROWTH AND VIABILITY UNDER TREATMENT WITH MEV-GFP, IMMUNE CHECKPOINT INHIBITORS AND PBMC / NK CELL COCULTURE 102
FIGURE 25, A - C: QUANTIFICATION OF ANTIVIRAL EFFECTS OF IMMUNE CHECKPOINT INHIBITORS IN A VIRAL GROWTH CURVE MODEL ON HT29 AND HCT-15 TUMOR CELLS .. 106
FIGURE 26: QUANTIFICATION OF ANTIVIRAL EFFECTS OF CHECKPOINT INHIBITORS VIA VIRUS TITRATION ON HT29 AND HCT-15 TUMOR CELLS 108

List of tables

TABLE 1: MATERIALS AND DEVICES FOR CELL CULTURE 42
TABLE 2: USED CELL LINES WITH THEIR CHARACTERISTICS (NCI-WEBPAGE, ACCESSED AUGUST 17, 2016) 43
TABLE 3: DIFFERENT CULTURE VESSELS AND CORRESPONDING AMOUNTS OF MEDIUM, TRYPSIN OR PBS 44
TABLE 4: DIFFERENT CULTURE PLATES AND FITTING NUMBERS OF CELLS BEING SEEDED PER WELL 47
TABLE 5: CONCENTRATIONS OF IMMUNE CHECKPOINT INHIBITORS USED IN DIFFERENT EXPERIMENTS 47
TABLE 6: MATERIALS AND DEVICES FOR FACS ANALYSIS 51
TABLE 7: STAINING ANTIBODIES FOR FACS ANALYSIS WITH THEIR CORRESPONDING ISOTYPES 51
TABLE 8: CD279 (PD-1) FACS ASSAY STAININGS AND THE RESPECTIVE AMOUNTS OF ANTIBODY PER STAIN 54
TABLE 9: MATERIALS AND DEVICES FOR SRB ASSAY 55
TABLE 10: MATERIALS AND DEVICES FOR XCELLIGENCE ANALYSIS 57
TABLE 11: CELL COUNTS PER WELL USED FOR XCELLIGENCE ANALYSIS OF DIFFERENT CRC CELL LINES 58
TABLE 12: AMOUNT OF TUMOR CELLS PER WELL USED FOR VIRAL GROWTH CURVES. 60
TABLE 13: CELL COUNTS, MOIS, E : T RATIOS AND ICI CONCENTRATIONS USED FOR VIRAL TITER DETERMINATION 63
TABLE 15, A - C: FACS ANALYSIS OF PD-L1 EXPRESSION ON MEV-GFP-INFECTED IN COMPARISON TO MOCK-INFECTED HUMAN COLORECTAL CANCER CELL LINES HT29, HCT-15 AND SW-620 77
TABLE 15: FACS ANALYSIS OF PD-1 EXPRESSION ON NK CELL POPULATIONS FROM DIFFERENT HEALTHY DONORS 85

1. Introduction

1.1. Colorectal cancer as a major health problem

1.1.1. Epidemiology of colorectal carcinoma

Colorectal carcinoma (CRC) is considered a major health problem especially in industrialized nations. All over the world, this tumor entity depicts the third most common diagnosis of cancer (GLOBOCAN 2012, 1.36 million of 14.1 million new cancer cases / 9.7 %) and the fourth most common cause for cancer death (694,000 of 8.2 million deaths / 8.5 %) with a higher incidence in more developed countries (12.1 % of new cancer cases in 2012 vs. 7.8 % in less developed countries) (Ferlay et al., 2015). Furthermore, referring to data from the US National Cancer Institute between 2012 and 2014, overall lifetime risk of the diagnosis of CRC is described with 4.3 % of men and women (NCI-Webpage, Accessed April 23, 2017).

In Germany, overall CRC mortality in men decreased by 36.7 % between 1989 and 2011, in women even by 47.3 % (Ait Ouakrim et al., 2015). In contrast, mortality in all 34 investigated European countries increased by 6 % in men, whereas it decreased by 14.7 % in women. Differences between various geographic regions may probably be influenced by factors such as access and possibility of screening (especially colonoscopy with the possibility to remove early precursor lesions presenting as polyps, thus making CRC partly preventable (Simon, 2016)) and of treatment modalities, as well as nutritive habits and health-related lifestyle.

Available access to early screening methods has also a great impact on overall CRC mortality, as localized CRC has a 5-year relative survival of 89.9 %, whereas the appearance of distant metastases goes along with a 5-year relative survival of only 13.9 %, citing data from the NCI webpage collected between 2007 and 2013 (NCI-Webpage, Accessed April 23, 2017). These data furthermore comprise the necessity of novel therapeutic treatment strategies, especially for advanced CRC.

***A)** Cancer incidence and mortality in 2012 in men*

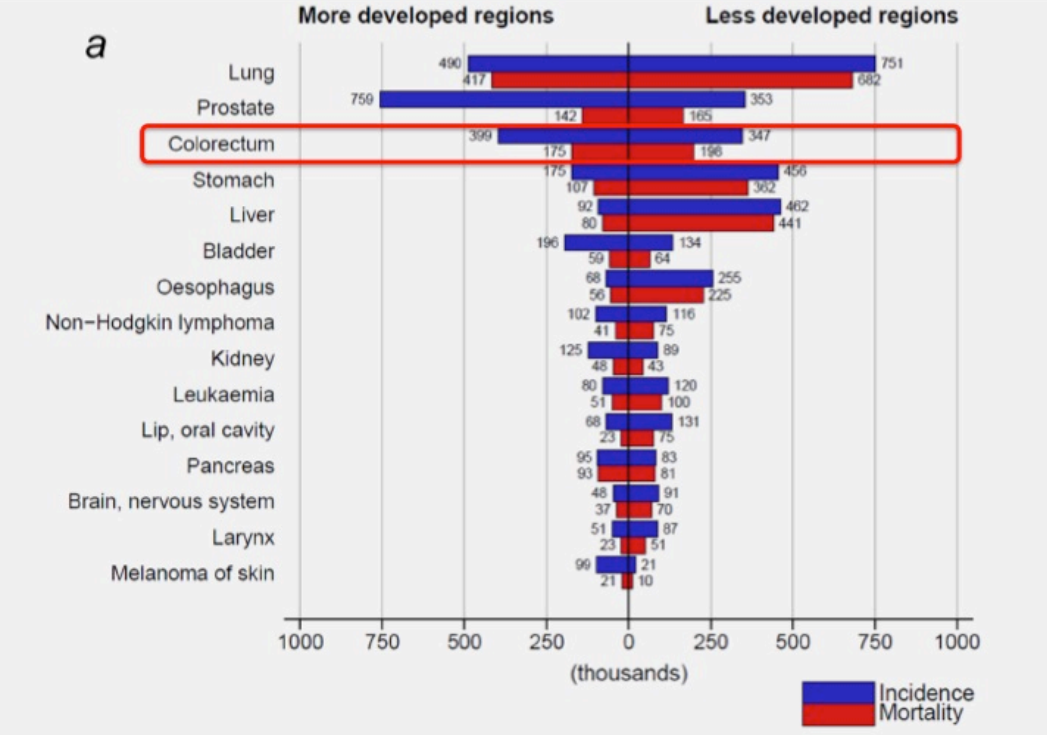

***B)** Cancer incidence and mortality in 2012 in women*

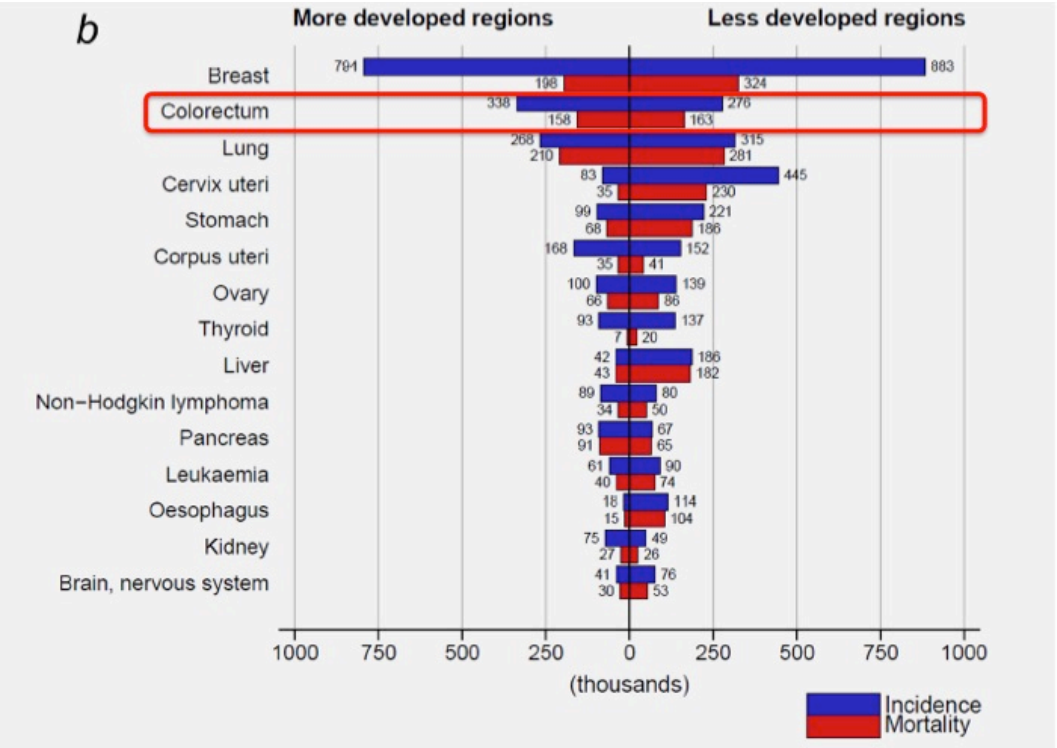

Figure 1, A - B: Cancer incidence and mortality in 2012.
Cancer incidence (blue colored) and mortality (red colored) in (A) men and (B) women in 2012, depicting the differences between more and less developed countries. Among different cancer

entities, CRC takes rank three in men and rank two in women in regard to incidence in more developed countries. Taken of (Ferlay et al., 2015).

1.1.2. Colorectal cancer - an overview of pathology and clinical presentation

Most colorectal cancers develop in a sporadic, non-hereditary manner, often referring to a somatic mutation in the Wnt / β-catenin signaling pathway, namely in the adenomatous polyposis coli *(APC)* tumor suppressor gene (Rowan et al., 2000).

Hereditary syndrome forms, on the contrary, are rather rare with approximately 5 % of CRC (Lung et al., 2015). One of the best known, the familial adenomatous polyposis (FAP), is also attributed to a mutation of *APC* on chromosome 5q21 - q22, but this time in the germ line, characterized by up to thousands of adenomatous polyps in adolescence (Bodmer et al., 1987; Nakamura et al., 1988; Groden et al., 1991). Another hereditary form of CRC displays Lynch syndrome, an entity of hereditary non-polyposis colon cancer (HNPCC) with germ line mutation leading to DNA mismatch repair deficiency, followed by an enormous rate of mutations. This inheritable defective DNA repair mechanism is also associated with numerous extracolonic cancers, most of all endometrial and ovarian (Carethers and Stoffel, 2015; Lung et al., 2015).

Prolonged inflammation as a key factor in carcinogenesis likewise concerns forms of CRC, for example in patients with diagnosed inflammatory bowel disease (IBD), such as ulcerative colitis or Crohn's disease (Lasry et al., 2016). Furthermore, this goes along with the finding that proinflammatory cytokines are able to increase Wnt signaling pathway activity (Ostaff et al., 2013). Emphasizing these links between inflammation and CRC, a further factor of carcinogenesis has to be taken into account: microbiota. To give only one example, investigations could show that the toxin of *Bacteroides fragilis* was able to increase transcription of β-catenin-regulated oncogenes (Sears, 2009; Saleh and Trinchieri, 2011).

Apart from discussed pathogenesis factors of hereditary impact, family history of CRC and inflammation, also advanced age, black race, obesity, diabetes mellitus and smoking as well as alcohol consumption have been revealed as risk factors for CRC development (Cai et al., 2014; Oluyemi et al., 2014). As for advanced age, about 90 % of CRC occur beyond age of 50 (Herold, 2015).

Clinical presentation of CRC does not go along with reliable early symptoms, but blood admixture in stool or sudden changes in dejection habits can belong to the clinical pattern.

Histopathological definition of a malignant polyp includes invasion of muscularis mucosae, hence being referred to as pT1 and being capable of metastasis (Engstrom et al., 2009).

The way of metastasis follows mainly the portal vein, turning the liver and, secondly, the lung into most preferred regions of early tumor filiae. For metachronous liver metastases, cumulative 10-year incidences after first diagnosis of CRC are ranked at about 6 % for stage I and up to 30 % at stage III (Landreau et al., 2015).

1.1.3. Existing therapeutic possibilities and problems in treatment of colorectal cancer

Surgery represents the therapy option with greatest significance in treatment of CRC in both primary tumor and metastases in liver or lung, if complete tumor resection is possible. With the total mesocolic or mesorectal excision and the ablation of lymph nodes as well as infiltrated neighboring organs, a maximal local radicalness is supported (Herold, 2015). Although 70 - 80 % of patients with CRC diagnosis can be resected *in sano* (R0), 40 - 50 % suffer recurrence or later metastases (Gustavsson et al., 2015).

Neoadjuvant or adjuvant (radio-) chemotherapy is used to treat higher UICC stages, including conventional chemotherapy with an oxaliplatin- or fluoropyrimidine-based regimen. For colon cancer, adjuvant chemotherapy is referred to as gold standard for stage III or higher in order to eliminate possible micrometastases and to improve progression-free survival (PFS) as well as overall survival (OS) (Lombardi et al., 2010; Gustavsson et al., 2015).

The basis of the existing chemotherapy protocols represents 5-fluorouracil (5-FU), since its converted form 5-fluorodeoxyuridine monophosphate (FdUMP) appeared to be a potent inhibitor of thymidylate synthetase as a suicide substrate (Danenberg, 1977). Thymidine-containing desoxyribonucleotides result from methylation of uracil-containing desoxyribonucleotides through thymidylate synthetase, thus being a key step of nucleic acid synthesis, which becomes blocked by 5-FU. Furthermore, incorporation of 5-FU into RNA as well as DNA is another mechanism of 5-FU-induced cytotoxicity

(Gill et al., 2003). Soon, folinic acid (leucovorin) was added to the treatment regimen, resulting in a prolonged survival, increased tumor response rates as well as improved PFS (Poon et al., 1989).

Together with the topoisomerase I inhibitor irinotecan, oxaliplatin and the oral 5-FU prodrug capecitabine, the existing treatment regimens were compiled.

As the era of monoclonal antibodies was introduced, *bevacizumab*, targeted against vascular endothelial growth factor (VEGF), and *cetuximab / panitumumab*, targeted against the epidermal growth factor receptor (EGFR) in patients with K-RAS wildtype (wt), replenished the spectrum of possible chemotherapeutics in CRC treatment. But yet, the median OS achieved in combination studies for metastatic disease in the last 30 years did not rise above 23.9 months (Gustavsson et al., 2015), thus making the research for new therapeutical approaches inevitable.

1.2. Virotherapy as an anti-cancer treatment approach

1.2.1. Principles of virotherapy - how an infectious virus becomes anti-cancer therapy

The idea behind virotherapy refers to the principle of tumor-specific oncolysis, therefore applying a virus with the hallmark of infecting tumor cells for replication and lysis afterwards, but sparing the surrounding healthy tissue. With the tumor cell lysis, viral progenies are released, which further infect neighboring tumor cells, thus representing a self-amplifying anti-cancer agent. Besides, concerning safety issues, the oncolytic virus (OV) should possess the trait of genetic stability as well as limited human pathogenicity, conceivably with well-known antiviral treatment available, also taking attenuated vaccine viruses or animal-pathogenic viruses into account (Kelly, 2007). Finally, a hurdle in introducing new virotherapeutics consists in production of needed virus doses in terms of good manufacturing practice (GMP) guidelines (Thorne et al., 2005).

Since the process of oncolysis leads to release of tumor-associated antigens (TAAs), thus setting an immunological stimulus, the direct tumor damage is completed by activating the host immune system against cancer, evading the tumorous immune escape mechanisms and thereby portraying virotherapy in an immunotherapeutical context (Naik et al., 2011; Russell et al., 2012). To put it into a nutshell, viral oncolysis

induces both innate immunity and adaptive anti-tumor immune response via tumor-specific T-cell priming (Melcher et al., 2011; Naik et al., 2011; Turnbull S, 2015). The highly immunogenic cell death (ICD) following viral lysis shapes the tumor microenvironment towards a pro-inflammatory background, for example through release of pathogen-associated molecular patterns (PAMPs) or danger-associated molecular patterns (DAMPs): PAMPs display conserved microbial molecules identified via pattern recognition receptors (PRRs), whereas DAMPs lead to activation of innate immune cells such as dendritic cells (DCs) or tumor macrophages, which further arrange adaptive anti-tumor immune responses (Prestwich et al., 2009; Donnelly et al., 2013; Woller N, 2014; Hardcastle et al., 2016; Marchini et al., 2016).

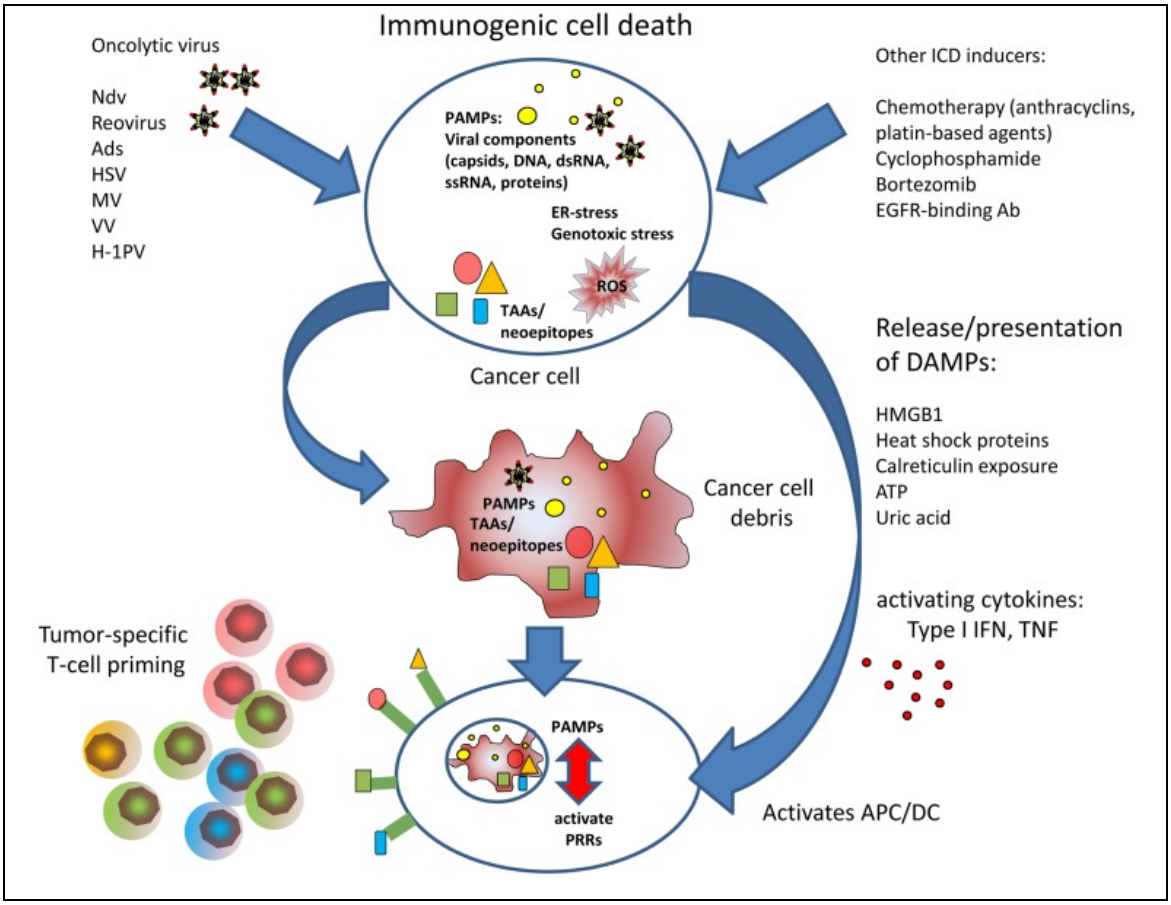

Figure 2: Virotherapy as highly immunogenic stimulus
OV-induced oncolysis functions as immunological impulse towards an innate as well as adaptive anti-tumor immune response. With the release of so-called pathogen-associated molecular patterns (PAMPs) and danger-associated molecular patterns (DAMPs), antigen-presenting cells (APC) such as dendritic cells (DC) are stimulated to mediate the immunological interplay against the foreign tumor neoepitopes. Figure from (Woller N, 2014).

Another mechanism of OV-induced tumor mass reduction involves strategies to impair tumor sustentative blood supply by targeting tumor endothelial cells (Breitbach et al., 2013). Moreover, OVs were even found to aim at cancer stem cells, which are often resistant to conservative radio- or chemotherapy and play a crucial role in tumor relapse (Smith et al., 2014; Marchini et al., 2016).

The leading characteristic of a candidate for virotherapy is certainly specificity in infection and replication behavior in terms of tumor cell tropism. Actually, several specifics of tumor cells make them more accessible for virus entrance and replication in comparison to related healthy tissue. To set an example, tumorigenesis mainly relies on the principles of avoiding apoptosis and of supplying autonomous growth, whereas a response to viral infection rather implements the opposite: apoptosis and inhibition of production of viral proteins via stop of translation (Russell et al., 2012). Namely, mutations in antiviral response pathways such as the interferon α / β response make the tumor cell incapable of defending against viral infection. Nevertheless, these mutations are common: As interferon simultaneously impedes tumor growth, interferon pathway deficiency turns out to be advantageous in carcinogenesis (Stojdl et al., 2000; Russell and Peng, 2009).

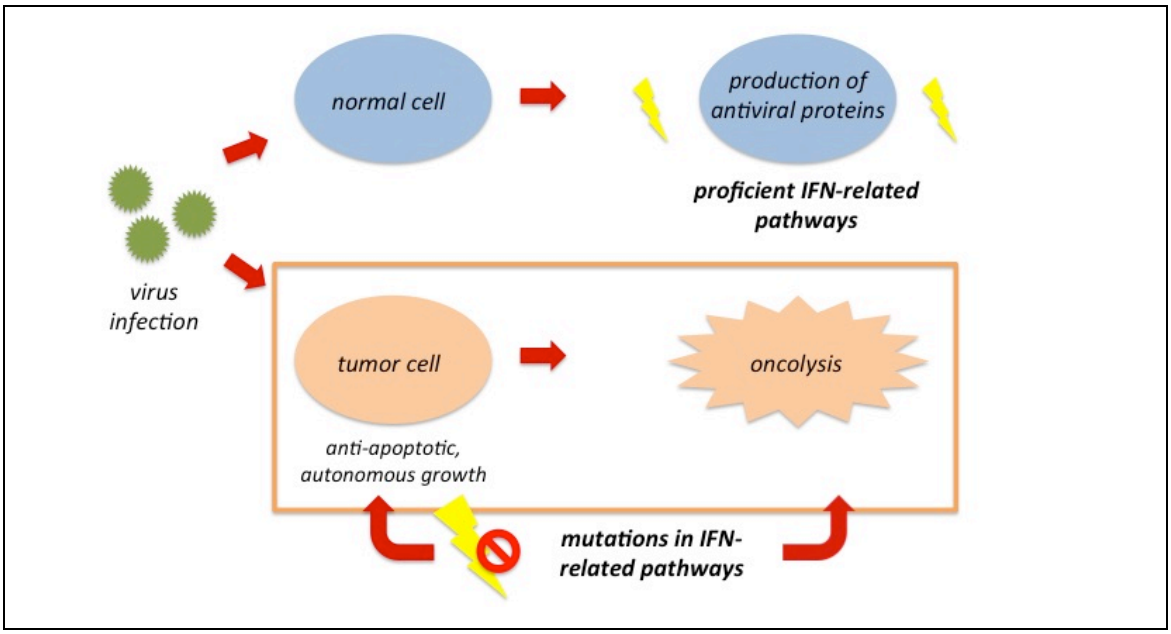

Figure 3: Principles of tumor-specific viral oncolysis
Tumor cells are preferentially accessible for viral infection, as important antiviral pathways such as the interferon (IFN) pathway appear to be impaired in favor of unhindered tumor growth. Figure modified after (Liu T.C., 2007).

Other ways of targeting virus to cancer cells imply the usage of OVs dependent on tumor-specific surface receptors and proteases for host cell fusion and entry, or involve the exploitation of distinct specificities of replication and transcription in tumor cells (Cattaneo et al., 2008).

A problem still to face in the field of virotherapy depicts the immunological clearance of systemically applied OV, especially of viruses also used for vaccination or with broad immunity-creating propagation (Fisher, 2006; Russell and Peng, 2009; Msaouel et al., 2013; Marchini et al., 2016). To elude such an early immunological clearance of OV by neutralizing antibodies in the bloodstream, several approaches were implemented in preclinical testing: combination of OVs with immunosuppressive drugs such as cyclophosphamide (Msaouel et al., 2013; Peng et al., 2013), protective coating of the virus particle (Fisher et al., 2001) or usage of so-called cell carriers (Iankov et al., 2007). It will be the challenge to get the balance between optimal OV-induced anti-tumor immune responses on the one hand and effective viral spread on the other hand.

1.2.2. History of virotherapy - from historical approaches to new generations of genetically engineered oncolytic viruses

In the early 20th century, the finding of viral oncolytic potential shortly followed the discovery of virus existence, when doctors witnessed cancer regression under naturally acquired viral infections (Kelly, 2007; Russell and Peng, 2009). But not until more than half a century had passed, clinical observances heralded the modern era of virotherapy in the 1970s and 1980s: In several cases, measles disease obtained shrinking of prominent Burkitt's lymphoma tumors, shortly after the typical measles exanthema was noticed (Bluming, 1971; Taqi et al., 1981). Moreover, several cases of tumor regression in patients with Hodgkin's disease (Greentree, 1983; Schattner, 1984) or chronic lymphatic leukemia (Hansen and Libnoch, 1978) were described after vaccination against measles or smallpox. Although the exact mechanisms of tumor-specific oncolysis were not fully understood, the immune-enhancing role of viral infection was assumed to be an important part of the resulting therapeutic effect, also considering the immunocompromised state accompanying those hematological tumor entities (Kelly, 2007). As early as 1973, Minton et al. used killed mumps virus for an immune stimulation protocol in melanoma patients, who had already undergone several

treatment strategies such as surgery and chemotherapy, but still, clinical benefit was not of long duration (Minton, 1973; Kelly, 2007).

Furthermore, several animal viruses were tested as an oncolytic therapeutic with controllable virulence: In contrast to many human pathogenic viruses, which are wide-spread as natural infections or part of vaccination programs, animal viruses implicate the advantage of not being exposed to immunological clearance by preexisting anti-bodies (Kelly, 2007).

When successful cultivation of virus in laboratories, establishment of human cancer models in rodents and, finally, reverse genetics entered the stage of clinical basic research, virotherapy experienced a new boom (Kelly, 2007; Cattaneo et al., 2008; Russell and Peng, 2009). With the partly insufficient tumor tropism, the problem of early OV clearance by the host immune system or the lack of oncolysis efficacy, the era of viral genome manipulation in the late 20th century implied an enormous progress in establishing virotherapy in the field of oncology. But as a matter of fact, first attempts to improve efficacy of virus-mediated oncolysis had already been made before, for example as Moore and colleagues discovered that Russian Far East encephalitis virus provided better results in oncolysis of sarcoma after having been propagated in sarcoma cells beforehand, thereby enabling an adaption of viral replication to the host cell (Moore, 1952; Kelly, 2007).

Utilizing the new options in genetic engineering, experiments of retargeting OVs to surface molecules expressed by cancer cells succeeded, with CD20 (Non-Hodgkin lymphoma) (Bucheit et al., 2003) or carcinoembryonic antigen (CEA) (Hammond et al., 2001) as exemplary targets for creating a more specific tumor tropism. Other approaches of viral genome manipulation made non-invasive monitoring of viral spread- and elimination-kinetics possible, for example via insertion of marker genes such as CEA or the β-unit of human chorionic gonadotropin (β-HCG), whose serum levels not only reflected viral replication kinetics, but also correlated with the therapeutic outcome in animal models (Peng et al., 2002a).

With regard to the field of radiovirotherapy, treatment with a measles vaccine virus (MeV) expressing the sodium iodide symporter (NIS), which can be found on thyroid follicular cells for iodide transport into the cell, was combined either with the application of I-123, or with the β-emitter I-131. Thereby, monitoring of viral growth

kinetics via positron emission tomography (PET) or single photon emission computed tomography (SPECT) in the former, as well as an additive therapeutic option in the latter case could be realized (Dingli et al., 2004).

Genetic engineering was also used in attempt to increase anti-tumor immunostimulatory effects, for example enabling herpes virus (T-Vec) or vaccinia virus (JX-594) to express the granulocyte-macrophage colony-stimulating factor (GM-CSF) (Park et al., 2008; Kaufman et al., 2010). Finally, suicide-gene functions were exploited to convert systemically administered, harmless prodrugs into highly effective, local chemo-therapies: By directly delivering necessary transforming enzymes via OV-vectors to the tumor location, preexisting resistances against virotherapy were successfully overcome (Graepler F., 2005; Lampe J, 2013; Lange S, 2013; Noll M., 2013; Yurttas C, 2014).

To put it into a nutshell, possibilities of genetic engineering induced metamorphosis of virotherapy into a multifunctional instrument in cancer treatment.

1.2.3. Oncolytic virus in clinical usage - from bench to bedside

With the introduction of the first FDA- and EMA-approved virotherapeutic on the market in 2015, *Imlygic*® (*Talimogene laherparepvec*, Amgen, also shortened as T-VEC and developed as OncoVEX$^{GM\text{-}CSF}$), a great hurdle was overcome in clinical development of virotherapy as an anti-cancer treatment. Approval of the GM-CSF expressing human herpes simplex virus HSV-1 for treatment of unresectable stage III / IV melanoma was given, after efficacy and, simultaneously, safety as well as feasibility of application were proven in a first phase III clinical trial with prolongation of overall survival (OS) from 18.9 months (GM-CSF only) to 23.3 months (T-VEC) ($P = 0.051$) (Andtbacka, 2015). Engineered to sustain major histocompatibility complex I (MHC I) presentation, to produce GM-CSF and to achieve effective, tumor specific viral replication and limited neuropathogenicity at the same time, T-VEC belongs to the third generation of OVs, genetically armed for better anti-tumor efficacy (Liu T.C., 2007; Andtbacka, 2015; Johnson et al., 2015).

Without this possibility of sophisticated viral gene modification in the middle of the last century, early clinical trials had been executed with wildtype viruses, domesticated through passage in cell culture, such as West Nile virus, adenovirus, mumps or vaccinia virus (Liu T.C., 2007).

Currently, along with herpes simplex virus, numerous virotherapeutics are under clinical development, for example MeV, focused on non-invasively trackable MeV-CEA and MeV-NIS (described in 1.2.2). Namely, a phase I trial of intratumoral or resection cavity application of MeV-CEA in glioblastoma multiforme patients investigated safety issues, with no dose limiting toxicities (DLTs) reported so far (ClinicalTrials.gov identifier NCT00390299) (Msaouel et al., 2009). In another phase I trial, MeV-NIS and MeV-CEA are tested for therapeutic efficacy against ovarian cancer, also exploring safety and toxicity in a dose escalation study, as well as shedding of replication-capable virus (NCT00408590) (Galanis et al., 2010). Along with predisposition to mutate or revert to wildtype, environmental shedding, for example in saliva, urine or blood, has to be particularly attributed in clinical trials with virotherapeutics, which descend from originally pathogenic strains (Buijs et al., 2015).

Addressing the tumor entity of treatment-refractory CRC, a first virotherapeutic phase Ib dose-finding trial was conducted with *i.v.* vaccinia virus Pexa-Vec, leading to a stable disease (SD) in 67 % of patients (Park et al., 2015). Furthermore, infusions of herpes simplex virus NV1020 or oncolytic adenovirus *dl*1520 (Onyx-015) into the hepatic artery were tested for CRC liver metastasis in phase I / II studies, resulting in acceptable toxicity profiles (Reid et al., 2002; Geevarghese et al., 2010).

To overcome tumor-immanent resistances against viral oncolysis, researchers and clinicians now head for combination therapies with conventional chemotherapy, radiotherapy, immunotherapy or targeted therapy. To give an example, squamous cell cancer of the head and neck is treated in a phase I/ II trial with T-VEC together with cisplatin and radiotherapy, resulting in 82.3 % of patients showing response according to RECIST criteria (Response Evaluation Criteria in Solid Tumors) (Harrington et al., 2010).

Multimodal immunovirotherapeutic treatment (for details, see 1.5), including immune checkpoint blockade, is evaluated in clinical phase Ib/II trials (T-VEC and *ipilimumab / Yervoy*®, Bristol-Myers Squibb, in patients with advanced melanoma, NCT01740297), as well as phase Ib/III trials (T-VEC and *pembrolizumab / Keytruda*®*,* MSD, also for treatment of advanced melanoma, NCT02263508). First results for T-VEC and *ipilimumab* prove tolerable safety without appearing DLTs and a 50 % objective response rate (ORR, 95 % CI, 26.0 to 74.0), including four patients (22 %) with

complete response (CR) (Puzanov et al., 2016). With regard to MeV virotherapy, a phase I study combining MeV-NIS with the immune checkpoint inhibitor (ICI) *nivolumab* (*Opdivo*®, Bristol-Myers Squibb) will start recruiting patients with recurrent non-small cell lung cancer in 2017 (NCT02919449).

One of the latest successes in the field of immunovirotherapy was the treatment of advanced melanoma with *Talimogene laherparepvec* and *pembrolizumab* in a phase Ib clinical trial (NCT02263508) (Ribas et al., 2017), resulting in no apparent increase in toxicity compared to the respective monotherapies. In the rather small patient cohort of 21, an ORR of 62 % was found, including CRs in 33 % of patients (both referring to immune-related response criteria). An ongoing phase III study allocates patients with advanced melanoma in a *Talimogene laherparepvec* plus *pembrolizumab* or a placebo plus *pembrolizumab* arm to further investigate OS as well as PFS (NCT02263508).

To summarize, virotherapy has made a fine step forward towards proving its worth in clinical oncology, considering numerous clinical trials and the approval of Imlygic®.

1.3. Measles virus - boon or bane in modern medicine?

1.3.1. Morphology and classification of measles virus

Measles virus, member of the family *Paramyxoviridae*, genus *Morbillivirus*, belongs to the enveloped viruses, containing a 16 kb negative strand genomic RNA coated with a nucleocapsid. The virion has a size of about 100 to 300 nm and is configured out of six structural proteins (Duke and Mgone, 2003; Knipe, 2013).

Two glycoproteins, viral transmembrane hemagglutinin (H) and the fusion protein (F), were found responsible for receptor targeting (H) and viral entrance via membrane fusion (F) in *Paramyxoviridae* such as measles (Navaratnarajah et al., 2011). Measles wildtype virus possesses the ability to bind to the signaling lymphocytic activation molecule (SLAM or CD150) on B- and T-lymphocytes (Tatsuo et al., 2000) or to nectin-4 on human airway epithelium (Mühlebach M. D., 2011) for cell entrance, but measles vaccine strains such as Edmonston strain are also able to target the so-called membrane cofactor protein (MCP or CD46), which plays a role in regulation of the complement system. Interestingly, CD46 is expressed ubiquitously on nucleated cells (Dorig et al., 1993) and also on human tumor cells, here even in a higher degree

(Russell and Peng, 2009), which makes measles vaccine virus (MeV) suitable as a viro-therapeutic.

Other structural proteins are the matrix protein (M), nucleocapsid protein (N), phosphoprotein (P) and large polymerase proteins (L). The basic matrix protein (M) is part of the virion's envelope, together with H and F. The nucleocapsid protein (N) is the protein transcribed first as well as most frequently, building the helical ribonucleocapsid together with the RNA genome. A component of replicase complex represents the large protein (L) with polymerase function, which is also part of the nucleocapsid and associated with the phosphoprotein (P), being a polymerase cofactor.

The wildtype virus phosphoprotein transcription unit also codes for the proteins C and V, which, together with P, circumvent the translocation of STAT to the nucleus as well as STAT1 and STAT2 phosphorylation, thus counteracting the antiviral interferon response and enabling viral spread more efficiently (Cattaneo et al., 2008; Russell and Peng, 2009). Interestingly, an oncolytic MeV, genetically engineered to code for the wildtype P gene, was able to circumvent innate tumor cell immunity via suppression of the IFN pathway (Haralambieva et al., 2007).

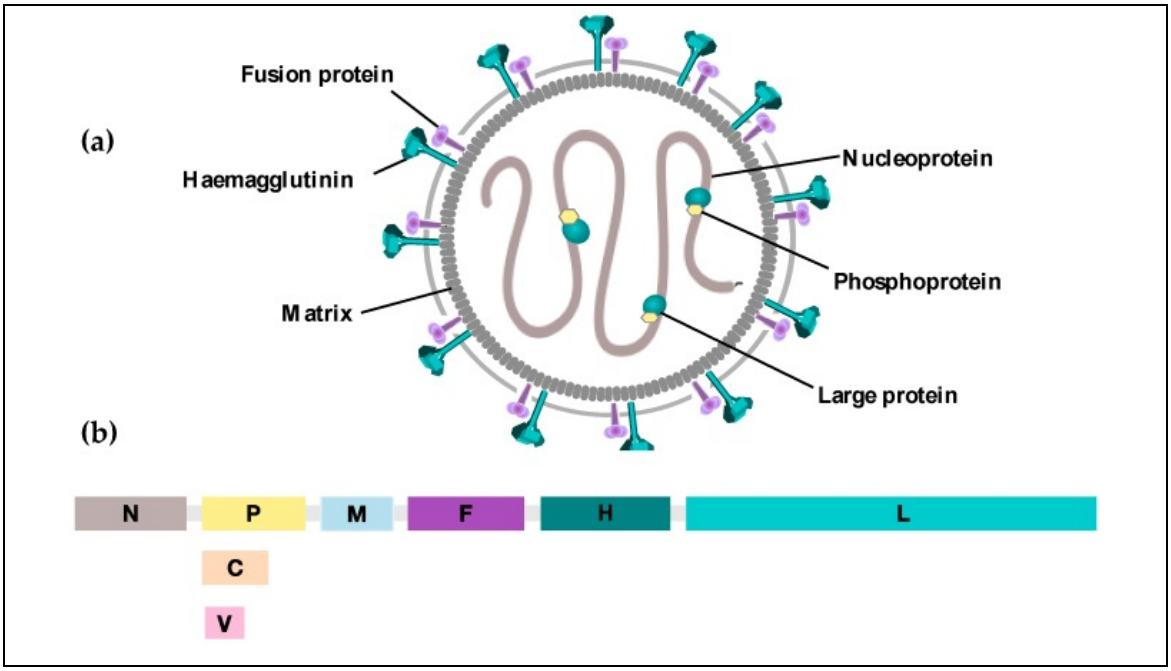

Figure 4, a - b: Schematic structure of the measles virus particle (a) and its respective genome (b)

The enveloped measles virus particle (a) consists of six structural proteins. The matrix proteins (M) encompass the so-called ribonucleoprotein complex, comprising the nucleoprotein (N), which coats the negative strand genomic RNA, the RNA-dependent RNA polymerase called large protein (L) and its cofactor, the phosphoprotein (P). Hemagglutinin (H) and fusion protein (F) are responsible for receptor targeting as well as viral invasion into the host cell via

membrane fusion. The measles viral genome (b) codes for the six viral proteins and implies a transcriptional gradient from the N protein to the L protein with a decreasing amount of resulting protein products. The proteins C and V are alternative products of P and play an important role in antagonizing antiviral interferon responses. Figure from (Aref et al., 2016).

Genetically engineered measles vaccine virus used in the field of virotherapy often encodes for further proteins, for example for the green fluorescent protein (GFP) to monitor successful infection, or for the prodrug-converting super-cytosine deaminase (SCD), which implements additional therapeutic effects in combination with the substrate and prodrug 5-fluorocytosine. Thereby, the transcriptional gradient from the N to the L protein implies that a gene position upstream of the region coding for the N protein results in maximal expression of the wanted protein product (see Fig. 5) (Lampe J, 2013; Hutzen et al., 2015).

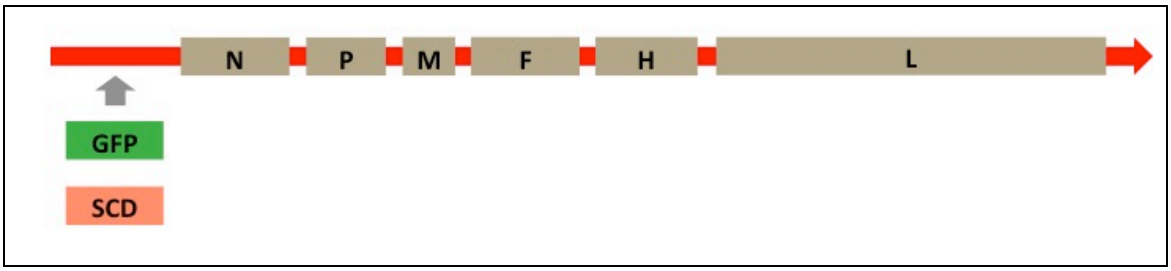

Figure 5: Schematic structure of the genetically engineered measles virus genome
Genetically engineering of measles vaccine virus in the field of virotherapy implicates new possibilities of enhanced therapeutic effects or monitoring of virus spread. Based on recombinant technologies, marker genes such as the green fluorescent protein (GFP) or therapeutic genes such as the super cytosine deaminase gene (SCD) can be inserted into the viral backbone.

The pathognomonic cytopathic effect (CPE) of measles infection depicts the formation of multinucleated syncytia after fusion of cells, also observable *in vitro* (Aref et al., 2016). Furthermore, syncytia formation was found to be dependent on CD46 expression, thereby leading to increased cell fusion in tumor cells, as they often overexpress CD46 (Anderson et al., 2004). Other cytopathic effects are altered cell shape as well as inclusion bodies (Nakai and Imagawa, 1969).

With only one serotype existent, a monovalent vaccine is sufficient to protect against measles disease, but still, eight different classes (A - H) as well as several genotypes are distinguished, taking the gene sequences coding for M and H into account (Duke and Mgone, 2003).

1.3.2. *Measles virus as an infectious pathogen - epidemiology and clinical appearance*

As a highly contagious illness, measles are a major health problem especially in developing countries, where vaccination is not available to everyone and where particularly children die as a consequence of severe measles infection. But also in industrialized nations with persisting vaccination gaps in the population, measles outbreaks are still on the agenda, listing 2.464 cases of measles in 2015 in Germany, with largest incidences in one-year-old and younger children (Robert-Koch-Institut, 2016). Measles infection is a droplet infection entering via respiratory tract and casually via conjunctivae, while dissemination takes place via reticuloendothelial system (Duke and Mgone, 2003). After an incubation time of 10 - 12 days, prodromal symptoms such as rhinitis, conjunctivitis, fever, cough or measles enanthema (the pathognomonic Koplik spots) and, a few days later, exanthema evolve. Pneumonia turned out to be the most common fatal complication, accounting for 56 - 86 % of measles-related deaths, also often due to bacterial or viral superinfection (Duke and Mgone, 2003; Herold, 2015). Acute postinfectious measles encephalitis (APME), measles inclusion body encephalitis (MIBE) and subacute sclerosing panencephalitis (SSPE) represent complications concerning the central nervous system in the context of measles infection, but are fortunately rather rare (Duke and Mgone, 2003).

Interestingly, on the one hand, measles infection is associated with an induced immunosuppression with lymphopenia, opening the floodgates to opportunistic infections, whereas on the other hand, the resulting anti-measles immune response leads to lifelong immunity (de Vries and de Swart, 2014).

1.3.3. *Measles vaccine virus as a virotherapeutic agent*

With the already mentioned advantageous characteristic of MeV being able to target CD46, which is often overexpressed in tumor cells, and with the acceptable low toxicity as an attenuated vaccine strain (Msaouel et al., 2012), MeV seems to be an outstanding candidate for the development of a virotherapeutic. Moreover, MeV is able to harbor transgenes of large size, still with proven genetic stability (Buijs et al., 2015).

Thus, measles OV already took part in numerous preclinical testing, resulting in successful virotherapy of various tumor entities such as melanoma (Donnelly et al.,

2013; Kaufmann et al., 2013), lymphoma (Grote et al., 2001; Heinzerling et al., 2005; Kunzi et al., 2006), myeloma (Peng et al., 2001; Liu et al., 2010), hepatocellular carcinoma and other tumors of the liver (Blechacz, 2006; Zimmermann et al., 2009), glioblastoma (Phuong et al., 2003), ovarian cancer (Peng et al., 2002b; Hasegawa et al., 2006) or pancreatic cancer (Penheiter et al., 2010), just to give some examples.

Nevertheless, the usage of oncolytic MeV, which mostly descends from the attenuated vaccine Edmonston strain, brings along several problems to deal with. First of all, the high rate of vaccination in our population results in the problem of immunological clearance of systemically applied measles virus - one of the main obstacles of implementation of MeV-based virotherapy into clinical practice (Russell and Peng, 2009). Yet, the anti-measles vaccination also displays a certain protection against unintended spread after application of MeV as virotherapeutic agent. Moreover, along with the clinical vaccination experience over the last decades, this virus can be referred to as fairly safe for usage in humans (Msaouel et al., 2009).

Facing the clinical introduction of MeV, the problem of appropriate model systems in animals emerged. As mice do express neither CD46 nor SLAM (Msaouel et al., 2009), transgenic CD46 expressing mice had to be developed for safety evaluation (Mrkic et al., 1998; Kemper et al., 2001). By retargeting MeV to CD20, a CD20 expressing murine B16 melanoma model was successfully introduced, implying the advantage of an immunocompetent murine model, which was an inevitable step for testing MeV in the background of cancer immunotherapy (Engeland CE, 2014). Furthermore, preclinical toxicity testing was performed in non-human primates such as rhesus macaques (Msaouel et al., 2009).

With the replication-trackable virotherapeutics MeV-CEA and MeV-NIS (as described in 1.2.2), representatives of the genus *Morbillivirus* finally entered the stage of clinical phase I and II trials (for details, see 1.2.3).

1.4. Immunotherapy as an anti-cancer treatment approach

1.4.1. Principles of immunotherapy - how to activate the body's defence against cancer

Gene mutations and dysfunctional epigenetics are distinctive hallmarks of carcinogenesis, resulting in expression of new proteins, which are foreign to our immunological self. With those potential epitopes for activation of an anti-cancer immune response, a tumor has to develop several immune escape mechanisms to circumvent an attack by the host's immune system. 'Immunoediting' and 'immunosubversion' are two main strategies, implying selection of the least immunogenic tumor subclones and, on the other hand, following active prevention of immunological clearance by involving cellular and humoral manipulation of tumor microenvironment and tumor-distinct mechanisms, such as downregulation of MHC or expression of so-called immune checkpoint ligands (Zitvogel et al., 2006). The cellular components of cancer immune escape contain regulatory T-cells as well as myeloid-derived suppressor cells, while interleukin 6, interleukin 10, vascular endothelial growth factor or transforming growth factor β are part of the soluble elements in abrogating anti-tumor immune responses (Topalian et al., 2011).

In the last decades, cancer research turned its attention to the role of immune checkpoints, which represent costimulatory or inhibitory receptors expressed on several immune effector cells. Together with their corresponding ligands, they were found to be responsible for modulating immune responses.

For stimulation of naïve T-cells through a particular epitope, descending from a mutated cancer cell, two signals are necessary. First of all, the processed host-foreign antigen is presented via MHC class I to the T-cell receptor (TCR), which is done by DCs, acting as professional APCs. But without costimulatory signals, the T-cell would become anergic, hence not reactive (Esensten et al., 2016). The CD28 receptor on naïve $CD4^+$ and $CD8^+$ T-cells provides such a coregulatory, antigen-independent signal in case of stimulation by APCs, which express the ligands B7.1 (CD80) and B7.2 (CD86) (Chen and Flies, 2013; Zamarin D, 2015). Activation of CD28, member of immunoglobulin superfamily (IgSF), finally results in T-cell survival, proliferation and differentiation (Esensten et al., 2016). By contrast, inhibitory receptors, so-called immune checkpoint receptors such as cytotoxic T-lymphocyte-associated antigen-4 (CTLA-4, also referred

to as CD152), compete against CD28, inhibiting IL-2 release and T-cell activity and furthermore possessing higher affinity for both CD28 ligands (Leach et al., 1996; Waldmann, 2003).

Physiologically, the mechanism of APCs expressing those immune checkpoint ligands avoids autoimmune incidents and ensures immunological homeostasis, while cancer cells abrogate this mechanism for immune evasion. This is emphasized in the fact that *Ctla-4*-knockout mice suffer from severe systemic immune hyperactivation, not being able to keep T-cell response against self-antigens under control (Waterhouse et al., 1995).

In contrast to this, as already described as a mechanism of 'immunosubversion', tumor cells express immune checkpoint ligands to impede anti-tumor immune response (Zitvogel et al., 2006). These are the requirements for the grand entrance of therapeutic antibodies called immune checkpoint inhibitors (ICI), targeting receptors or ligands of immune checkpoint pathways to abrogate tumor immune escape or, in other words, create an anti-tumor immunity (Leach et al., 1996).

Whereas CTLA-4 represents an immune checkpoint pathway which modulates initial T-cell activation, some other immune checkpoint receptors such as programmed cell death 1 receptor (PD-1 or CD279) and its ligands PD-L1 (also known as B7-H1 or CD274) and PD-L2 (also known as B7-DC or CD273) play an outstanding role in the regulation of ongoing T-cell immune responses (Topalian et al., 2011; Bauzon M, 2014; Postow et al., 2015). In contrast to CTLA-4, PD-1 can also be found on non-T-lymphocytic cells such as NK cells, B-cells, activated monocytes or DCs (Keir et al., 2008). As main ligand of PD-1 on solid tumors (Bauzon M, 2014), PD-L1 is found to be overexpressed in many human carcinomas, whereas healthy tissues do not express PD-L1 (Dong H., 2002). Receptor / ligand interaction downregulates T-cell proliferation and cytokine production, and thus counteracts anti-tumor immune response. Moreover, IFN type I and IFN type II signaling both work as possible inductors of PD-L1 expression (Keir et al., 2008).

High degrees of PD-L1 expression in the tumor microenvironment, especially on tumor-infiltrating immune cells, proved to be favorable for developing responses on ICI therapy influencing PD-1 / PD-L1 pathway (Topalian et al., 2012; Taube et al., 2014). In a broader sense, a preexisting anti-tumor immune response such as tumor infiltration

with tumor-infiltrating lymphocytes (TILs) is in favor of ICI therapy success, as in this case, immune checkpoint blockade is able to counteract ensuing processes of tumor immune escape (Herbst et al., 2014; Tumeh et al., 2014). It thus seems to be the challenge to combine immunotherapeutics in a way that induces and improves anti-tumor immune responses, even in poorly immunogenic cancer entities.

1.4.2. Immune checkpoint inhibitors entering the stage of clinical trials as anti-cancer drugs

With the anti-CD20 antibody *rituximab,* the first monoclonal antibody (mAb) was approved as anti-cancer drug in the 1990s, followed by numerous other mAbs against specific tumor-related antigens (Waldmann, 2003). Thus, the era of passive immunotherapy was initiated with a focus on targeted tumor therapy.

Along with immune checkpoint blockade and anti-tumor-targeted mAbs, cancer vaccines and adoptive cell transfer also belong to the today's spectrum of immuno-therapy. But until the first ICI, the CTLA-4-targeted antibody *ipilimumab* (*Yervoy*®, Bristol-Myers Squibb), was FDA-approved for grade 3 and 4 melanoma in 2011, active immunotherapy was quite underestimated in clinical practice.

Pembrolizumab (*Keytruda*®, MSD) was the first immune checkpoint targeted against PD-1 to be approved by FDA in 2014, and several others such as *nivolumab* (*Opdivo*®, Bristol-Myers Squibb, 2014) against PD-1 or *atezolizumab* (*Tecentriq*®, Roche, 2016) against PD-L1 followed, partly in fast-track approval procedure (Martin-Liberal et al., 2017).

MDX-1106, later *nivolumab*, which is now approved for unresectable or metastatic melanoma (2014), non-small cell lung cancer, renal cell carcinoma (both 2015), Hodgkin lymphoma and squamous-cell carcinoma of the head and neck (both 2016), was one of the first anti-PD-1 antibodies to enter phase I clinical trials (Martin-Liberal et al., 2017). Primarily safety and toxicity issues had to be examined: In this regard, good tolerability without any DLTs after a single dose could be proven (Brahmer et al., 2010). For anti-tumor efficacy, this first trial showed several tumor regressions, along with one complete response (CR) in a CRC patient and two partial responses (PR) in melanoma and renal cell cancer, thus stating a therapeutic chance even for carcinomas considered to be rather non-immunogenic such as CRC (Brahmer et al., 2010).

Clinical trials with *nivolumab* continued up to phase III, for example in patients suffering from advanced melanoma as a second-line therapy after pretreatment with *ipilimumab* and, if BRAF mutation diagnosed, BRAF inhibitors, resulting in an improvement of objective responses from 10.6 % in the group receiving chemotherapy of investigator's choice to 31.7 % in *nivolumab* group (Weber et al., 2015).
With *atezolizumab*, FDA-approved since 2016 for second-line treatment of urothelial cancer after platinum-based chemotherapy (Markham, 2016), a representative of ICIs targeting PD-L1 was tested in several clinical trials, for example against cancer of the lung (Fehrenbacher et al., 2016) or against metastatic renal cell carcinoma (McDermott et al., 2016). In a phase II clinical trial of *atezolizumab* against urothelial carcinoma (NCT02108652), Rosenberg et al. described an ORR of 26 % in patients with ≥ 5 % of immune cells in the tumor microenvironment expressing PD-L1 in comparison to an ORR of 15 % in the whole study group irrespective of PD-L1 expression. As a consequence of those results, PD-L1 expression was given an important role in prediction of response to immune checkpoint blockade in urothelial carcinoma patients (Rosenberg et al., 2016). Moreover, it is discussed to supplement examination of PD-L1 expression as sole biomarker with the investigation of preexisting T-cells specific for tumorous antigens to make predictions about patient-specific response to inhibition of PD-1 / PD-L1 signaling (Shin and Ribas, 2015). To summarize the clinical revolution of ICI in cancer immunotherapy, ICI not only became part of the everyday business of oncologists, but also progressed to the stage of personalized medicine.

1.4.3. Immunotherapy and colorectal cancer - a way of treatment worthy to go?

The role of immunotherapy in the treatment of CRC is quite controversial, as two different entities have to be differentiated: microsatellite stable (MSS) tumors and, on the other hand, CRC with defects in genes coding for DNA mismatch repair, which leads to an enormous mutational load and the phenomenon of microsatellite instability (MSI) (Boland and Goel, 2010). As those mutations result in numerous proteins foreign to our immunological self, thereby potentially serving as epitopes for T-cell activation, the consideration has to be why such highly immunogenic tumors can still grow and metastasize. This is even underlined with the observation of active $CD8^+$ cytotoxic T-lymphocytes (CTL) and T helper cells type 1 (TH1 cells) infiltrating the tumor micro-

environment (Llosa et al., 2015). Apart from that, it is generally accepted that the degree of T-cell infiltration of CRC is of high prognostic as well as predictive relevance, emphasizing the outstanding role of interplay between tumor and immune system (Galon et al., 2006; Jager et al., 2016).

The fact that immune checkpoint receptors and ligands such as PD-1 and PD-L1 are upregulated to a great extent in MSI colorectal tumors does not only explain the mechanism of immune escape, but also depicts an interesting relation between genotype and tumor microenvironment and a possibility of therapeutical intervention with ICI (Llosa et al., 2015; Xiao and Freeman, 2015).

As a matter of fact, early phase trials with PD-1 blockade in patients with MSS CRC resulted in an absence of any immune-related objective responses (immune-related ORR of 0%), compared to 40% in the group of MSI patients. Moreover, the immune-related PFS at week 20 was significantly higher in the MSI group (11% MSS vs. 78% MSI) (Le et al., 2015).

To touch on a subject already raised in 1.1.2, the eminent role of microbiota in the immune cell / tumor cell interaction will have to be considered when discussing immunotherapy of CRC. To give only one example, it could be proven that some bacteria are able to impair NK cell-mediated anti-tumor immune responses, thus enabling tumor immune escape (Gur et al., 2015; Lasry et al., 2016). Even though this surely exceeds the topic of the dissertation thesis, such considerations with new possible therapeutic impacts should be followed, facing the growing awareness of the gastrointestinal microbiome as one of the main players in carcinogenesis.

To put it into a nutshell, immunotherapy in CRC, especially with MSI status, depicts a treatment regimen worthy of being taken into account with a focus on modulation of the immunosuppressive tumor microenvironment.

1.5. Combination of virus and immune checkpoint inhibitors in cancer therapy

The rationale for combining virotherapy with ICI results from the experience with partly improvable therapeutical success with the respective monotherapies in different tumor entities. Synergistic effects are hoped for, since virotherapy is able to induce an active anti-tumor immune response inclusive of an ICI-favorable tumor micro-environment, while immune checkpoint blockade showed to strengthen preexisting

immune responses by abrogating immune escape mechanisms, even creating immunological memory (Vile, 2014; Rajani and Vile, 2015).

As viral-induced oncolysis leads to release of multiple foreign tumor antigens, thus establishing a prerequisite for activation of DCs and, following, cross-presentation of TAAs to T-cells in the lymph nodes, even poorly immunogenic tumors become a target of highly effective anti-cancer immune mechanisms (see 1.2.1). Furthermore, the presence of an OV itself with associated immunogenic viral antigens could serve as immunostimulans. But still, with the immunosuppressive mechanisms exploited by the tumor, including immune checkpoint ligand production, an immune response induction by virotherapy alone will probably not lead to long-time regression.

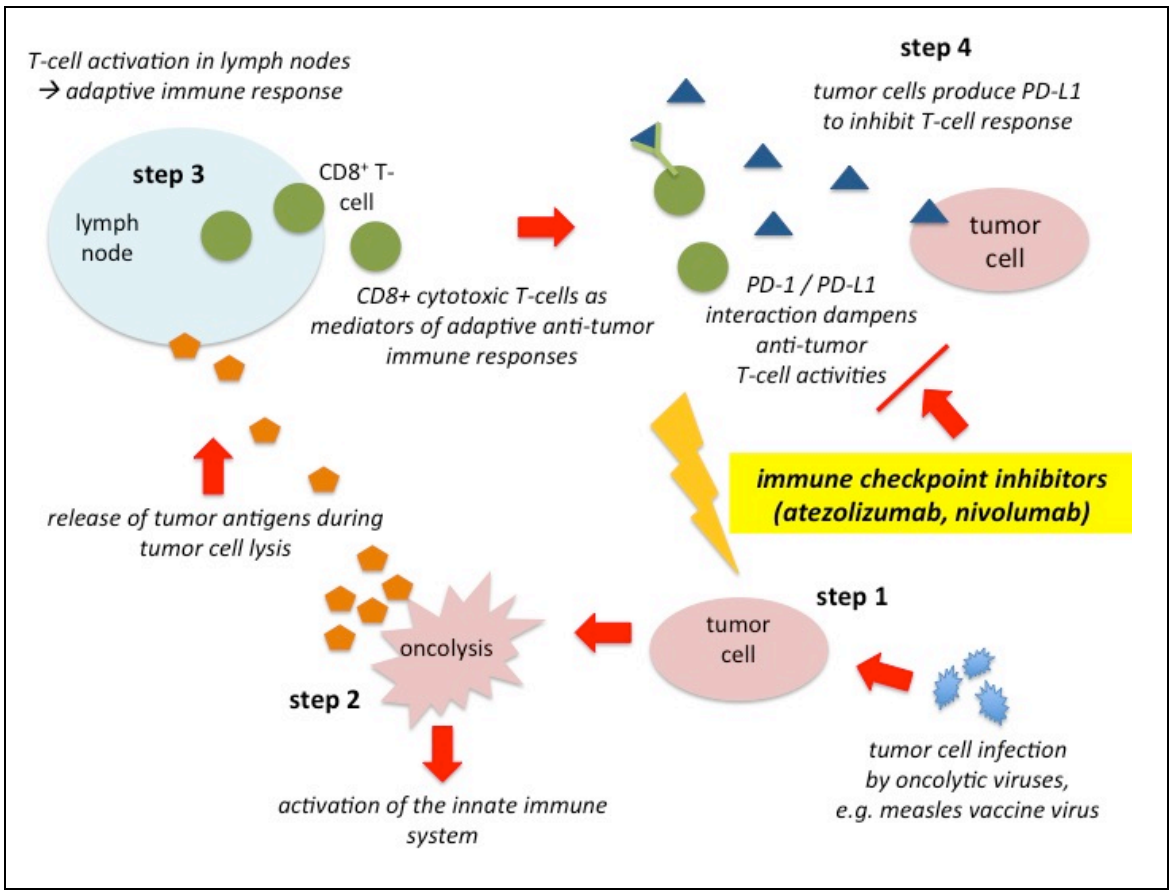

Figure 6: Principle of combining oncolytic virus (MeV) with immune checkpoint blockade (*atezolizumab, nivolumab*)

Tumor-specific viral infection, followed by replication and production of virions, results in highly immunogenic tumor cell lysis with release of antigens, which are foreign to the immunological self. These TAAs derive from genetic mutations or from epigenetic alterations, and depict potent epitopes for T-cell activation after presentation by DCs in lymph nodes. $CD8^+$ CTLs, to name only one of the main actors in anti-tumor immune response, are impaired in their activity by PD-1 / PD-L1 checkpoint pathway, which is exploited by tumor cells for immune escape. Here, ICI such as atezolizumab or nivolumab interfere to strengthen and prolong OV-induced anti-tumor immune response. Figure modified after (Vile, 2014).

Gao and colleagues achieved to cure four out of five mice with peritoneal mammary tumor implants, using a combination therapy of recombinant replicating vesicular stomatitis virus (rrVSV), which was retargeted to infect Her2/neu positive cells, together with anti-CTLA4 mAb, whereas virotherapy alone could not induce any cure, but only prolong survival (Gao Y, 2009). Moreover, rechallenging trials without any further therapy in mice, which had received combination therapy before, resulted in tumor resistance: Those findings underlined the dynamic, active character of such a treatment regimen, obtaining immunological memory function.

Woller et al. showed that systemic resistance against ICI therapy could be overcome by localized adenovirus-induced oncolysis in CMT64 lung adenocarcinomas, as an efficient elimination of disseminated lung tumors could be induced in mice (Woller N, 2015). Interestingly, this $CD8^+$ T-cell-dependent process of immune response went along with a broader spectrum of presented MHC class I T-cell epitopes. Moreover, it was proven that viral oncolysis could induce PD-L1 expression on APCs infiltrating cancer nodes of liver and lung, thus creating an ICI-favorable microenvironment.

One possibility to investigate immune effects of a combination therapy *in vitro* was presented by Rajani and colleagues in a B16 melanoma cell culture model under NK cell coculture (Rajani K, 2016): The ICI-augmented NK cell activation by reovirus, resulting in improved tumor cell killing, confirmed the results of cure in a B16 model in immunocompetent C57Bl/6 mice after combination therapy of *i.t.* reovirus with *i.v.* anti-PD-1 mAb.

With the realization of transgenic manipulation of virotherapeutics, several achievements were made in the subject of tumor-specific delivering of ICI, expressed by the virus itself with remaining oncolytic potential (Dias JD, 2012; Engeland CE, 2014). Those results depict a possibility of not only increased efficacy, but also of reduction of unwanted immune-related adverse events in case of systemic ICI application.

Investigating relevant effector cells mediating such a immunovirotherapy-induced anti-tumor immune response, $CD8^+$ T-cells as well as NK cells seem to be rudimental, but not $CD4^+$ T-cell subsets (Juan J. Rojas, 2015; Rajani K, 2016).

But still, combination therapy implies difficulties in scheduling, as ICI-increased antiviral immune responses could be detrimental to viral replication when applied simultaneously. Rojas et al. therefore could prove the benefit of delayed ICI administration with regard to tumor regress and to survival in mice with renal adenocarcinoma, enabling an early phase of unhindered viral replication (Juan J. Rojas, 2015).

With those promising results from *in vitro* and animal model research, the first early-phase clinical trials combining virotherapy and immune checkpoint blockade are already ongoing (as described in 1.2.3), and results will soon show clinical feasibility and response rates in the subset of the complex human immune system.

In regard to clinical testing of immunovirotherapy in patients, one of the latest findings was made by Ribas and colleagues who applied combined *Talimogene laherparepvec* and *pembrolizumab* treatment in advanced melanoma (NCT02263508; for details, see 1.2.3) (Ribas et al., 2017). Interestingly, taking tumor samples into account obtained prior to the first application of OV, response rates seemed to correlate neither with initial $CD8^+$ T-cell-infiltration, nor with also frequently discussed predictive parameters such as PD-L1 or IFN-γ expression (Herbst et al., 2014; Tumeh et al., 2014). Especially in combination therapy responders, pretreatment with the herpes virotherapeutic itself achieved a shift towards a highly ICI-favorable tumor microenvironment, including not only immigration of $CD8^+$ T-cells and enhanced expression of both PD-L1 and IFN- γ at the tumor site, but also a rise in $CD4^+$ and $CD8^+$ T-cells in blood samples. OV was therefore the prerequisite for implementation of a systemic anti-tumor response, strengthened by following ICI and OV applications - another *in vivo* proof of immuno-virotherapy overcoming poor tumor immunogenicity (Ribas et al., 2017).

1.6. Aim of this dissertation

This dissertation aimed to investigate a combination therapy of measles vaccine virus (MeV-GFP) together with immune checkpoint blockade, targeted against PD-1 (*nivolumab*) or PD-L1 (*atezolizumab*). We focused on examination of (i) whether measles OV could induce ICI-favorable effects in the tumor microenvironment in regard to PD-L1 expression in CRC cell lines, (ii) synergistic therapeutical effects in the subset of CRC cell lines in coculture with NK cells or PBMC, namely an improved anti-tumor immune

response resulting in an increased tumor cell killing, and (iii) antiviral immune effects, considering the impact of ICI on efficient MeV-GFP replication and spread in colorectal tumor cells.

Those cell culture experiments depict a necessary prerequisite to translate a combination treatment regimen of oncolytic measles vaccine virus and ICI influencing the PD-1 / PD-L1 pathway into animal models and, finally, early phase clinical trials for patients with advanced colorectal cancer disease. Paying attention to both anti-tumor and antiviral immune effects of such a combination has its eligibility in planning a future time schedule for a conceivable therapeutic regimen, thus respecting a possible impairment of measles replication by ICI-induced immune responses.

2. Materials and methods

2.1. Cell culture of tumor cells

2.1.1. Materials and devices for cell culture

Table 1: Materials and devices for cell culture

Materials and devices for cell culture	
Dulbecco's modified Eagle's medium (DMEM) (+ L-glutamine + 4.5 g / l glucose)	SIGMA life science
Dulbecco's phosphate buffered saline (PBS) without Mg^{2+} and Ca^{2+}	SIGMA life science
Fetal calf serum (FCS)	PAA Laboratories GmbH
Opti-MEM®I + GlutaMAX™-I	Gibco by life technologies™
Dimethylsulfoxide (DMSO)	PanReac AppliChem
RPMI 1640 (+ L-Glutamine + 25 mM HEPES)	Gibco by life technologies™
Pen Strep (Penicillin Streptomycin)	Bio Whittaker, Lonza
Recombinant Human Interleukin-2 (IL-2)	ImmunoTools
Trypsin-EDTA solution 0.25 %	SIGMA life science
Trypan Blue solution 0.4 %	SIGMA life science
Neubauer improved haemocytometer	Karl Hecht Assistent GmbH
Culture flask, 750 ml, 175 cm^2 growth area	Greiner Bio-One GmbH
Culture flask, 300 ml, 75 cm^2 growth area	TPP
15 ml Cellstar tubes®	Greiner Bio-One GmbH
50 ml polypropylene conical tube	Corning
Cell strainer	Greiner Bio-One GmbH
1.5 ml safe-lock tube	eppendorf
2.0 ml safe-lock tube	eppendorf
C-Chip (disposable haemocytometer)	Kisker Biotech GmbH & Co. KG
Cryogenic vial	Corning

Incubator for virus-free cell culture (HERA cell)	Heraeus
Incubator for virus-infected cell culture	Memmert
Megafuge 2.0 R centrifuge	Heraeus SEPATECH
Light microscope Olympus CK40	Olympus

DMEM, PBS, Trypsin-EDTA and FCS were stored at 4 °C after opening, so DMEM + 10 % FCS as well as PBS had to be incubated in the water bath at 37 °C before usage, while Trypsin-EDTA was warmed up at room temperature (RT).
FCS and Trypsin-EDTA were stored frozen at -20 °C before usage. FCS had to be heat-inactivated for 30 minutes at a temperature of 56 °C to inactivate proteins of the complement system.

2.1.2. Used cell lines

The used tumor cell lines derive from the National Cancer Institute NCI-60 tumor cell panel with the similarity of being of human colorectal carcinoma origin, but differing significantly in their characteristics of oncolysis resistance towards measles vaccine virus MeV-SCD as illustrated in the table below. African green monkey Vero cells were used for virus titration.

Table 2: Used cell lines with their characteristics (NCI-Webpage, Accessed August 17, 2016)
The different NCI-60 human colorectal carcinoma cell lines differed substantially in their oncolysis resistance behavior after infection with MeV-SCD.

Cell line	Species	Origin	Doubling time in hours	Oncolysis resistance against MeV-SCD
SW-620	human	colorectal carcinoma	20.4	intermediate resistant
HT29	human	colorectal carcinoma	19.5	susceptible
HCT-15	human	colorectal carcinoma	20.6	high resistant

Vero	African green monkey	kidney epithelial cells	24 - 96 (Nahapetian et al., 1986)	-

2.1.3. Cell culture

Cells were cultured permanently in plastic culture flasks of 750 ml and 300 ml volume, being stored humidified, 37°C-tempered and with 5 % CO_2 in separated incubators for virus-infected cells as well as uninfected cells. Moreover, cultured cells were regularly tested for mycoplasma contamination.

For excellent growth in monolayers, cells were passaged every three or four days. Cultivation took place in Dulbecco's Modified Eagle's Medium, supplemented with 10 % fetal calf serum (FCS, also fetal bovine serum / FBS), which had been heat-inactivated at 56 °C for 30 minutes before use.

For splitting, cells were washed with phosphate buffered saline (PBS) and then detached with Trypsin-EDTA. Supporting the effect of the trypsin, culture flasks were incubated for about five minutes at 37°C. The EDTA additionally enhanced the trypsinization, creating an acidic environment. Detachment of cells from the flasks' bottom could be controlled by light microscopy. The trypsin was inhibited by the FCS in the medium, which was used to remove the cells from the flasks' ground. The cell suspension was collected in falcon tubes, followed by optional centrifugation at RT, 1000 revolutions per minute (rpm), for 4 minutes. After centrifugation, the cell pellet was resuspended in about 5 ml of fresh medium, depending on the pellet's size. At last, the cell suspension was returned into a culture flask in ratios of 1:2 to 1:20, depending on the growth kinetics of the respective cell line, and filled up with fresh medium. If the cells empirically tended to agglutination, the cell suspension was passed through a cell strainer.

Table 3: Different culture vessels and corresponding amounts of medium, trypsin or PBS

Culture vessel size	DMEM + 10 % FCS	Trypsin-EDTA	PBS for washing
Large culture flask (175 cm^2)	30 ml	3 ml	10 ml
Medium culture	15 ml	1,5 ml	10 ml

flask (75 cm^2)			
6 well plate	2 ml	0.5 ml	2 ml
24 well plate	0.5 ml	0.2 ml	0.5 ml

2.1.4. Counting of cells via Neubauer haemocytometer

To count the number of cells in a solution, a Neubauer improved haemocytometer was used. Therefore, cells were trypsinized and centrifuged as described above. The cell pellet was resuspended in DMEM + 10 % FCS. 10 µl of cell suspension was added to 90 µl of Trypan Blue solution 0.4 % in a 1.5 ml Eppendorf cup and after vortexing, the haemocytometer was charged with 10 µl of the stained cell suspension.

Cells were counted in four large quadrants, using light microscopy, and the amount of cells per milliliter medium was calculated by the following formula. Vital cells could be distinguished from dead cells, as they were bright, whereas dead cells were stained dark blue by trypan blue. For counting, cells which were placed either on the left or on the lower, but not on the right or the upper margin of the quadrant were taken into account.

$$Concentration\ of\ cells\ per\ ml\ suspension = \frac{Counted\ cells}{4} \times 10 \times 10^4$$

Cell count was divided by four and multiplied by 10^4 to calculate the amount of cells per milliliter, afterwards multiplied by 10 as the original cell suspension was diluted with trypan staining at 1 : 10.

The amount of counted cells in four quadrants should not exceed 300 or go below 50 to make the result reliable, so dilution could be necessary. If cells were too agglutinated, usage of a cell strainer was required.

For counting of virus-infected cells, disposable haemocytometer chips were used.

2.1.5. Cryopreservation of cells

Tumor cell lines were cryopreserved at -150 °C. Therefore, the cells were washed, trypsinized and centrifuged as described. The cell pellet was resuspended in a special medium for cryopreservation, consisting of FCS + 10 % DMSO (dimethylsulfoxide).

1 ml of the suspension was used for one aliquot, being pipetted into a labeled cryotube. For optimal results, the tumor cells were frozen overnight in an isopropanol-filled freezing box at -80 °C, before they could be stored at -150 °C.

2.1.6. Thawing of cells for recultivation

Cells were thawed by carefully warming the cryotubes in the water bath at 37°C. Afterwards, cells were suspended in 8 ml of preheated DMEM + 10 % FCS in a 15 ml falcon tube and centrifuged for 4 minutes at 1000 rpm and 20 °C.

The supernatant was discarded before the cell pellet could be resuspended in 5 ml of fresh medium and the suspension was added with 10 ml of medium in a middle-sized culture flask, which was stored in the incubator. Cell growth was controlled the next day by light microscopy. The medium was exchanged if necessary.

2.1.7. Seeding of cells

Tumor cells were seeded in different culture plates at diverging cell amounts, dependent on the cell line's growth characteristics.

After being washed with PBS, trypsinized and centrifuged, the cells were counted as described in 2.1.4. Furthermore, the needed amount of cell suspension for the distinct number of wells was calculated with the formula below and replenished with DMEM + 10 % FCS.

$$Volume\ of\ cell\ suspension\ in\ ml = \frac{Required\ amount\ of\ cells\ per\ well}{Counted\ concentration\ of\ \frac{cells}{ml}}\ x\ Number\ of\ required\ wells$$

The cell lines which tended to agglutinate were passed through a cell strainer before, a multi-stepper was used and the cell suspension was thoroughly resuspended with medium to guarantee uniformity of the cell amount in the different wells. Conformity could be proved via light microscopy the day after.

The table below shows the different culture plate sizes with the needed amount of tumor cells.

Table 4: Different culture plates and fitting numbers of cells being seeded per well

Cell line		HT29	SW-620	HCT-15
Required number of cells per well	6-well plate	3×10^5	4×10^5	3×10^5
	24-well plate	3×10^4	4×10^4	2.5×10^4
	96-well plate	5×10^3	5×10^3	2.5×10^3

2.1.8. Treatment of cells with immune checkpoint inhibitors

Immune checkpoint inhibitors (ICI) targeted against PD-1, such as *nivolumab* (Nivolumab BMS®, Bristol-Myers Squibb) or *pembrolizumab* (Keytruda®, MSD), and against PD-L1, here *atezolizumab* (Tecentriq®, Roche), were a kind gift of PD Dr. Marcus Schittenhelm, University Hospital Tübingen, and stored at 4 °C.

The concentrations of immune checkpoint blockade antibodies used for the respective experiments are listed below.

Table 5: Concentrations of immune checkpoint inhibitors used in different experiments

Experiments	**Concentration of ICI**
xCELLigence	5 µg / ml
Viral growth curves	10 µg / ml
Determination of viral titers	5 µg / ml

2.2. Cell culture of virus-infected cells

2.2.1. Used virus strains

For infection with oncolytic measles vaccine virus, two different virus strains were used: MeV-GFP (GFP = green fluorescent protein) and MeV-SCD (SCD = super-cytosine deaminase, a suicide gene functioning as prodrug-converting enzyme of 5-fluorocytosine). Virus was stored at -80 °C in aliquots of 100 µl, 200 µl and 500 µl.

2.2.2. Infection of cells

For virus infection, tumor cells were seeded the day before in DMEM +10 % FCS in culture plates as described in 2.1.7.

Uniformity of cell seeding was verified the next day by light microscopy, before cells were infected with virus at different multiplicities of infection (MOI). Multiplicity of infection describes the ratio of virus particles per target cell, meaning that infection at a MOI of 1 implies that one plaque forming unit (PFU) of virus is used per tumor cell. The formula below was used to calculate the needed amount of virus suspension in regard to MOI, count of cells per well, virus titer and number of wells.

$$Required\ amount\ of\ virus\ suspension$$

$$= MOI \times \frac{count\ of\ cells\ per\ well}{virus\ titer} \times number\ of\ wells$$

For infection, virus suspensions were prepared in Opti-MEM®I + GlutaMAX™-I (in the following abbreviated as Opti-MEM). Therefore, aliquots with the respective virus were thawed at RT, carefully vortexed and pipetted into calculated volumes of Opti-MEM, optionally using dilution series to prepare all needed MOIs.

Cells were washed once with preheated PBS and infected with the respective virus solution. At 2.5 - 3 hpi, the inoculum was removed and DMEM + 10 % FCS was added. Phase contrast and, for MeV-GFP, fluorescence microscopy could verify success of infection as described in 2.2.3.

As a matter of laboratory safety, UV-light irradiation of cell culture materials took place after working with virus under the laminar flow hood for complete virus inactivation.

2.2.3. Control of tumor cell infection with MeV-GFP using fluorescence microscopy

Successful infection of tumor cells with MeV-GFP could be monitored via fluorescence microscopy, using the OLYMPUS IX50 with connected upstream OLYMPUS U-RFL-T. Phase contrast and fluorescence microscopy pictures could be taken with the F-View Soft Imaging System and anaLYSIS software.

The MeV-GFP-infected CRC tumor cells could be detected as green lightening cell syncytia, as GFP (green fluorescent protein) implicates the intrinsic ability to fluoresce when stimulated with blue light. Therefore, fluorescence microscopy was used to determine viral titers (as described in 2.8.3).

2.3. Cell culture of NK cells and peripheral blood mononuclear cells

Both NK cells and peripheral blood mononuclear cells (PBMC) were isolated from various healthy donors and a kind gift of AG Salih, either fresh in culture or as frozen aliquots. We therefore thank Stefanie Maurer, AG Salih, Internal Medicine II, University Hospital Tübingen, for providing the immune cells.

2.3.1. Cultivation of immune cells

NK cells were cultivated in 24 well plates with 1 x 10^5 irradiated feeder cells in 1 ml of NK cell medium (RPMI-1640 with 10 % FCS, 1 % Pen Strep (Penicillin Streptomycin) and 2 mM L-glutamine). To protect medium from evaporation, only eight wells in the middle of the plate were used for NK cell cultivation, whereas the other wells were filled with 1 ml PBS.

For medium exchange, 200 µl of medium were carefully exchanged by 200 µl of fresh medium every two days.

NK cells were stimulated by addition of interleukin 2 (IL-2) to the medium at 25 U / ml. For cocultivation with tumor cells, stimulation could be omitted on the last day of medium exchange to decrease NK cell-induced tumor cell killing activity.

PBMC were also cultured in fluid culture, using plastic culture flasks of different sizes (see 2.1.1) and the same medium used for NK cells. Storage of immune cells took place in a humidified and 37 °C-tempered incubator, containing 5 % of CO_2.

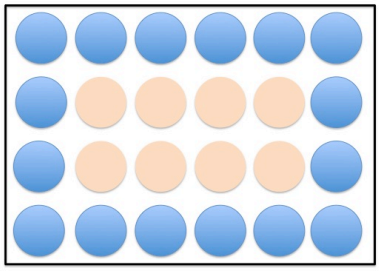

Figure 7: Schematic illustration of NK cell cultivation
NK cell cultivation took place in 24-well plates containing 1 ml of PBS in edging wells (blue colored wells) for evaporation protection and 1 ml of NK cell suspension on 1 x 10^5 feeder cells in the middle wells (fawn colored wells).

2.3.2. Thawing of NK cells

Frozen NK cells were stored at -150 °C until the day before cocultivation. For thawing, NK cells were added to fresh NK cell medium as described before (2.3.1) and were centrifuged for 8 minutes at 800 rpm and RT. Afterwards, cells were resuspended in medium, together with IL-2 for stimulation (25 U / ml), and counted. 2 x 10^6 NK cells per well were cultured overnight in 1 ml of medium, considering the PBS evaporation protection mentioned in 2.3.1.

2.3.3. Cocultivation of tumor cells with immune cells

For xCELLigence analysis and virus titrations, tumor cell lines HCT-15 and HT29 were cocultured with NK cells (or PBMC, respectively) at different effector : target ratios (E : T ratios). An E : T ratio of 10 : 1 means that for each tumor cell, 10 immune cells were used for coincubation.

Coincubation took place in 6-well or 96-well plates at different E : T ratios, after CRC tumor cells had been seeded and treated in the respective regimen (for coincubation during xCELLigence analysis, see 2.7.4, and for coincubation for viral titrations, see 2.9). Tumor cells were counted again on the day of coincubation, since growth of the cells had to be considered for exact composition of NK cell suspensions, or particular growth factors were calculated in test runs.

For the next step, NK cells (or PBMC) were pooled and wells were resuspended once with RPMI in the case of cultivation in well plates. Afterwards, cells were counted via Neubauer improved haemocytometer as described in 2.1.4 after centrifugation at 1200 rpm and RT for 4 minutes, using 10 µl of cell suspension and 90 µl of trypan blue.

To achieve the required immune cell amount for different E : T ratios in the exact volume of immune cell medium, cells were centrifuged again and the cell pellet was resuspended in the calculated amount of RPMI. Serial dilution was used to produce the different E : T ratios and coculture was realized by pipetting the needed amount of immune cell suspension into each well of the seeded tumor cell plates with incubation times from 48 to 58 hours at 37 °C.

2.4. Quantification of PD-L1 expression on tumor cell lines via FACS analysis

2.4.1. Materials and devices for FACS analysis

Table 6: Materials and devices for FACS analysis

Materials and devices for FACS analysis	
Dulbecco's phosphate buffered saline (PBS) without Mg^{2+} and Ca^{2+}	SIGMA life science
Fetal calf serum (FCS)	PAA Laboratories GmbH
Accutase® solution	SIGMA life science
4 % paraformaldehyde (PFA)	Otto Fischar GmbH
Gamunex 10% 100 mg / ml (FC block)	Talecris Biotherapeutics GmbH
5 ml polypropylene round-bottom tube	Corning
BD CellQuest™ analysis software	BD Biosciences
BD FACSCalibur™	BD Biosciences
Attune™ NxT Acoustic Focusing Cytometer	ThermoFisher Scientific
Megafuge 2.0 R centrifuge	Heraeus SEPATECH

2.4.2. Staining antibodies for FACS analysis with their corresponding isotypes

Table 7: Staining antibodies for FACS analysis with their corresponding isotypes

Staining antibody		**Isotype**	
FITC anti-human CD3	BioLegend	FITC Mouse IgG1, κ Isotype Ctrl	BioLegend
FITC anti-human CD56 (NCAM)	BioLegend	FITC Mouse IgG1, κ Isotype Ctrl	BioLegend
PE anti-human CD46	BioLegend	PE Mouse IgG1, κ Isotype Ctrl	BioLegend
PE anti-human CD274 (B7-H1, PD-L1)	BioLegend	PE Mouse IgG2b, κ Isotype Ctrl	BioLegend
PE anti-human CD279 (PD-1)	BioLegend	PE Mouse IgG1, κ Isotype Ctrl	BioLegend

2.4.3. Staining for FACS analysis

For the quantitative analysis of PD-L1 expression on the CRC cells, the immunohistochemical method of fluorescence-activated cell sorting (FACS) was used.

Therefore, cells were seeded in 6-well plates and infected with MeV-GFP or MeV-SCD (see 2.1.7 and 2.2.2 for seeding and infection of cells). For each staining approach, 5 x 10^5 tumor cells were needed. Cells were washed with PBS and detached with accutase, which was used instead of trypsin in case of staining of surface markers. After 8 ml of FACS buffer (PBS + 10 % FCS) were added to the solved cells, the suspension was centrifuged for 4 minutes at 1000 rpm and RT. 5 x 10^5 tumor cells were diluted with 3 ml PBS in FACS tubes and centrifuged again for 5 minutes at 1000 rpm and 4 °C. Afterwards, the supernatant was discarded and the pellet was resuspended in 50 µl of FACS buffer. 10 µl of Fc-block Gamunex were added to block unspecific binding sites. After 5 min of incubation on ice, PE-anti-human CD274 (PD-L1) antibody was added, and mouse IgG2b κ was used as isotype control. One sample remained unstained each. Incubation was performed for 30 minutes on ice after carefully vortexing each sample. Then 3 ml PBS were added and cells were again centrifuged for 5 minutes at 1000 rpm and 4 °C. The cell pellet was finally resuspended in 200 - 500 µl FACS buffer. Cells were fixed with paraformaldehyde (PFA, final concentration 1.3 %) so that they could be stored in the refrigerator until analysis.

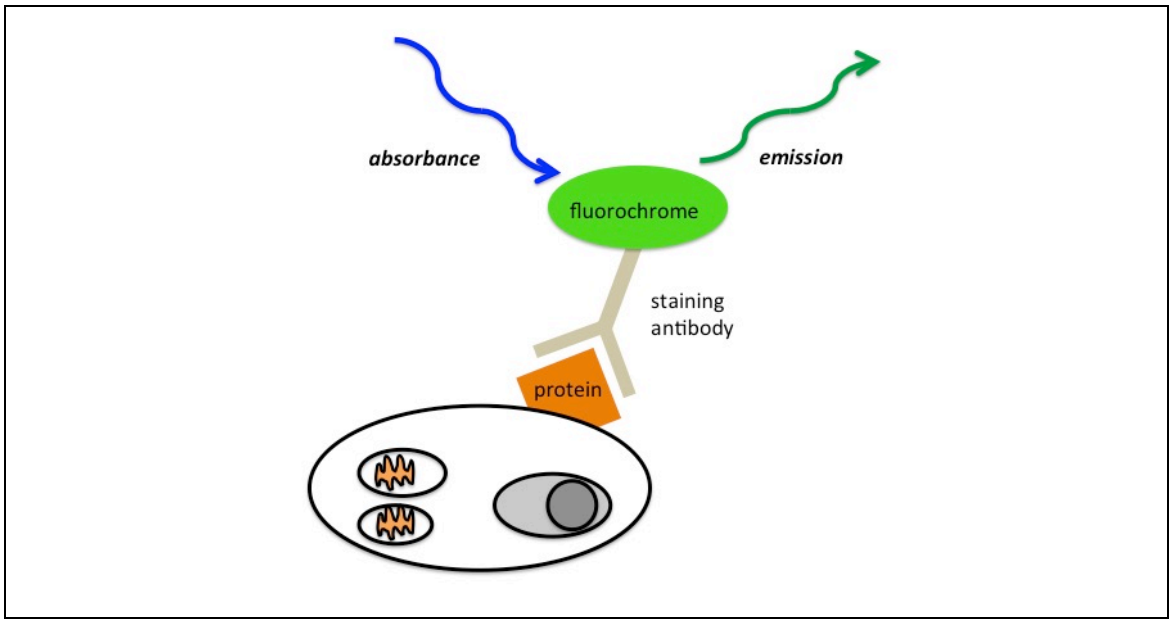

Figure 8: Principle of immunhistochemical staining for flow cytometry
Flow cytometry allows qualitative and quantitative analysis of expression of particular proteins, for example the immune checkpoint ligand PD-L1 expression on PD-L1 positive tumor cells. As

many proteins such as PD-L1 are not able to fluoresce intrinsically, a specific antibody with conjugated fluorochrome, for example phycoerythrin (PE) or fluorescein isothiocyanate (FITC), is used for labeling. With a laser stimulus of defined wavelength, the fluorochrome is able to emit light with a higher wavelength, which can be transformed by the photomultiplier into an electric signal.

2.4.4. Procedure of FACS analysis

For FACS measurement and analysis of PD-L1 expression in HT29 and HCT-15, the cytometer FACSCalibur and the program CellQuest were used. For FACS measurement and analysis of PD-L1 expression in SW-620, Attune™ NxT Acoustic Focusing Cytometer and the corresponding analysis software were used.

2.5. FACS analysis of PD-1 expression on NK cell populations from different healthy donors

For analysis of CD279 (PD-1) expression on NK cell subpopulations from either expanded NK cells or PBMC cultures of different healthy donors, flow cytometry was used. The amount of PD-1 expression was analyzed to investigate preconditions for immune checkpoint inhibitor interaction between PD-L1 expressing tumor cells and PD-1 expressing immune cells.

2.5.1. Staining for CD279 (PD-1) expression

CD279 expression on CD56 positive NK cell populations in both NK cells and PBMC cultures was analyzed. Therefore, cells were stained with FITC anti-human CD56 as well as PE anti-human CD279 and with the corresponding isotype controls FITC / PE Mouse IgG1, κ Isotype Ctrl (all BioLegend®). 5 x 10^5 immune cells were used per stain, which were added to 2 ml of FACS buffer (PBS + 10 % FCS) and centrifuged at 1200 rpm, RT, for 4 minutes. Afterwards, staining took place in 50 µl of FACS buffer together with 10 µl of Gamunex, which was incubated on ice for 5 min beforehand. Single stains as well as one unstained sample were prepared for fluorescence compensation.

Samples were incubated for 15 min on ice and then washed with 2 ml PBS. After centrifugation, the stained immune cells were resuspended in 300 µl of FACS buffer. The samples were stored in the refrigerator until time of analysis.

The amount of antibody used for the staining procedure can be extracted from the table below.

Table 8: CD279 (PD-1) FACS assay stainings and the respective amounts of antibody per stain
5 x 10^5 NK cells or PBMC were used for one stain.

Staining	Antibody	Amount of antibody	Amount of FACS buffer
PE and FITC isotype control (PBMC and NK cells)	mIgG1-PE mIgG1-FITC	5 µl 1 µl	50 µl buffer + 10 µl Gamunex
PE isotype control (PBMC and NK cells)	mIgG1-PE CD56-FITC	5 µl 1 µl	50 µl buffer + 10 µl Gamunex
CD279-PE staining (PBMC and NK cells)	CD279-PE CD56-FITC	5 µl 1 µl	50 µl buffer + 10 µl Gamunex
Single stain FITC (PBMC only)	CD3-FITC	1 µl	50 µl buffer + 10 µl Gamunex
Single stain PE (PBMC only)	CD46-PE	1 µl	50 µl buffer + 10 µl Gamunex
Unstained (PBMC only)	-	-	50 µl buffer + 10 µl Gamunex

2.5.2. Analysis of CD279 expression via flow cytometry

For CD279 expression analysis and presentation in dot plots with quadrant stats, FACSCalibur and the software CellQuest were used.

2.6. Investigation of anti-tumor effects via sulforhodamine B cytotoxicity assay

Sulforhodamine B (SRB) assays were used to investigate the degree of cytotoxicity after treatment of adherent human tumor cells with oncolytic drugs or measles vaccine virus. Thereby, the measured optical density correlated with the content of proteins and thus with the number of surviving cells (Skehan, 1990).

2.6.1. Materials and devices for SRB assay

Table 9: Materials and devices for SRB assay

Materials and devices for SRB assay	
sulforhodamine B	SIGMA® life science
trichloroacetic acid (TCA, 10 % w/v)	Carl Roth GmbH + Co. KG
acetic acid 1 %	Merck (100 %)
Tris base solution (TBS, 10 mM)	SIGMA® life science
Tecan GENios Microplate Elisa Reader	MTX lab systems

2.6.2. Procedure of SRB assay

Tumor cells were seeded in 24-well plates in each 0.5 ml DMEM +10% FCS, as described in 2.1.7, and treated in the respective manner in quadruplicates.

Fixation took place at different time points, washing each well with 0.5 - 1 ml PBS and fixing tumor cells in 250 µl of 10 % trichloroacetic acid (TCA) afterwards, both stored at 4 °C. TCA fixation was used to make intracellular proteins accessible for the SRB staining. Incubation time was at least 30 min before TCA could be tipped and collected for toxic waste. The plates were washed at least four times with tap water before they were dried at 40 °C overnight or longer.

Staining was conducted for ten minutes at room temperature with 250 µl of SRB staining solution (0.4 % w/v SRB in 1 % acetic acid), targeting the basic amino acids. The excess dye was washed out with 1 % acetic acid, before being dried one more time over night at 40 °C.

For measurement, the dye was resolved under basic conditions (pH 10.5) in about 1 ml of 10 mM Tris base, depending on the intensity of the pink staining. Finally, optical density (OD) was determined in 96-well plates at 550 nm, using Tecan GENios Elisa Reader. Therefore, 80 µl per well of the dissolved suspension were pipetted into the 96-well plate in duplicates. If the OD of a single sample was over 2.0, all samples had to be diluted with 10 mM Tris to ensure exact measurement.

The cell mass of treated cells was calculated in relation to MOCK-infected or untreated samples. Afterwards, for each experiment, means of the resulting quadruplicates were calculated. Data were illustrated using GraphPad Prism 4.0 software, showing the mean of three experiments with calculated standard error of the mean (SEM). If only one

representative experiment was shown, mean and standard deviation (SD) were calculated.

2.7. xCELLigence real-time cell proliferation assay

The xCELLigence Real-Time Cell Analyzer was used to examine the cell growth of adherent tumor cell lines continuously up to 130 hours. Moreover, the interactions of measles vaccine virus MeV-GFP, immune checkpoint inhibitors (*nivolumab, atezolizumab*) and immune cells (NK cells or PBMC) with the different CRC cell lines could be evaluated quantitatively throughout measurement.

Therefore, the xCELLigence system analyzes the change of the electric impedance, which is influenced by cells adhering to gold boards in 96-well electronic microtiter plates, so-called E-Plates, thus creating an isolating monolayer and decreasing impedance.

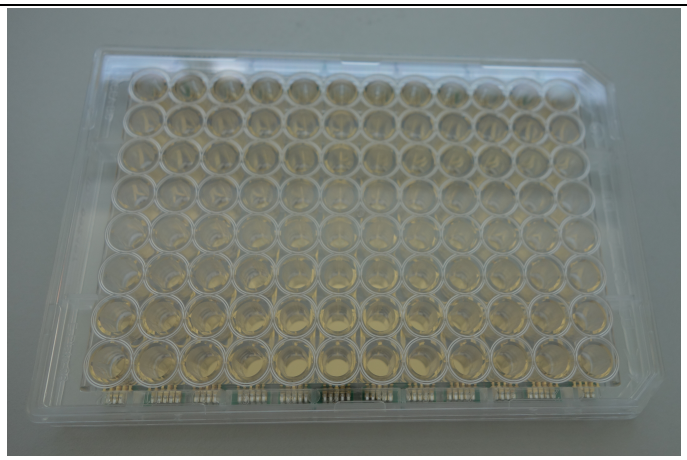

Figure 9: 96-well electronic microtiter plate

The system works with a calculated cell index (CI), representing the change of impedance in relation to the background impedance with medium only (DMEM + 10 % FCS). The cell index is not only affected by the count of cells, which adhere to the bottom of the plate, but also by their shape and viability.

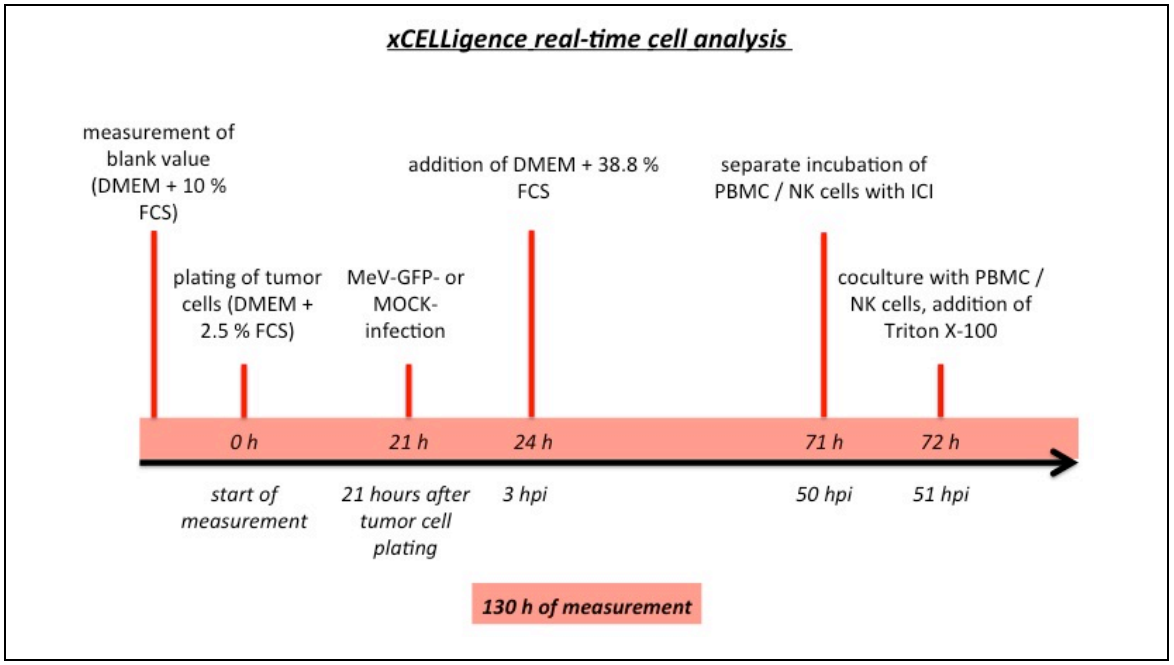

Figure 10: Procedure of xCELLigence analysis
The schema represents the procedure of xCELLigence analysis of CRC tumor cell lines (HT29, HCT-15) under the influence of MeV-GFP- or MOCK-infection 21 hours after plating of tumor cells. Furthermore, coculture with PBMC or NK cells and application of immune checkpoint blockade took place at 51 hpi. For viral infection, a total FCS concentration of 5 % per well was chosen. Incubation of immune cells with ICI took place in RPMI + 10 % FCS for one hour before cocultivation.

2.7.1. Materials and devices for xCELLigence analysis

Table 10: Materials and devices for xCELLigence analysis.

Materials and devices for xCELLigence analysis	
Triton X-100	Roth
atezolizumab	Genentech/Roche
nivolumab	Bristol-Myers Squibb
E-Plate 96	AACEA Biosciences Inc.
xCELLigence Real-Time Cell Analyzer (RTCA)	Roche / AACEA Biosciences Inc.
Biosafe eco (incubator)	Integra Biosciences

2.7.2. Seeding tumor cells for xCELLigence analysis

The human CRC tumor cell lines HT29 and HCT-15 had to be seeded at a density where they remained in an exponential growth phase during the measurement period of

up to 130 hours. Suitable cell numbers were determined in pretest xCELLigence runs; cell counts used for each tumor cell line are listed in the table below. For seeding of tumor cells, see 2.1.7.

Table 11: Cell counts per well used for xCELLigence analysis of different CRC cell lines

Tumor cell line	Cell count per well
HT29	5×10^3
HCT-15	2.5×10^3

The samples were analyzed in triplicates per condition and for controls in sextuplicates. Allocation of the samples had to be planned considering the effects of drying-out in the wells at the E-plate margin. Those wells were best occupied with the Triton X-100 1 % control, which represented a standard value for maximal tumor cell killing.

An exemplary plan of allocation for an E-plate used for xCELLigence analysis is shown below.

PBS was filled into the spaces between the wells to prevent drying-out of the wells. Afterwards, 50 µl of DMEM + 10 % FCS were pipetted into each well for measurement of the background impedance value. Tumor cells were then added in 100 µl of DMEM + 2.5 % FCS, resulting in a total FCS content of 5 % for viral infection the day after.

	MOCK						MeV-GFP MOI 2.5					
	1	2	3	4	5	6	7	8	9	10	11	12
A	Titon HT29 MOCK	Triton HT29 MOCK	20:1 PBMC Ate x	20:1 PBMC Niv x	Niv MOCK	Ate MOCK	Ate M 2.5	Niv M 2.5	20:1 PBMC Niv M2.5	20:1 PBMC Ate M2.5	Triton HT29 MOI2.5	Triton HT29 MOI2.5
B	Triton HT29 MOCK	20:1 PBMC MOCK	20:1 PBMC Ate x	20:1 PBMC Niv x	Niv MOCK	Ate MOCK	Ate M 2.5	Niv M 2.5	20:1 PBMC Niv M2.5	20:1 PBMC Ate M2.5	20:1 PBMC M 2.5	Triton HT29 MOI2.5
C	20:1 PBMC MOCK	20:1 PBMC MOCK	20:1 PBMC Ate x	20:1 PBMC Niv x	Niv MOCK	Ate MOCK	Ate M 2.5	Niv M 2.5	20:1 PBMC Niv M2.5	20:1 PBMC Ate M2.5	20:1 PBMC M 2.5	20:1 PBMC M 2.5
D	1:1 NK Niv x	1:1 NK Niv x	1:1 NK Niv x	1:1 NK A+N x	1:1 NK A+N x	1:1 NK A+N x	1:1 NK A+N M2.5	1:1 NK A+N M2.5	1:1 NK A+N M2.5	1:1 NK Niv M2.5	1:1 NK Niv M2.5	1:1 NK Niv M2.5
E	1:1 NK Ate x	1:1 NK Ate x	1:1 NK Ate x	1:1 NK MOCK	1:1 NK MOCK	1:1 NK MOCK	1:1 NK M2.5	1:1 NK M2.5	1:1 NK M2.5	1:1 NK Ate M2.5	1:1 NK Ate M2.5	1:1 NK Ate M2.5
F	2.5:1 NK MOCK	2.5:1 NK MOCK	2.5:1 NK Ate x	2.5:1 NK Niv x	Control MOCK	Control MOCK	Control MOI 2.5	Control MOI 2.5	2.5:1 NK Niv M2.5	2.5:1 NK Ate M2.5	2.5:1 NK M2.5	2.5:1 NK M2.5
G	Triton HT29 MOCK	2.5:1 NK MOCK	2.5:1 NK Ate x	2.5:1 NK Niv x	Control MOCK	Control MOCK	Control MOI 2.5	Control MOI 2.5	2.5:1 NK Niv M2.5	2.5:1 NK Ate M2.5	2.5:1 NK M2.5	Triton HT29 MOI2.5
H	Triton HT29 MOCK	Triton HT29 MOCK	2.5:1 NK Ate x	2.5:1 NK Niv x	Control MOCK	Control MOCK	Control MOI 2.5	Control MOI 2.5	2.5:1 NK Niv M2.5	2.5:1 NK Ate M2.5	Triton HT29 MOI2.5	Triton HT29 MOI2.5

Figure 8: Allocation of sample combinations for xCELLigence analysis of HT29 CRC cells
On the left hand side: MOCK-infected cells using 10 µl of Opti-MEM.

On the right hand side: MeV-GFP-infected cells (MOI 2.5).
Orange: Control. Blue: Triton X-100 1 % control. Red: Nivolumab or atezolizumab only, without immune cell coincubation.
Wells located at the margin of the E-plates were used for Triton control or for maximum one well per triplet to not falsify the results by drying-out.
Abbreviations: x: MOCK; M 2.5: MOI 2.5; Ate: atezolizumab; Niv: nivolumab; A+N: atezolizumab and nivolumab; 20:1 / 2.5:1 / 1:1 as effector : target ratios for immune cell coculture.

2.7.3. Infection of tumor cells for xCELLigence analysis with MeV-GFP at different MOIs

Viral infection with MeV-GFP at different MOIs, namely MOI 1 (in pretest runs) or MOI 2.5 for HT29 and MOI 10 for HCT-15, took place in 10 µl of Opti-MEM®. For HT29, a MOI of 2.5 was used in further experiments, considering well size and infection volume different from infection modus for FACS analysis or SRB assays.
For MOCK infection, the same amount of Opti-MEM® was pipetted into the corresponding wells using a new pipette tip for each step. Viral infection had to take place within 30 minutes to not interfere with the measurement schedule of the xCELLigence analyzer.
After the incubation time of three hours, 30 µl of DMEM + 38.3 % FCS were added to the E-plate to achieve a FCS concentration of 10 % in a total volume of 190 µl.

2.7.4. Coincubation with peripheral blood mononuclear cells or NK cells at different effector : target ratios and treatment with immune checkpoint inhibitors

Coincubation with PBMC or NK cells was performed in 20 µl of RPMI + 10 % FCS 51 hours after infection with MeV-GFP. Additionally, 20 µl of 10 % Triton X-100 were added to control triplets to achieve maximal tumor cell killing.
For the coculture, PBMC or NK cells were counted with the haemocytometer as described in 2.1.4. Effector : target (E : T) ratios from 20 : 1 to 0.5 : 1 were calculated considering a growth factor for the tumor cell lines which resulted from former FACS experiments with MeV-GFP- or MOCK-infected cells 48 hpi or, for HT29 infected at a MOI of 2.5, from separately plated cells which were counted 48 hpi. The required number of immune cells was pipetted into Eppendorf cups, centrifuged, and resuspended in the needed amount of RPMI + 10 % FCS.

For additional treatment with ICI, the immune cells were incubated with *atezolizumab*, *nivolumab* or both at a concentration of 5 µg / ml one hour before coincubation.

2.7.5. Evaluation of xCELLigence analysis

For analysis of the xCELLigence measurements, RTCA Software 1.2, version 1.2.1 (Roche) was used. Graphs were generated with GraphPad Prism 4.0.

2.8. Viral growth curves of MeV-GFP on HT29 and HCT-15 tumor cells

2.8.1. Viral infection of HT29 and HCT-15 cells for preparation of virus growth curves

For the measurement of viral replication, tumor cells were seeded in 6-well plates in 2 ml DMEM + 10 % FCS in amounts listed in the table below. The day after, infection with the virotherapeutic MeV-GFP was performed as described in 2.2.2, using MOIs also specified in the table below.

Infection took place in 1 ml of Opti-MEM, paying attention that the plates were swayed approximately every 15 minutes to ensure equability of infection. At 3 hpi, cells were washed three times with PBS and 1 ml of DMEM + 10 % FCS was added per well.

To analyze the influence of the checkpoint inhibitors *pembrolizumab* (Merck / MSD) and *atezolizumab* on viral replication, the respective drug was added directly after infection with the new medium in a concentration of 10 µg / ml.

Table 12: Amount of tumor cells per well used for viral growth curves.
Cells were seeded in 6-well plates in 2 ml of DMEM + 10 % FCS.

Tumor cell line	Amount of tumor cells per well	MOI used for viral growth curves
HT29	2 x 10^5	MOI 5
HCT-15	2 x 10^5	MOI 10

Directly subsequent to that, the first samples were frozen at -80°C. Supernatants were transferred into test tubes and cells were scraped into 1 ml of Opti-MEM and also transferred into test tubes.

This procedure was repeated after 24, 48, 72 and 96 hours. For each point of time, the supernatant and the cell lysate of one well was used.

2.8.2. Titration for virus growth curves

The day before the viral titration, 1 x 10^4 Vero cells per well were seeded in 200 µl DMEM + 5% FCS in 96-well plates. After controlling the uniformity of cell adherence, the titration of the virus samples took place. Therefore, a 96-well plate was prepared for the serial dilution, providing 270 µl of DMEM + 5 % FCS in each well except for the first row.

The samples were thawed in the water bath, vortexed and centrifuged at 3000 rpm for 2 minutes. The supernatants were transferred into new Eppendorf cups, and 300 µl out of each sample were pipetted into the first empty well of the rows of the dilution plate. Now, 30 µl of the first well were transferred into the well below and so forth to create series of 1:10 dilutions, as shown in the picture below (Fig. 11).

The diluted virus suspensions were used to infect Vero cells in quadruplicates, using 50 µl of suspension per well. After 96 hours of infection in the incubator, the titration could be evaluated using fluorescence microscopy.

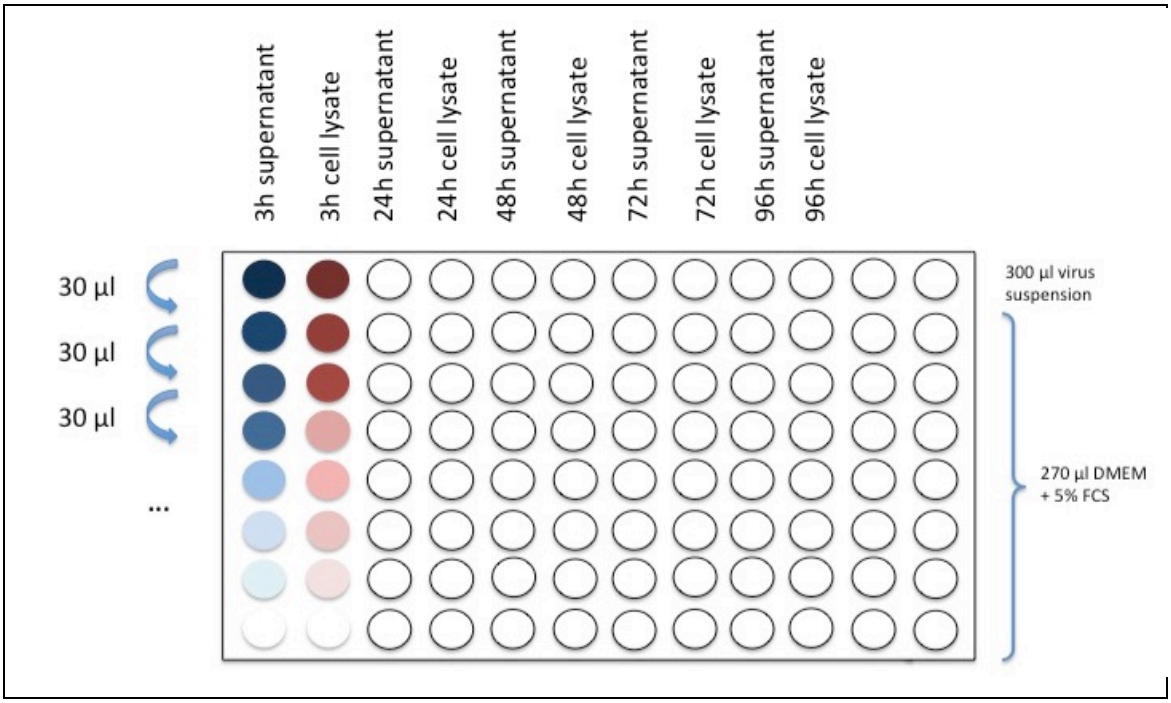

Figure 11: 96-well plate of dilution series for MeV-GFP virus growth curves
1 : 10 dilution series were used for the titration of MeV-GFP virus growth curves. Therefore, 300 µl of the collected supernatants or cell lysates were pipetted into the first row of the plate.

Dilution was realized by transferring 30 µl out of those into 270 µl of DMEM + 5 % FCS, repeating that step seven times.

2.8.3. Analysis of viral growth curves

Growth curve samples were evaluated in quadruplicates via fluorescence microscopy. As the GFP expressed by MeV-GFP-infected tumor cells fluoresces green, infected wells could be detected easily as described in 1.2.4.

For analysis, the amount of positive wells in each quad row was listed in Excel, calculating the viral titer in [PFU / ml]. Therefore, titers were deduced from the 50 % Tissue Culture Infective Dose ($TCID_{50}$), describing the virus amount needed to induce cytopathic effects in 50 % of infected cells, which was calculated with a formula by Spearman and Kärber (Spearman, 1908; Kärber, 1931).

$$\frac{TCID_{50}}{ml} = \frac{viral\ particles}{ml} = \frac{10^{1+\sum infected\ wells - 0.5\ x\ log10}}{0.03\ ml\ inserted\ viral\ solution}$$

A single well was considered as positive in case that at least one green fluorescing plaque / syncytium could be observed.

With the calculated titers, line diagrams could be designed in GraphPad Prism 4.0.

2.9. Determination of viral titers on HT-29 and HCT-15 tumor cells after coculture with NK cells or PBMC and treatment with atezolizumab or nivolumab

To investigate the quantitative influence of ICI therapy and immune cell cocultivation on viral replication and spread in CRC cell lines, virus titers were determined.

24 hours after seeding in 6-well plates, HT29 or HCT-15 tumor cells were infected with MeV-GFP at MOI 1 and 10, respectively. 48 hpi, both tumor cells and PBMC or NK cells were separately incubated for one hour with 5 µg / ml of each *atezolizumab*, *nivolumab* or both. Importantly, for treatment of tumor cells with ICI, a medium exchange was done, replacing the old medium with 1.8 ml of fresh DMEM + 10 % FCS. Incubation of immune cells took place in RPMI and the needed amount of PBMC / NK cells was added after one hour in a volume of 200 µl to each well.

For control, one well was left without coincubation or ICI treatment, one well was coincubated with immune cells but without ICI and one well was coincubated with PBMC / NK cells and treated with control IgG Gamunex.

Both supernatants and cell lysates were frozen 48 hours after coculture at -80° C, proceeding as described in 2.8.1. Therefore, supernatants were additionally centrifuged at 4000 rpm for 4 minutes to separate and discard NK cells or PBMC from supernatants.

Table 13: Cell counts, MOIs, E : T ratios and ICI concentrations used for viral titer determination

Tumor cell line	Amount of tumor cells per well	MOI used	E : T PBMC	E : T NK	ICI concentration
HT29	2 x 10^5	MOI 1	10:1	2.5:1	5 µg / ml
HCT-15	2 x 10^5	MOI 10	10:1	2.5:1	5 µg / ml

Titration on Vero cells and calculation of the resulting MeV-GFP titers in PFU / ml were performed as described in 2.8.2 and 2.8.3. Bar diagrams were designed using GraphPad Prism 4.0.

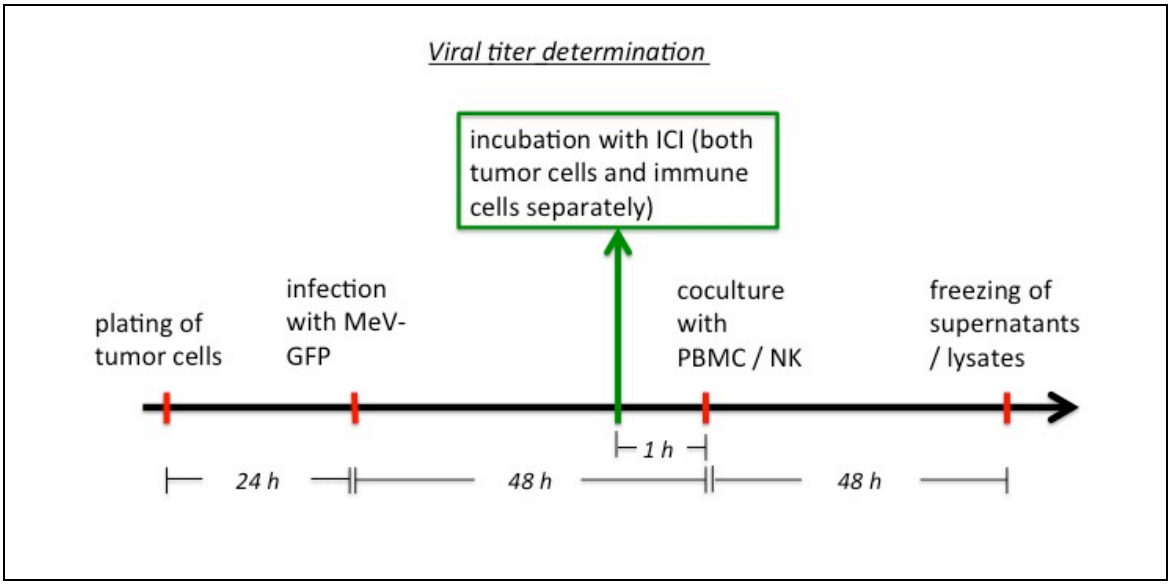

Figure 12: Workflow of virus titer determination after coincubation with NK cells / PBMC and treatment with ICI

Treatment with atezolizumab and / or nivolumab took place separately for tumor and immune cells, using a concentration of 5 µg / ml.

3. Results

Aim of this dissertation thesis was to investigate a novel multimodal therapeutic approach for the treatment of advanced colorectal carcinoma (CRC). Thereby, a measles vaccine virus (MeV) virotherapeutic was combined with immune checkpoint inhibitors (ICI) under coculture with NK cells or peripheral blood mononuclear cells (PBMC) *in vitro*, using three CRC cell lines from the NCI-60 human tumor cell panel, i.e. cell lines HT29, HCT-15 and SW-620.

For cytotoxicity analysis of the respective monotherapies, Sulforhodamine B (SRB) assays were performed to uncover preexisting resistances in the different tumor cell lines.

After the basal expression rates of immune checkpoint ligand PD-L1 on CRC cell lines were investigated under different culturing conditions using flow cytometry, a next step was to focus on the influence of treatment with measles oncolytic virus (OV) on PD-L1 expression. Furthermore, the existence of immune checkpoint receptor PD-1 on NK cell subpopulations was quantified via flow cytometry.

The functional xCELLigence real-time cell proliferation assay was used to depict conceivable anti-tumor effects of our immunovirotherapeutic approach for CRC treatment under immune cell coculture. On the other hand, antiviral effects of immune checkpoint blockade were examined in a viral growth curve model and, secondly, in viral titrations of supernatants and lysates of measles-infected CRC cells after immune cell cocultivation.

3.1. Quantification of anti-tumor effects of monotherapeutic treatment with measles virotherapeutic or immune checkpoint blockade in colorectal carcinoma

3.1.1. Measurement of cytotoxicity under MeV-GFP-infection in human colorectal carcinoma cell lines HCT-15, HT29 and SW-620

To reveal possible preexisting resistances against the respective monotreatments, cytotoxic influence of MeV-GFP-infection on three human CRC cell lines from the NCI-60 human tumor cell panel was determined by SRB cytotoxicity assays. Fixation of tumor cells was performed at 72 and 96 hours post infection (hpi).

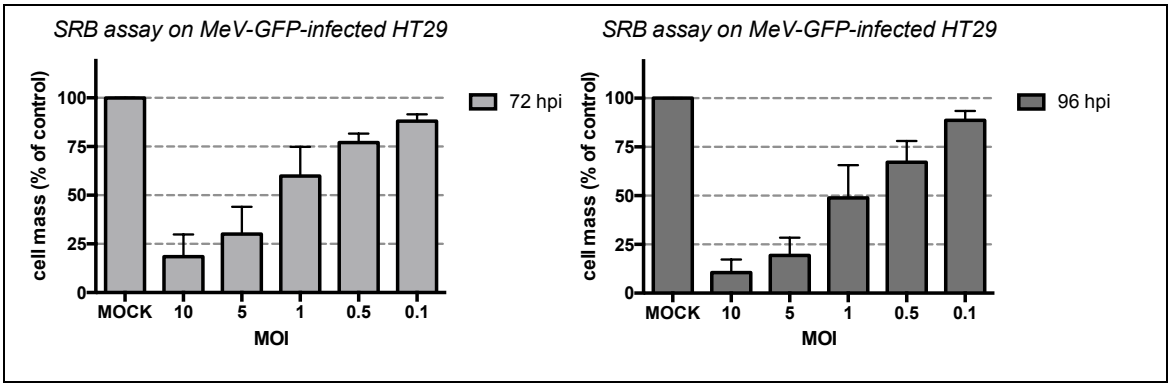

Figure 13: SRB cytotoxicity assays of the MeV-GFP-infected human CRC cell line HT29
Infection of HT29 tumor cells took place at different multiplicities of infection (MOI), namely 0.1, 0.5, 1, 5 or 10. MOCK-infected HT29 cells served as control and were equalized with 100 % of the overall cell mass. Fixation of tumor cells took place at 72 or 96 hours post infection (hpi).
Three independent experiments are shown, depicting mean and standard error of the mean (SEM). Analysis was performed in quadruplicates for each single experiment. For calculation of SEM, see 2.6.

In HT29 tumor cells, MeV-GFP-infection achieved a multiplicity of infection (MOI)- and time-dependent reduction of tumor cell mass. Thus, HT29 turned out to be susceptible towards MeV-GFP-induced oncolysis, as already described by Noll et al. for the infection with MeV-SCD at a MOI of 1 (Noll M., 2013). Our results showed that viral infection at the highest MOI of 10 already reduced cell mass to an extent of 18.4 % ± 11.4 (mean and SEM) of control at 72 hpi. After 96 hours, the cell mass residue decreased to a percentage of 10.6 % ± 6.7; so most tumor cells had been killed by then, which could also be observed via light microscopy with the dead cells being solved from the monolayer.

The HT29 tumor cell killing decreased at lower MOIs, as the trends in SRB assays clearly showed. Namely, referring to the lowest MOI of 0.1, tumor cell mass was only reduced to 88.1 % ± 3.4 of control cell mass at 72 hpi, whereupon a longer time of cultivation could not improve tumor cell killing in this single case with 88.7 % ± 4.8 at 96 hpi.

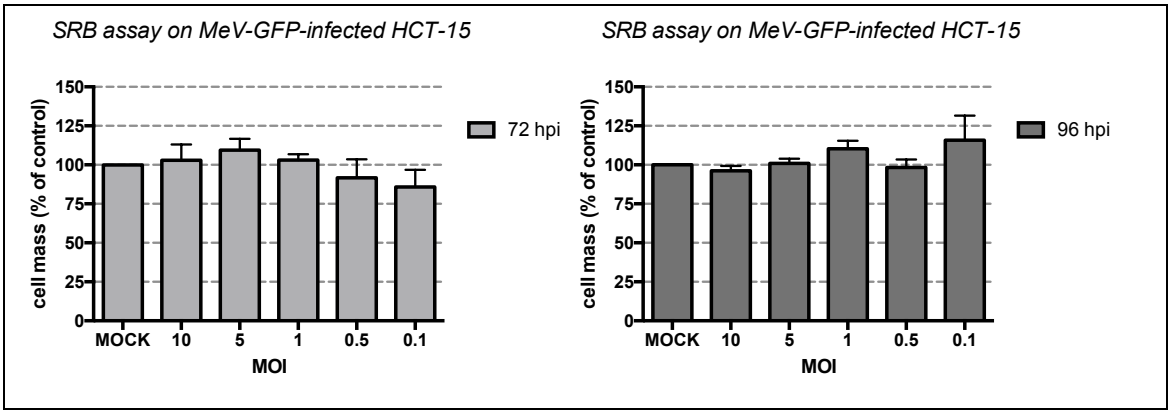

Figure 14: SRB cytotoxicity assays of the MeV-GFP-infected human CRC cell line HCT-15

Infection of HCT-15 tumor cells took place at different MOIs of 0.1, 0.5, 1, 5 or 10, respectively. MOCK-infected HCT-15 cells served as control and were equalized with 100 % of the overall cell mass. Fixation of cells took place at 72 or 96 hpi.
Three independent experiments are shown, depicting mean and SEM. Analysis was performed in quadruplicates for each single experiment. For calculation of SEM, see 2.6.

On the other hand, another human CRC cell line from the NCI-60 panel, HCT-15, was observed to be highly resistant towards MeV-GFP-induced oncolysis, also consistent with the results of Noll et al. for MeV-SCD. In this case, even the highest MOI of 10 could not achieve a tumor cell mass reduction, neither at 72 hpi with 102.9 % ± 10.2 of control cell mass, nor at 96 hpi with 96.2 % ± 3.2 of control cell mass.

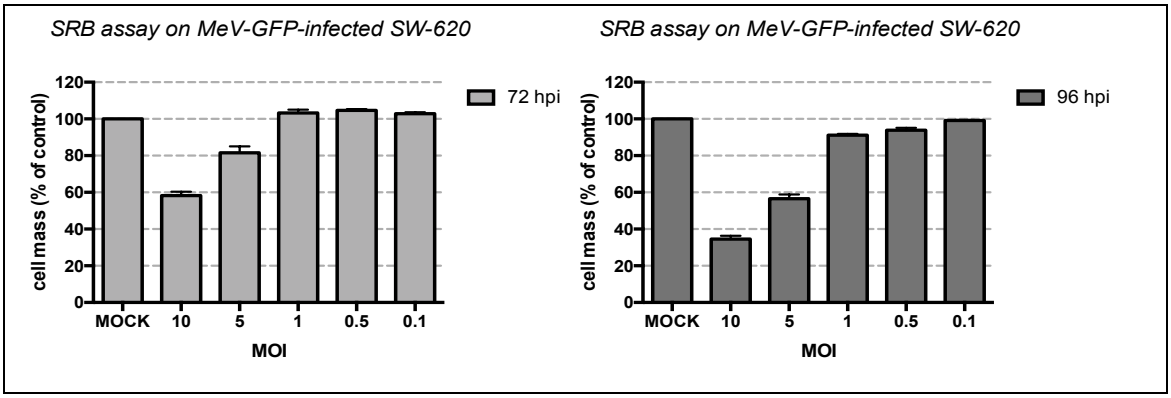

Figure 15: SRB cytotoxicity assays of the MeV-GFP-infected human CRC cell line SW-620
Infection of SW-620 tumor cells took place at different MOIs of 0.1, 0.5, 1, 5 or 10, respectively. MOCK-infected SW-620 cells served as control and were equalized with 100 % of the overall cell mass. Fixation of cells took place at 72 or 96 hpi.
Three independent experiments are shown, depicting mean and SEM. Analysis was performed in quadruplicates for each single experiment. For calculation of SEM, see 2.6.

The last cell line depicted here, SW-620, was tested intermediate resistant to MeV-GFP-oncolysis.

With a remaining tumor cell mass of 58.3 % ± 2.1 (mean and SEM) at 72 hpi and of 34.5 % ± 1.9 at 96 hpi using the highest MOI of 10, a time-dependent tumor cell mass reduction could be observed in SW-620. Furthermore, a MOI-dependent susceptibility to MeV-GFP could be proven. However, higher MOIs were necessary for effective tumor cell mass reduction. Namely, at 96 hpi, the remaining tumor cell mass after virotherapeutic treatment diminished from 99.1 % ± 0.4 for MOI 0.1 to 93.9 % ± 1.3 for MOI 0.5, 91.1 % ± 0.8 for MOI 1, 56.5 % ± 2.3 for MOI 5 and finally 34.5 % ± 1.9 for MOI 10. Whereas the MOIs of 0.1, 0.5 and 1 could not or only slightly achieve tumor cell killing at 72 and 96 hpi, a tumor cell mass decline could be found for the MOIs of 5 and 10 at both times of measurement.

To sum it up, MeV-GFP-infection achieved a MOI- and time-dependent reduction of HT29 and SW-620 tumor cell mass at 72 and 96 hpi *in vitro*. In contrast to those findings, the human CRC cell line HCT-15 was observed to be highly resistant to MeV-GFP-induced oncolysis at both 72 and 96 hpi, referring to MOIs from 0.1 to 10.

3.1.2. *Examination of cytotoxicity after treatment with immune checkpoint inhibitors nivolumab or atezolizumab in human colorectal carcinoma cell lines HCT-15 and HT29*

SRB assays of human CRC cell lines HT29 and HCT-15 were performed to analyze possible anti-tumor effects of monotherapeutic treatment with immune checkpoint inhibitors *nivolumab*, targeted against PD-1, and *atezolizumab*, with PD-L1 as its target. Tumor cell lines HT29 (permissive to MeV oncolysis) and HCT-15 (resistant to MeV oncolysis) were investigated, as both were used for xCELLigence analysis in the following.

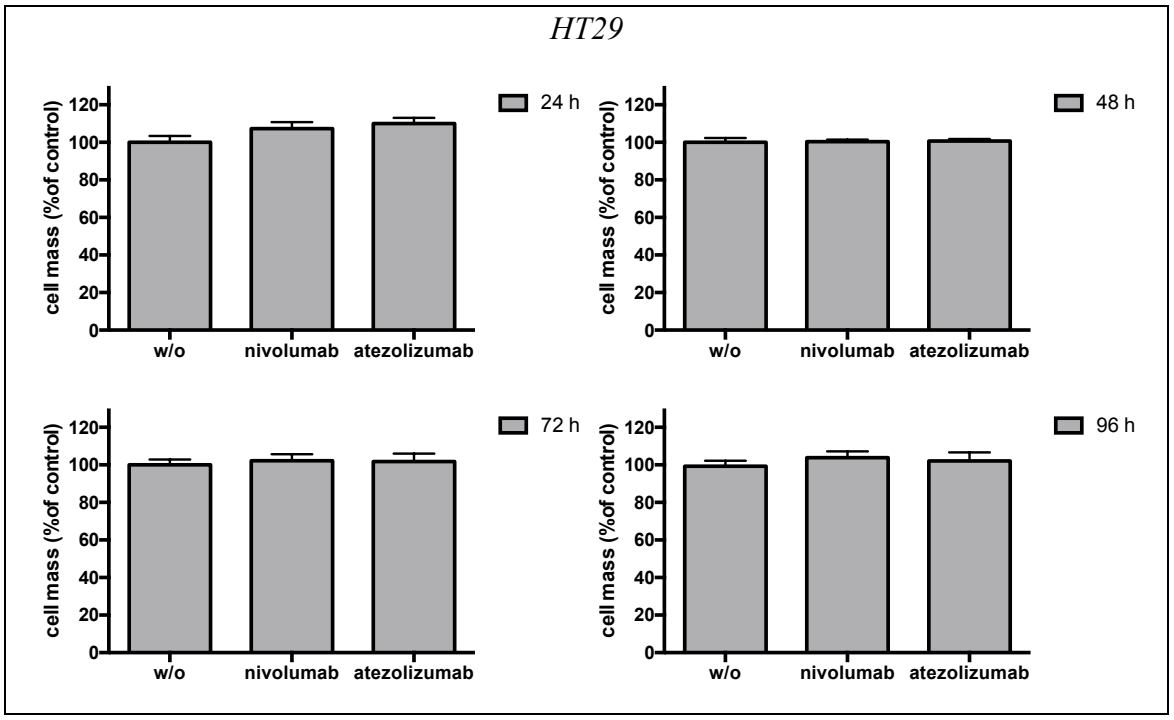

Figure 16: SRB cytotoxicity assays of HT29 tumor cells after treatment with immune checkpoint inhibitors *atezolizumab* or *nivolumab*

One day after plating, HT29 and HCT-15 tumor cells were treated with 5 µg / ml of atezolizumab or nivolumab, or were left without ICI treatment after a medium exchange, respectively. At each 24, 48, 72 and 96 hours after treatment, cells were fixed and prepared for SRB analysis.

Means ± SD of the cell mass relative to control cell mass of untreated cells are shown. Analysis was performed in quadruplicates. One representative experiment is depicted.

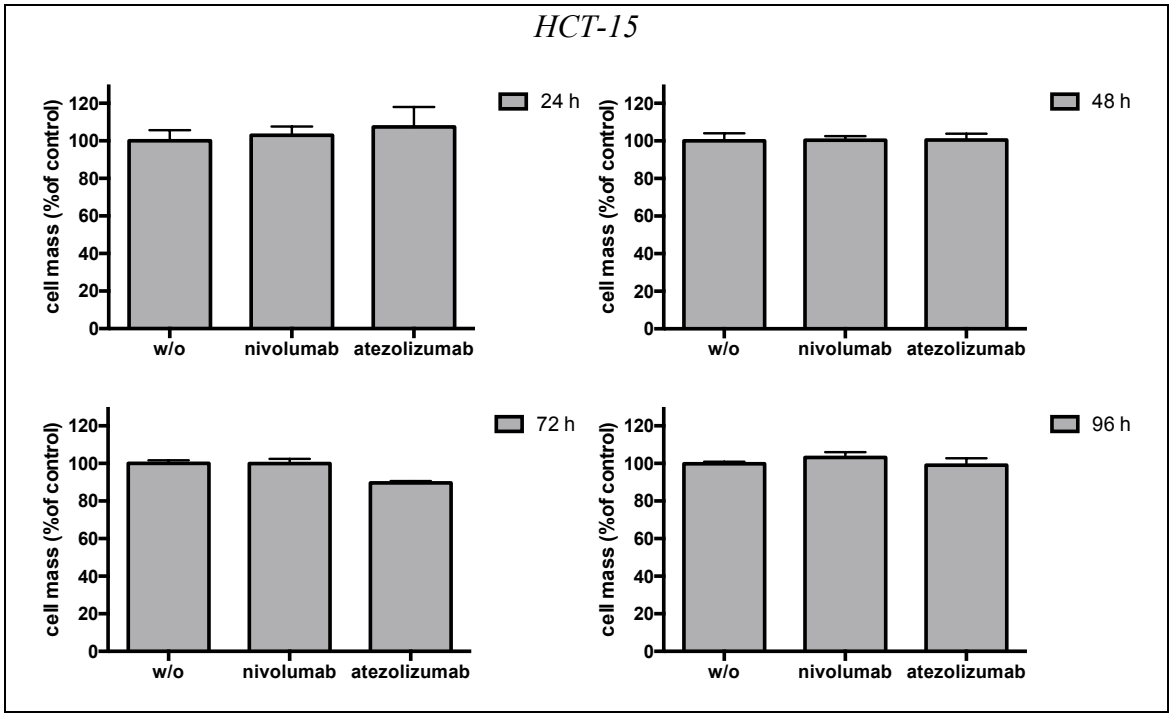

Figure 17: SRB cytotoxicity assays of HCT-15 after treatment with immune checkpoint inhibitors *atezolizumab* or *nivolumab*

Monotherapeutic treatment of both CRC cell lines HT29 and HCT-15 with 5 µg / ml of ICI *nivolumab* or *atezolizumab*, respectively, did not influence tumor cell viability *in vitro*, neither increasing nor decreasing the remaining cell mass at 24, 48, 72 or 96 hours after treatment.

According to these observations and to our expectations, both drugs were not found to possess independent anti-tumor efficacy in the absence of immune cells, as no PD-1 / PD-L1 interaction could take place.

3.2. Analysis of PD-L1 expression on different human colorectal carcinoma cell lines under the influence of measles-induced oncolysis

As immune checkpoint ligand (PD-L1) expression on tumor cells and immune checkpoint receptor (PD-1) expression on immune cells both display key factors for a possible therapeutic ICI interaction, these parameters were investigated in further steps. Thereby, a focus was set on the influence of measles virotherapeutic-infection on the expression of PD-L1 on human CRC cell lines at first.

3.2.1. Basal PD-L1 expression in human colorectal carcinoma cell lines HT29, HCT-15 and SW-620 under the influence of different culturing conditions

As a standard of comparison, basal expression rates of the immune checkpoint ligand PD-L1 on tumor cell lines HT29, HCT-15 and SW-620 were investigated via FACS analysis, taking different culturing conditions into account.

On the one hand, cells were cultured in DMEM + 10 % FCS, and on the other hand, cells were additionally incubated for three hours in the virus incubator with Opti-MEM, which was normally used for viral infection.

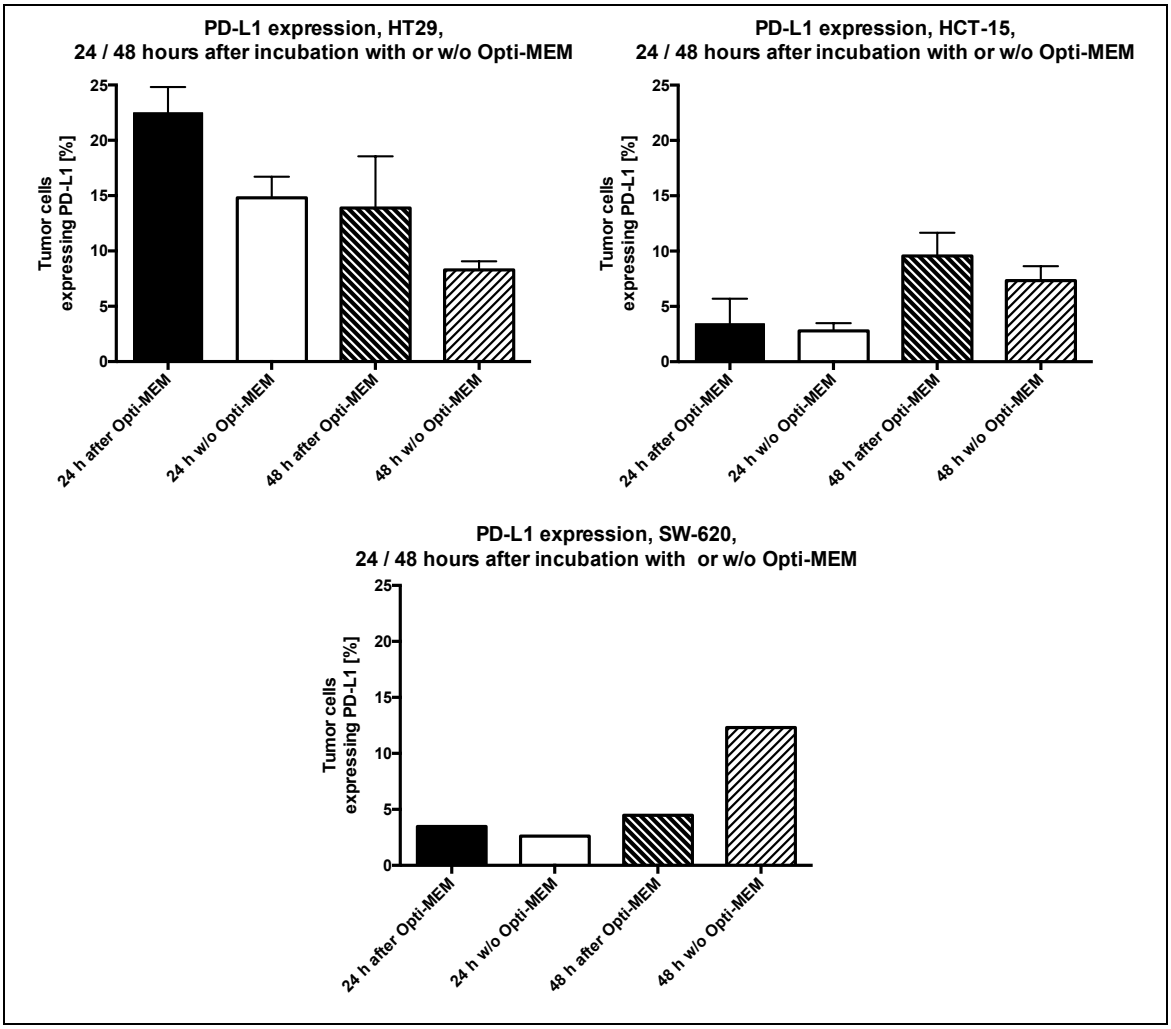

Figure 18: FACS analysis of the basal PD-L1 expression on human colorectal carcinoma cell lines HT29, HCT-15 and SW-620 under different culturing conditions

Tumor cells were plated and incubated with Opti-MEM in the virus incubator, similarly to the process of viral infection, or were left in DMEM + 10 % FCS in the incubator for uninfected cells instead. After three hours of incubation, medium was replaced by fresh DMEM + 10 % FCS in each case. 24 or 48 hours later, cells were collected for FACS staining of PD-L1 with PE anti-human CD274 (PD-L1). In case of HT29 and HCT-15, three independent experiments were performed, showing means ± SD of the percentages of PD-L1 expressing tumor cells. Regarding SW-620, one representative experiment is shown. W/o = without.

The three human CRC cell lines showed different degrees of basal PD-L1 expression. In detail, 14.8 % of HT29 cells, 2.8 % of HCT-15 cells and 2.6 % of SW-620 cells were found to express PD-L1 without addition of Opti-MEM.

Moreover, PD-L1 expression of the three tumor cell lines reacted differently in regard to time of culturing and variation of used media. In SW-620 tumor cells, a time-dependent increase in expression of PD-L1 could be observed (24 versus 48 hours of cultivation), namely a difference of 9.7 percentage points in cells cultured without Opti-MEM (from 2.6 % of analyzed tumor cells to 12.3 %) and a difference of 1.0 percentage points in cells cultured including Opti-MEM incubation (from 3.5 % of analyzed tumor cells to 4.5 %).

In the HCT-15 tumor cell line, an increase in PD-L1 expression with respect to duration of culture (24 versus 48 hours) could be observed, just as described for SW-620, namely a difference of 4.5 percentage points in cells cultured without Opti-MEM (from 2.8 % ± 0.7 of analyzed tumor cells to 7.3 % ± 1.3) and a difference of 6.2 percentage points in cells cultured with Opti-MEM incubation (from 3.4 % ± 2.3 of analyzed tumor cells to 9.6 % ± 2.1).

An inverse effect could be found addressing HT29 tumor cells, where a time-dependent decrease in expression of PD-L1 could be observed, namely a difference of 6.5 percentage points in cells cultured without Opti-MEM (from 14.8 % ± 1.9 of analyzed tumor cells to 8.3 % ± 0.8) and a difference of 8.6 percentage points in cells cultured including Opti-MEM incubation (from 22.5 % ± 2.3 of analyzed tumor cells to 13.9 % ± 4.7).

In HT29, a difference of PD-L1 expression could be observed when comparing the different culturing conditions DMEM + 10 % FCS versus Opti-MEM. A higher PD-L1 expression was observed when cells were cultured in Opti-MEM with a difference of 7.7 percentage points in cells collected after 24 hours (14.8 % ± 1.9 of tumor cells without Opti-MEM versus 22.5 % ± 2.3 of cells with Opti-MEM incubation) and a difference of 5.6 percentage points in cells collected after 48 hours (8.3 % ± 0.8 of analyzed tumor cells without Opti-MEM versus 13.9 % ± 4.7 of cells with Opti-MEM incubation).

In HCT-15 as well as SW-620, no consistent difference in expression of PD-L1 with respect to different culturing conditions could be observed. A decrease of PD-L1

expression in SW-620 from 12.3 % of analyzed CRC cells without Opti-MEM to 4.5 % of cells with Opti-MEM incubation after 48 hours could not be reproduced for the first time of measurement after 24 hours.

To summarize, culturing conditions with regard to medium and time of culturing could partly influence PD-L1 expression on human CRC cell lines, but not homogeneously in all three tested tumor cell lines.

These pretests were of relevance to appraise whether in the following experiments infection with oncolytic measles vaccine virus was a reason for a change in PD-L1 expression rates, or whether different culturing conditions pretended such an effect.

3.2.2. PD-L1 expression in human colorectal carcinoma cell lines HT29, HCT-15 and SW-620 after infection with MeV-GFP

After comparison of basal PD-L1 expression rates under different culturing conditions, FACS analysis of MeV-GFP-infected tumor cells HT29, HCT-15 and SW-620 was performed to examine the influence of viral infection on the expression of the immune checkpoint ligand.

MeV-GFP as a virotherapeutic implicates the advantage that the viral infection of tumor cells can be quantified, as infected cells express the green fluorescent protein (GFP), which in turn can be detected by flow cytometry. First of all, appropriate viral infection of the three human CRC cell lines was proven by flow cytometry.

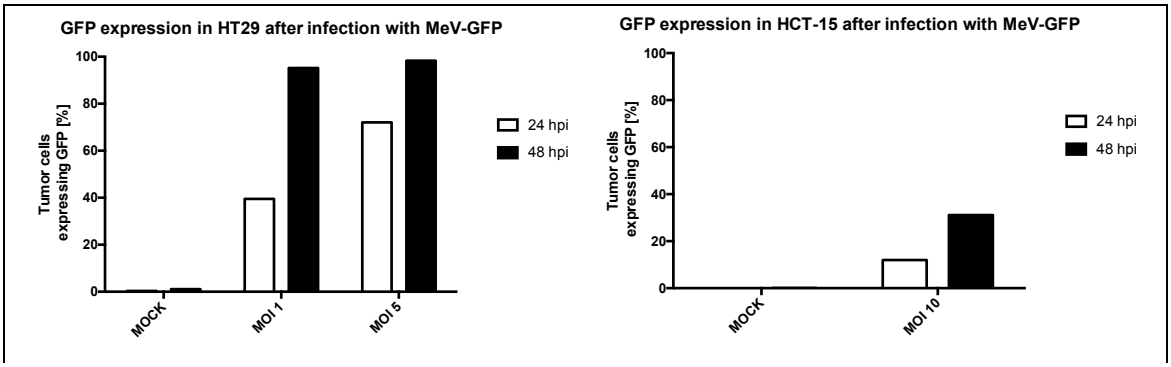

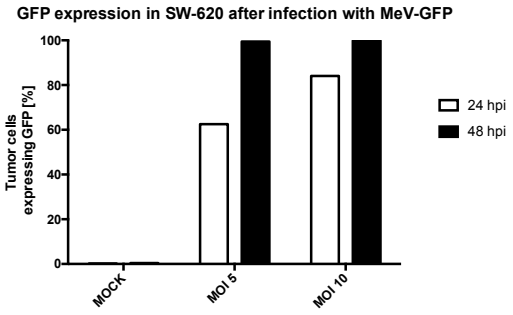

Figure 19: FACS analysis of GFP expression on MOCK- or MeV-GFP-infected human colorectal carcinoma cell lines HT29, HCT-15 and SW-620
Tumor cells were infected with MeV-GFP using different MOIs of 1, 5 or 10, or were MOCK-infected. Tumor cells were fixed for FACS analysis at 24 and 48 hpi.
The percentages of GFP positive cells are given, representing successfully infected tumor cells.

Time- and MOI-dependent MeV-GFP-infection could be proven in all three CRC cell lines by measuring GFP expression of infected tumor cells.

Addressing HT29 cells infected at a MOI of 1, only 39.5 % of tumor cells at 24 hpi and 95.2 % at 48 hpi revealed GFP expression. Referring to infection at the higher MOI of 5, 72.1 % of cells expressed GFP at 24 hpi, further increasing to 98.3 % at 48 hpi.

In contrast to this, only 12.0 % of HCT-15 tumor cells showed GFP expression at 24 hpi and 31.1 % at 96 hpi, albeit the higher MOI of 10 was used for infection.

In SW-620 cells, a MOI of 5 achieved infection of 62.5 % of tumor cells at 24 hpi and 99.5 % at 48 hpi. With an increase of MOI to 10, infection rates could be further augmented to 84.1 % of tumor cells at 24 hpi and stayed at a high level of 99.9 % at 48 hpi. These observations seemed consistent with the different MeV-GFP susceptibilities found in SRB assays before.

In a next step, PD-L1 expression on infected tumor cells was analyzed.

***A)** PD-L1 expression on HT29 tumor cells, infected with MeV-GFP*

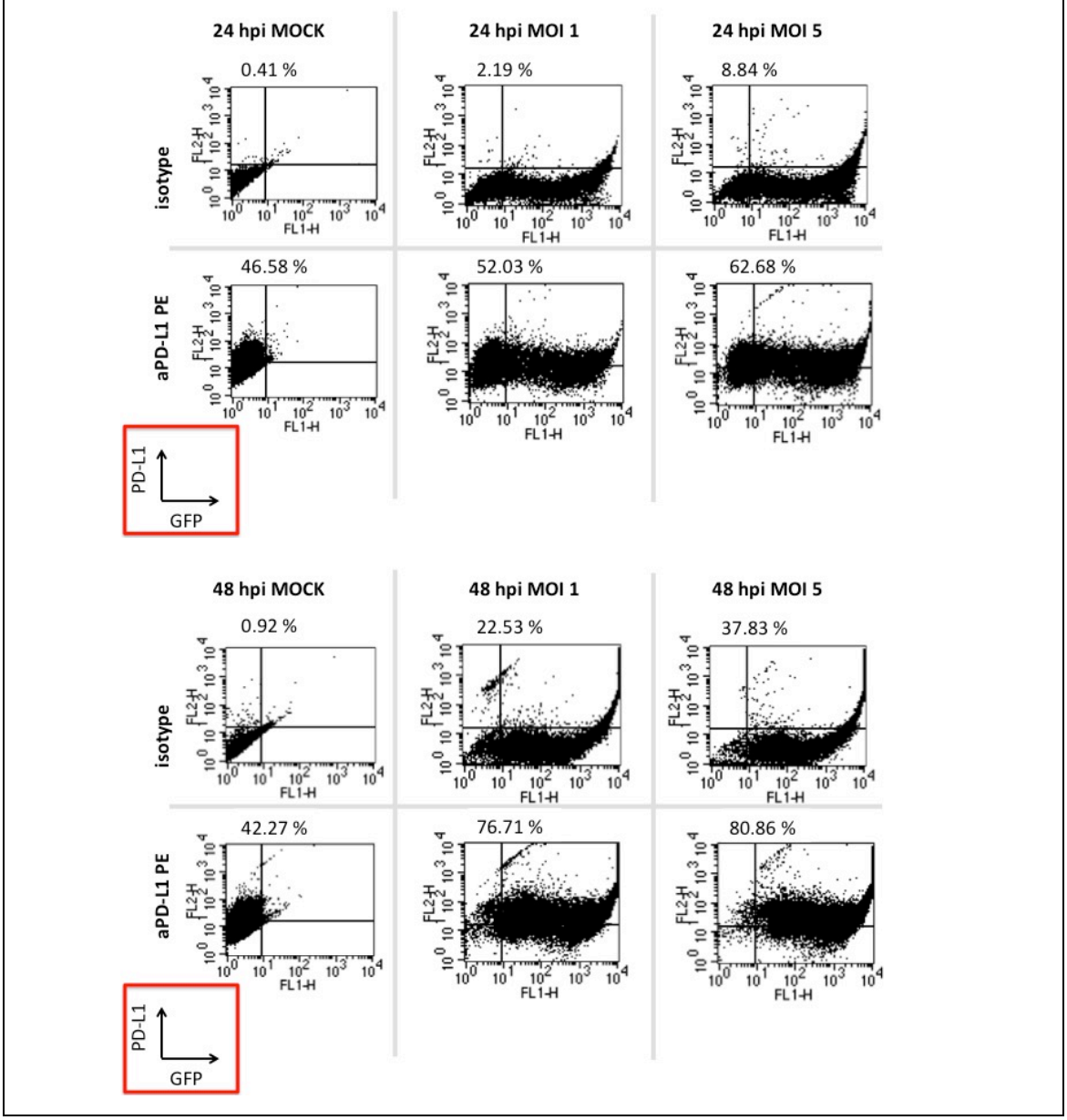

***A)** PD-L1 expression on HT29 tumor cells, infected with MeV-GFP*

24 hpi	GFP positive [%]	PD-L1 positive [%]	GFP and PD-L1 positive [%]	**48 hpi**	GFP positive [%]	PD-L1 positive [%]	GFP and PD-L1 positive [%]
MOCK	0.37	46.58	0.37		1.09	42.27	0.98
MOI 1	39.52	52.03	19.59		95.20	76.71	73.63
MOI 5	72.06	62.68	44.82		98.32	80.86	79.68

B) *PD-L1 expression on HCT-15 tumor cells, infected with MeV-GFP*

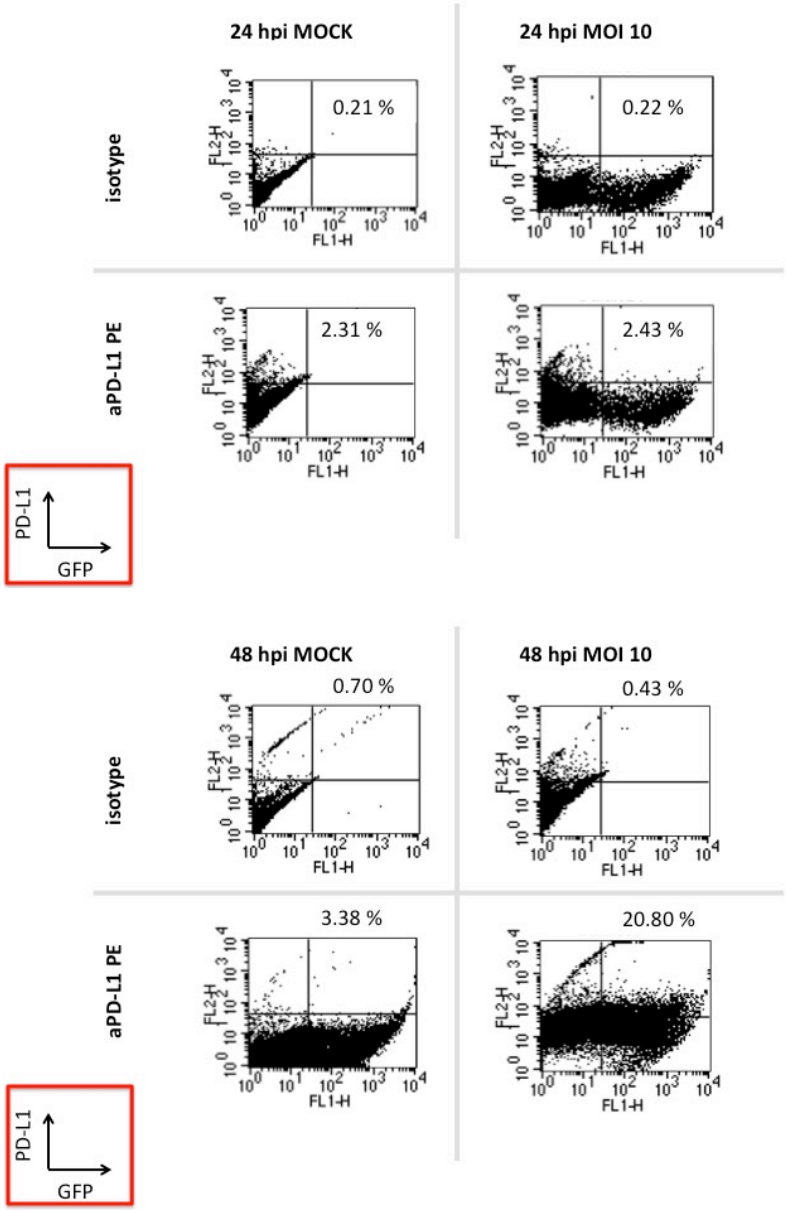

B) *PD-L1 expression on HCT-15 tumor cells, infected with MeV-GFP*

24 hpi	GFP positive [%]	PD-L1 positive [%]	GFP and PD-L1 positive [%]	**48 hpi**	GFP positive [%]	PD-L1 positive [%]	GFP and PD-L1 positive [%]
MOCK	0.04	2.31	0.04		0.09	3.38	0.09
MOI 10	12.01	2.43	0.16		31.09	20.80	10.32

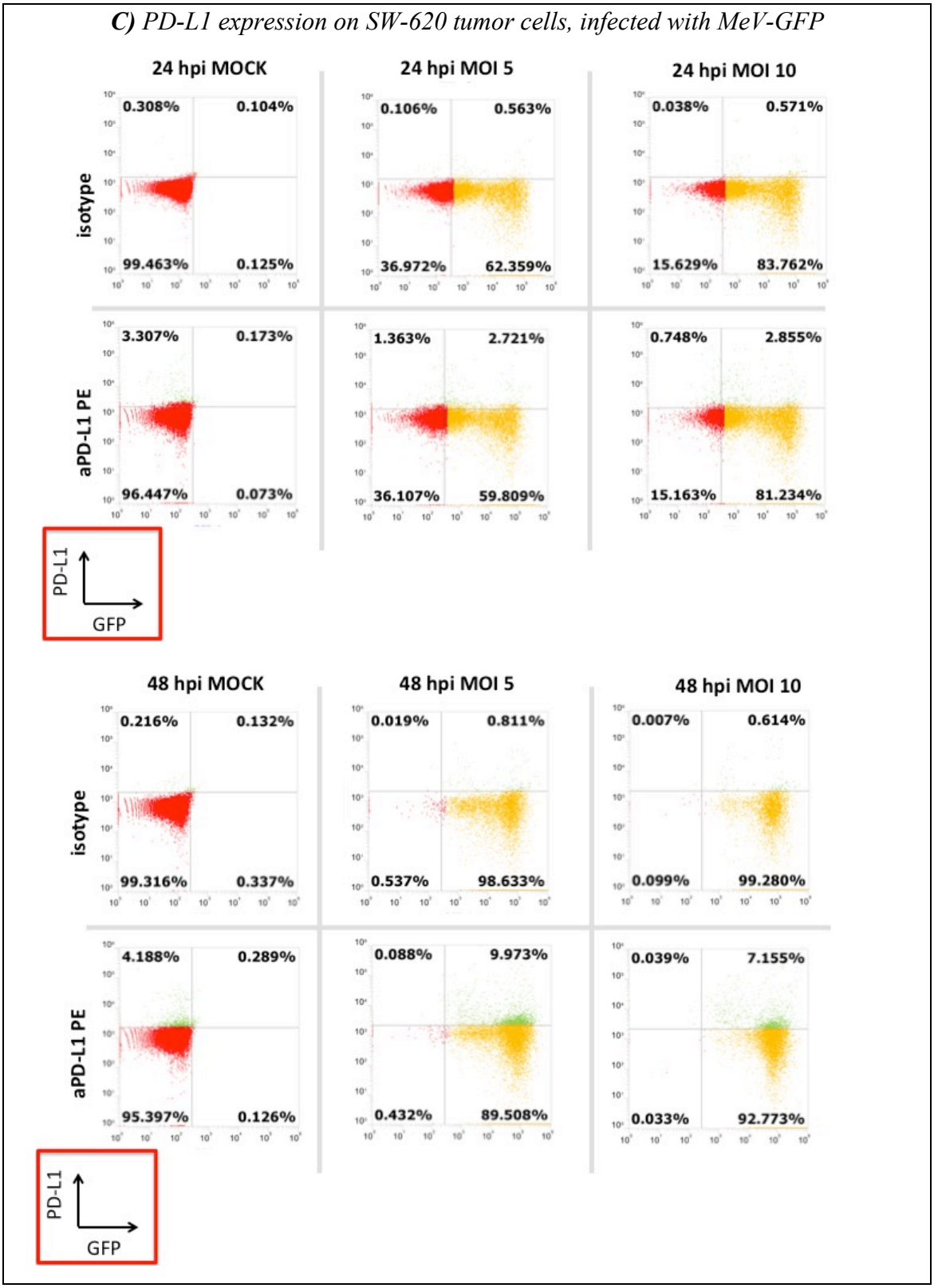

Figure 20, A - C: FACS analysis of PD-L1 expression on MeV-GFP-infected in comparison to MOCK-infected human colorectal cancer cell lines HT29, HCT-15 and SW-620

MeV-GFP-infection of CRC cells was performed using different MOIs (MOI 1 and MOI 5 for HT29, MOI 10 for HCT-15 and MOI 5 and MOI 10 for SW-620) or cells were MOCK-infected.

Tumor cells were analyzed for PD-L1 expression at 24 and 48 hpi. Staining was performed with PE anti-human CD274 (aPD-L1 PE) or the respective PE IgG2b isotype control (isotype). In the dot plots of HT29 and HCT-15, percentages of PD-L1 positive cells are given irrespective of GFP expression status. In the dot plots of SW-620, the percentages of cells in each quadrant region are shown.

Table 14, A - C: FACS analysis of PD-L1 expression on MeV-GFP-infected in comparison to MOCK-infected human colorectal cancer cell lines HT29, HCT-15 and SW-620
The respective tables below list the percentages of GFP positive, PD-L1 positive and both GFP and PD-L1 positive tumor cells, referring to cells labeled with PE anti-human CD274.

***C)** PD-L1 expression on SW-620 tumor cells, infected with MeV-GFP*

24 hpi	GFP positive [%]	PD-L1 positive [%]	GFP and PD-L1 positive [%]	**48 hpi**	GFP positive [%]	PD-L1 positive [%]	GFP and PD-L1 positive [%]
MOCK	0.25	3.48	0.17		0.42	4.48	0.29
MOI 5	62.53	4.08	2.72		99.48	10.06	9.97
MOI 10	84.09	3.60	2.86		99.93	7.19	7.16

In HT-29 cells, PD-L1 expression 24 hpi increased from an initial level of 46.6 % of uninfected cells to a level of 62.7 % of cells infected at MOI 5. Further augmentation of PD-L1 expression could be observed at 48 hpi, finally reaching a level of 80.9 % of cells infected using MOI 5.

In HCT-15, PD-L1 expression at 24 hpi did not change from an initial level of 2.3 % of MOCK-infected cells to a level of 2.4 % of cells infected at MOI 10, but an increase in PD-L1 expression could be observed at 48 hpi, finally reaching a level of 20.8 % of cells infected using MOI 10.

In SW-620 cells, PD-L1 expression at 24 hpi could not be increased by MeV-GFP infection, with 3.5 % of uninfected cells expressing PD-L1 compared to 3.6 % of cells infected at MOI 10. Nevertheless, augmentation of PD-L1 expression could be observed at 48 hpi with 4.5 % of uninfected cells expressing PD-L1 versus 7.2 % of cells infected at MOI 10. However, no MOI-dependent relation of PD-L1 upregulation could be described, as even 10.1 % of tumor cells infected at MOI 5 expressed PD-L1 at 48 hpi.

To sum it up, a MOI- and time-dependent upregulation of PD-L1 could be shown for HT29 and HCT-15 CRC cells. In SW-620, a greater proportion of MeV-GFP-infected tumor cells expressed PD-L1 than of uninfected tumor cells, but no MOI-dependency could be proven. Still, the PD-L1 expression in SW-620 rose with time of cultivation after OV infection.

As high levels of GFP expression unfortunately interfered with the PE fluorochrome, the percentage of PE positive cells increased in MeV-GFP-infected isotype controls as well. This has to be taken into account when considering results of PD-L1 expression, especially in the MeV-GFP susceptible cell line HT29, where high GFP expression levels were achieved with MOIs of up to 5 (see Fig. 19). Therefore, after effective infection was proven, MeV-SCD (not encoding the GFP marker gene) was used for measurement of PD-L1 expression in further experiments to avoid interference.

3.2.3. PD-L1 expression in human colorectal carcinoma cell lines HCT-15, HT29 and SW620 after infection with MeV-SCD

In a next step, the influence of MeV-SCD-infection on PD-L1 expression on human CRC cell lines was examined by flow cytometry, whereupon the interference of fluorescing GFP with PE fluorochrome, as described in 3.2.2, could be avoided.

A) *PD-L1 expression on HT29 cells, infected with MeV-SCD*

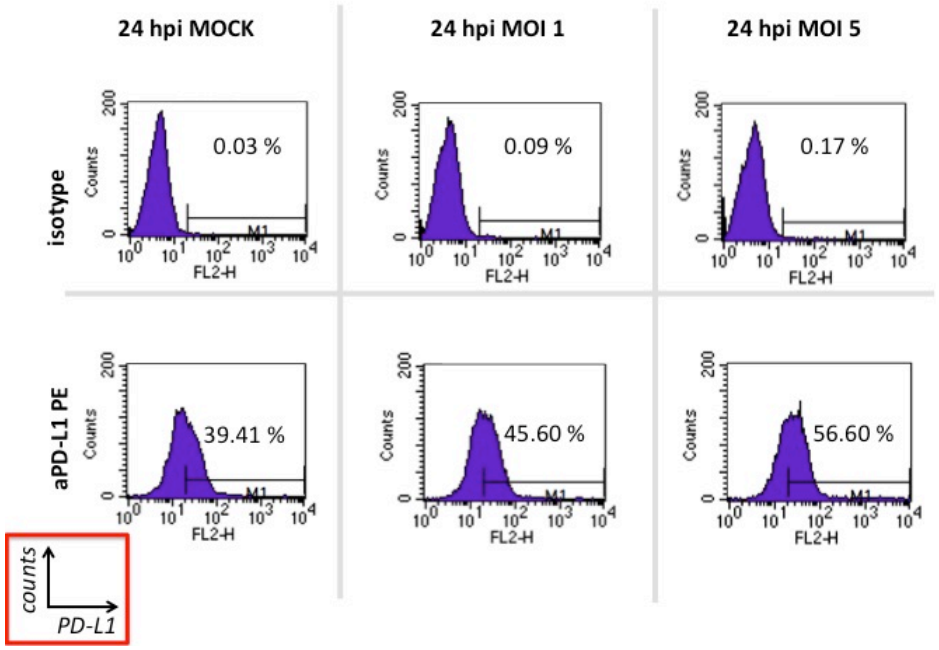

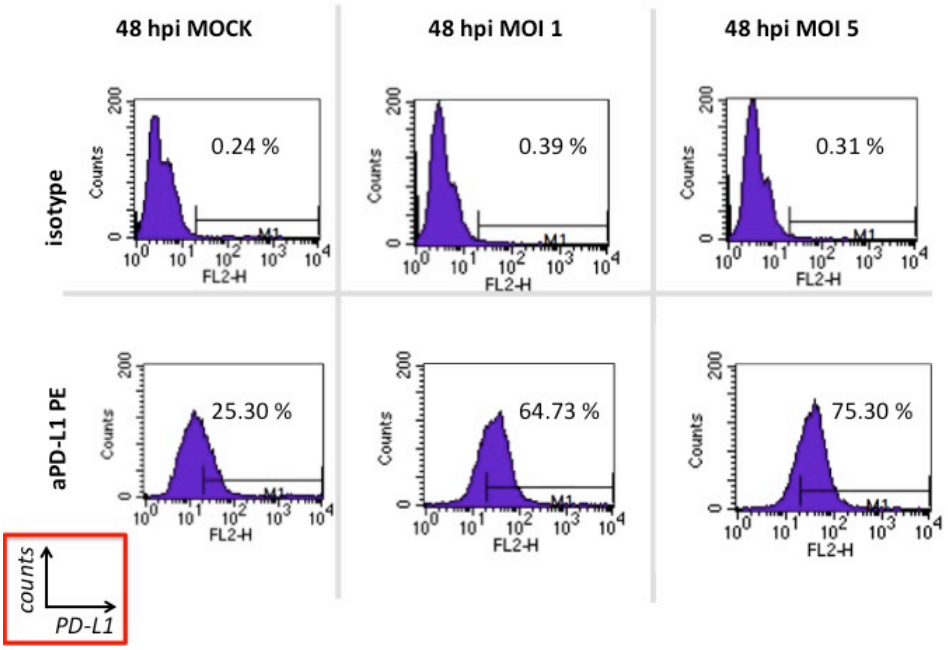

PD-L1 expression, HT29, 24 / 48 hpi with MeV-SCD at different MOIs

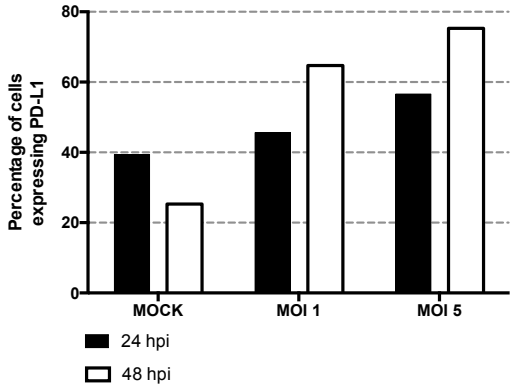

B) *PD-L1 expression on HCT-15 cells, infected with MeV-SCD*

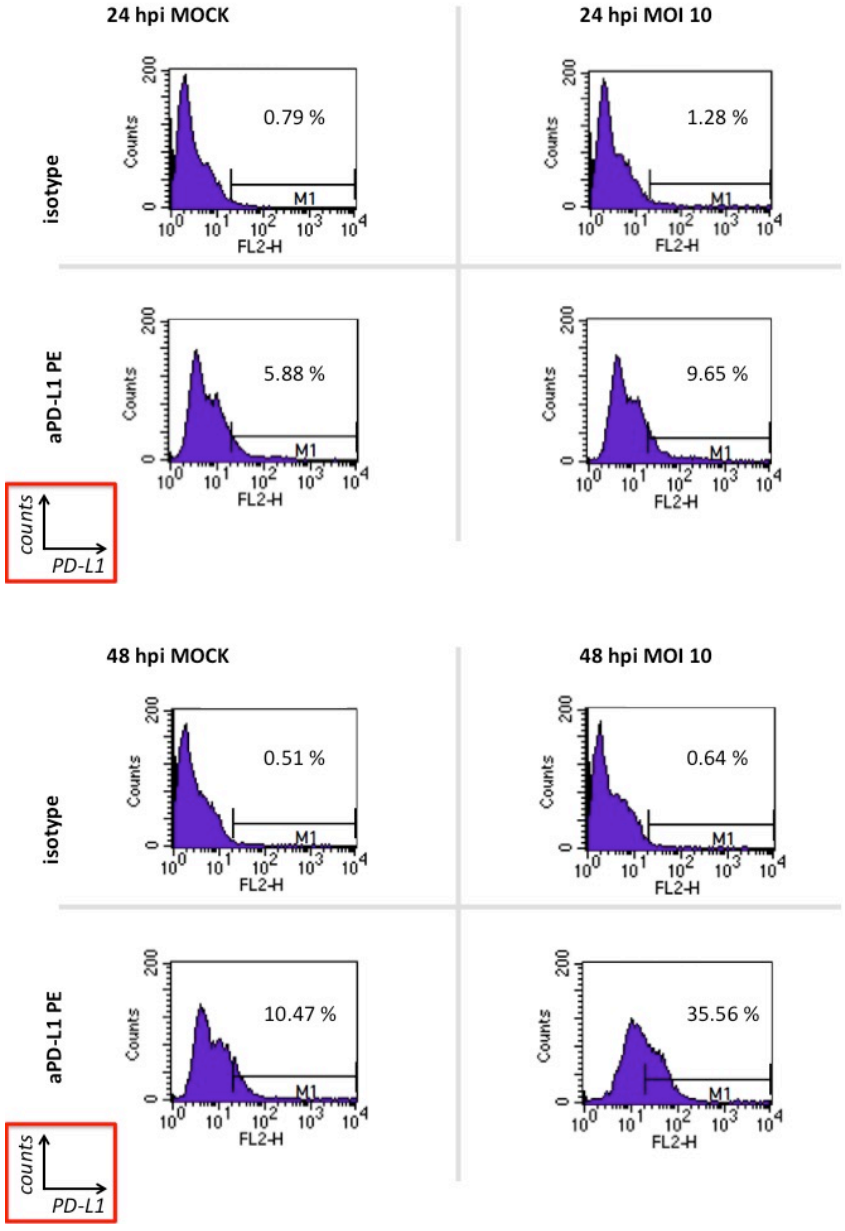

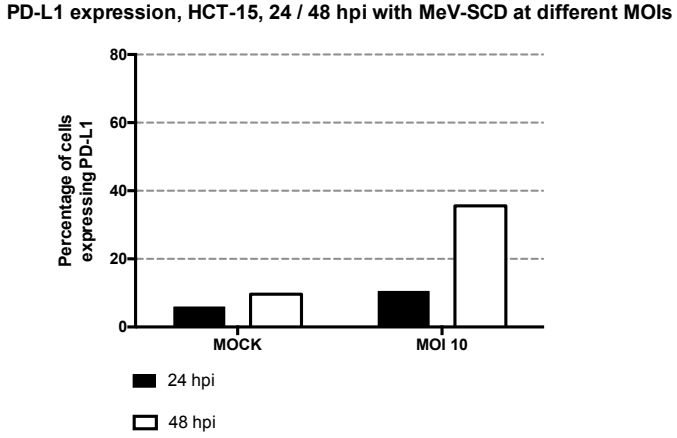

C) *PD-L1 expression on SW-620 cells, infected with MeV-SCD*

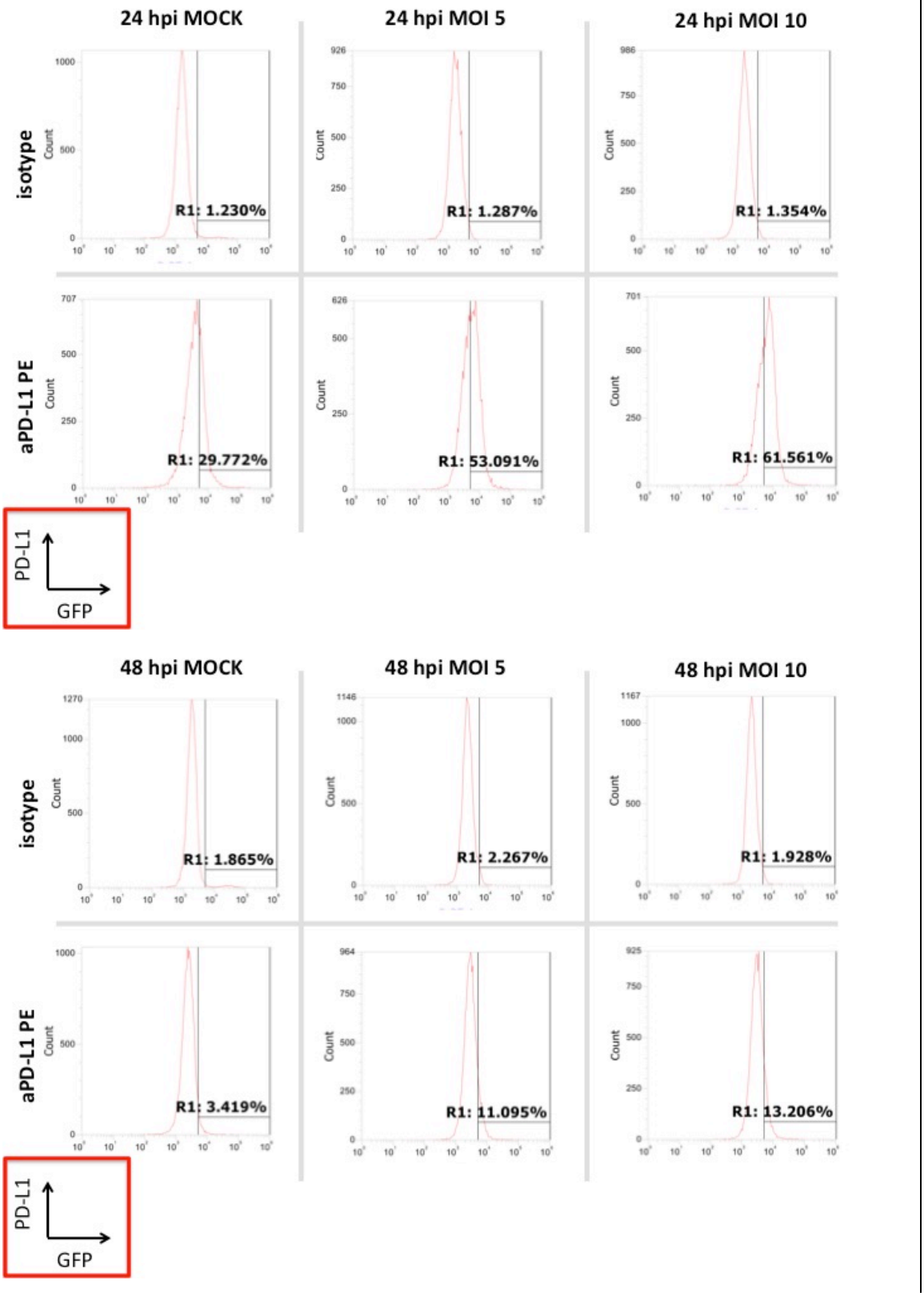

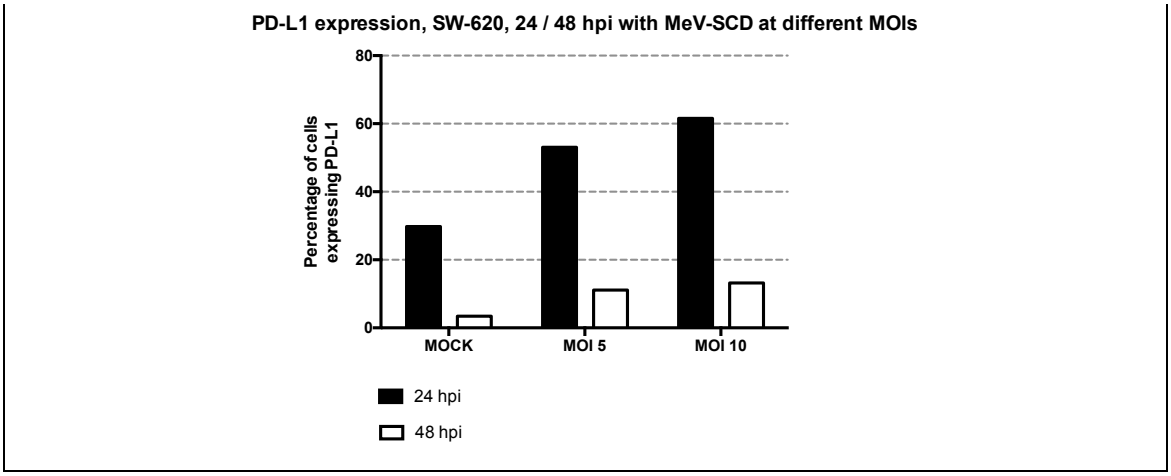

Figure 21, A - C: FACS analysis of PD-L1 expression on MeV-SCD-infected in comparison to MOCK-infected human colorectal cancer cell lines HT29, HCT-15 and SW-620

MeV-SCD-infection of CRC cells was performed using different MOIs (MOI 1 or MOI 5 for HT29, MOI 10 for HCT-15 and MOI 5 or 10 for SW-620), or cells were MOCK-infected. Staining for PD-L1 analysis was performed at 24 or 48 hpi. Tumor cells were labeled with PE anti-human CD274 (aPD-L1 PE) or the respective PE IgG2b isotype control (isotype). In the graphs of HT29 and HCT-15, percentages of PD-L1 positive tumor cells, which were covered by the marker M1, are given. In the graphs of SW-620, percentages of PD-L1 positive tumor cells, covered by the region R1, are given.

Comparable to our results for MeV-GFP, we could show that infection with MeV-SCD increased PD-L1 expression in all three human CRC cell lines *in vitro*. Expression further rose with augmentation of MOI and time of culture after infection for HT29 and HCT-15, whereas in SW-620, expression rose with increase of MOI but not with augmentation of time of culturing after infection with MeV-SCD.

In HT29, an initial PD-L1 expression of 39.4 % of analyzed tumor cells at 24 hours after MOCK-infection could be increased to 56.6 % of tumor cells by MeV-SCD infection, using a MOI of 5. At 48 hpi, the initially lower level of PD-L1 positive HT29 cells, namely 25.3 % of analyzed MOCK-infected tumor cells, could be enhanced to a PD-L1 expression on 75.3 % of cells via MeV-SCD-infection at MOI 5, thus PD-L1 expression could be tripled by MeV treatment. Similar tendencies were observed with infection at a lower MOI of 1 (see Fig. 21, A).

In HCT-15, an initially very low PD-L1 expression level of 5.9 % of MOCK-infected tumor cells was augmented to 9.7 % of tumor cells by MeV-SCD-infection at MOI 10, analyzed at 24 hpi. At 48 hpi, the slightly increased level of 10.5 % in MOCK-infected cells mounted to 35.6 % by OV treatment, thus again, PD-L1 expression rate even more than tripled.

Finally, in SW-620 tumor cells, an initial PD-L1 expression of 29.8 % of analyzed cells was increased to 53.1 % 24 hpi at MOI 5 and further to 61.6 % at MOI 10. Referring to measurements at 48 hpi, an initial expression of 3.4 % of SW-620 tumor cells rose to 11.1 % at MOI 5 and to 13.2 % at MOI 10. Surprisingly, for SW-620 tumor cells, the dependency on time of culturing after OV infection was this time inverse in comparison to HT29 and HCT-15, as the PD-L1 expression in SW-620 CRC cells declined at 48 hpi for MOCK and both MOIs (see Fig. 21, C). However, this effect of decreased PD-L1 expression rates after an augmented time of cultivation could not be reproduced in our experiments comparing different culturing media (Fig. 18) or analyzing PD-L1 expression rates after MeV-GFP infection (Fig. 20 C).

Summing up, those *in vitro* findings of PD-L1 expression analysis after infection with MeV-SCD confirmed our hypothesis, based on experiments with MeV-GFP (described in 3.2.2), that measles OV infection could consistently increase expression of immune checkpoint ligand on all three CRC cell lines. Hence, these results promise success of an immunovirotherapeutic treatment approach for colorectal cancer, blazing a trail for ICI application by PD-L1 upregulation through MeV-treatment. Even the tumor cell line with very low basal PD-L1 expression rates, HCT-15, which, at the same time, had to deal with the highest MeV resistance rates, achieved PD-L1 expression rates of 35.6 % at 48 hpi with MeV-SCD at MOI 10, increased from only 5.9 % for MOCK-infected cells at 24 hpi.

Moreover, referring to HT29 tumor cells, the effect of PD-L1 upregulation via treatment with measles virotherapeutic could also compensate the trend of lower PD-L1 expression rates due to longer time of cultivation. Effects are visible when comparing measurement at 24 and 48 hours after treatment with MeV or MOCK-infection, as depicted in Fig. 18, 20 A and 21 A. Referring to the effects of Opti-MEM incubation instead of cultivation in standard DMEM + 10 % FCS medium (see 3.2.1), PD-L1 expression on HT29 tumor cells was augmented about 1.7-fold by Opti-MEM, whereas MeV-SCD-infection could even triple PD-L1 expression rates, both analyzed at 48 hours after infection or after Opti-MEM incubation.

3.3. FACS analysis of PD-1 expression on NK cell populations from different healthy donors

PD-1 / PD-L1 interaction displays the therapeutic target for both immune checkpoint inhibitors *nivolumab* and *atezolizumab*. Thus, after upregulation of PD-L1 on human CRC cell lines HT29, HCT-15 and SW-620 through MeV-GFP- as well as MeV-SCD-infection could be proven, expression of immune checkpoint receptor PD-1 on CD56 positive NK cell populations was investigated. NK cells and PBMC were a friendly gift from AG Salih, Tübingen, and had been isolated from four different healthy donors, labeled #1 to #4. Furthermore, NK cells from donor #3 and PBMC from donor #2 were used for coincubation in xCELLigence analysis of HCT-15 tumor cells later (Fig. 24 A - G).

PD-1 expression on NK cell populations from different healthy donors

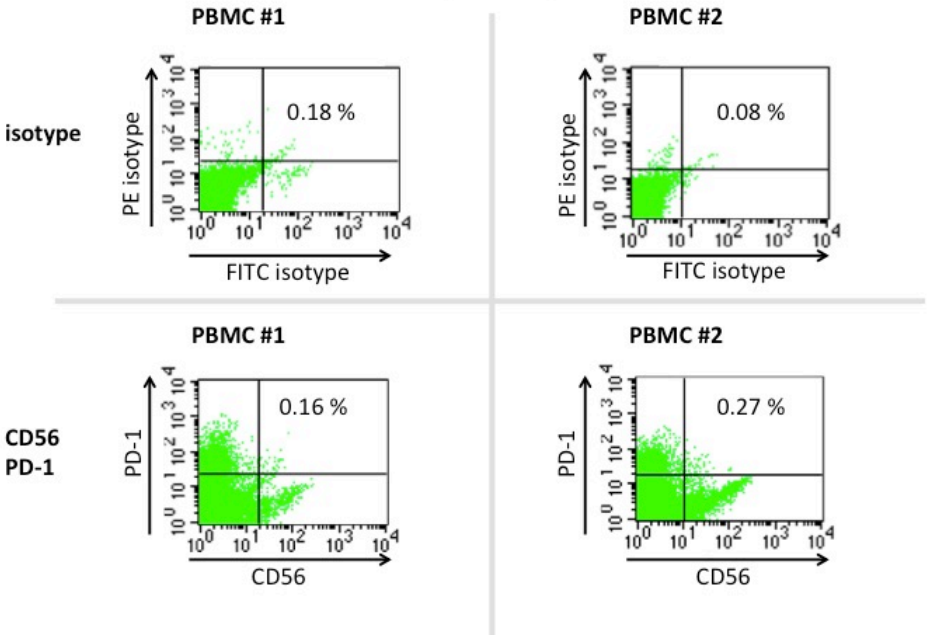

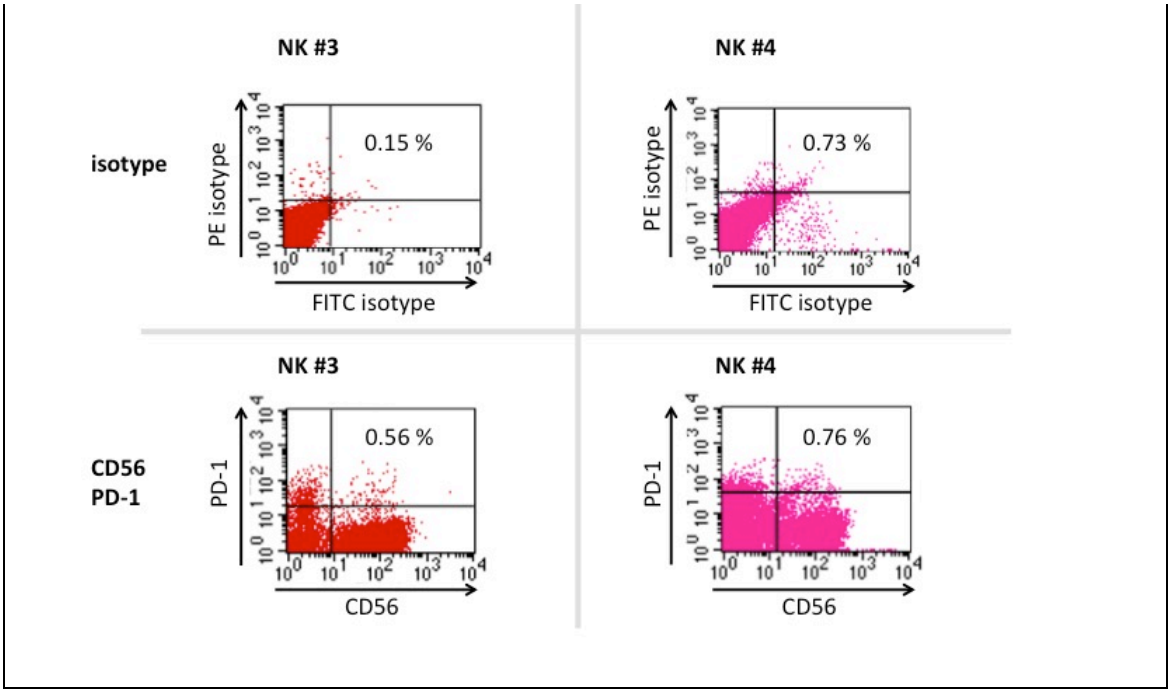

Figure 22: FACS analysis of PD-1 expression on NK cell populations from different healthy donors

PD-1 expression was analyzed on CD56 positive NK cell subsets from NK cells or from cultured PBMC, both from different healthy donors identified with #1 to #4. NK cell subsets were stained with FITC anti-human CD56 and PE anti-human CD279 (PD-1) or the respective FITC / PE IgG1 isotype controls. In the dot plots, percentages of both CD56 and PD-1 positive cells are given.

Table 15: FACS analysis of PD-1 expression on NK cell populations from different healthy donors

The percentages of CD56 positive, PD-1 positive and both CD56 and PD-1 positive cells are given.

	CD56 positive [%]	PD-1 positive [%]	CD56 and PD-1 positive [%]
PBMC #1	2.33	15.1	0.16
PBMC #2	8.32	11.59	0.27
NK #3	87.17	2.45	0.56
NK #4	36.72	3.51	0.76

FACS analysis of PBMC from donor #1 resulted in 2.3 % of CD56 positive cells, representing a NK cell subset; but only 0.2 % of analyzed cells were also positive for PD-1. Altogether, 15.1 % of PBMC expressed PD-1.

PBMC from donor #2 showed a higher proportion of CD56 positive cells, namely 8.3 % of cells; but again, only 0.3 % of analyzed PBMC were simultaneously expressing PD-1 and CD56. From the whole entity of PBMC, 11.6 % were positive for PD-1.

The NK cells from donor #3 consisted of 87.2 % of CD56 positive cells; and 0.6 % of these were also positive for PD-1. PD-1 expression of the overall cell population was measured in 2.5 % of investigated cells.
The NK cells from donor #4 possessed only 36.7 % CD56 positive cells, maybe as a result of a shorter time of cultivation after preparation from blood samples. 0.8 % of these NK cells were double positive for CD56 and PD-1, whereas 3.5 % of the whole cell population was only PD-1 positive.
Summing up, neither the CD56 positive cell subset of PBMC nor the CD56 positive expanded NK cells were found to have more than 1 % of PD-1 positive cells as a pre-condition to take place in a direct PD-1 / PD-L1 interaction. Yet, it should be considered that only the CD56 positive NK cell subset was investigated for PD-1 expression. Namely, PD-1 expression on overall PBMC or NK cells ranged from 2.5 % to 15.1 %.

3.4. In vitro therapeutic effects of combining MeV-GFP with immune checkpoint inhibitors and immune cell coculture in human colorectal carcinoma cell lines

xCELLigence real-time cell proliferation assay was used for analysis of the anti-tumor effects of the three different therapeutics measles vaccine virus, immune cells and ICI in monotherapy, as well as the effects of combined treatment with (i) measles vaccine virus plus ICI, (ii) measles vaccine virus plus immune cells, (iii) immune cells plus ICI and (iv) measles vaccine virus plus immune cells plus ICI.

For analysis, the two human CRC cell lines HT29 and HCT-15 were chosen, representing a MeV-GFP-susceptible as well as a MeV-GFP-resistant tumor cell line. The suitable tumor cell counts for the E-plates, MOIs as well as effector : target (E : T) ratios were established in multiple test runs (not shown here). For cell counts, it had to be taken into account that tumor cells remained in an exponential growth phase over the measurement period of 130 hours. MOIs as well as E : T ratios were selected accordingly that monotherapy did not lead to a complete tumor cell killing, making it possible to observe potential additional therapeutic effects of the combined treatment approaches.
The influence of MHC mismatch between human tumor cell lines and different healthy immune cell donors posed a problem in examination of the suitable E : T ratios and had to be considered when comparing individual xCELLigence runs.

3.4.1. xCELLigence real-time cell proliferation assay for analysis of HT29 / HCT-15 growth and viability under the influence of MeV-GFP-infection together with nivolumab and / or atezolizumab treatment

First of all, it was examined whether addition of ICI *nivolumab* or *atezolizumab* alone could improve therapeutic effects in uninfected CRC cells or in tumor cells infected with the virotherapeutic MeV-GFP.

In general, a supposable improvement of therapeutic effect has to be equated with a decrease of the cell index (CI), being influenced by tumor cell growth as well as tumor cell viability over the measurement period as described in 2.7.

A) *HT29 (5.000 cells / well), infected with MeV-GFP (MOI 2.5) or MOCK-infected, together with ICI atezolizumab or nivolumab*

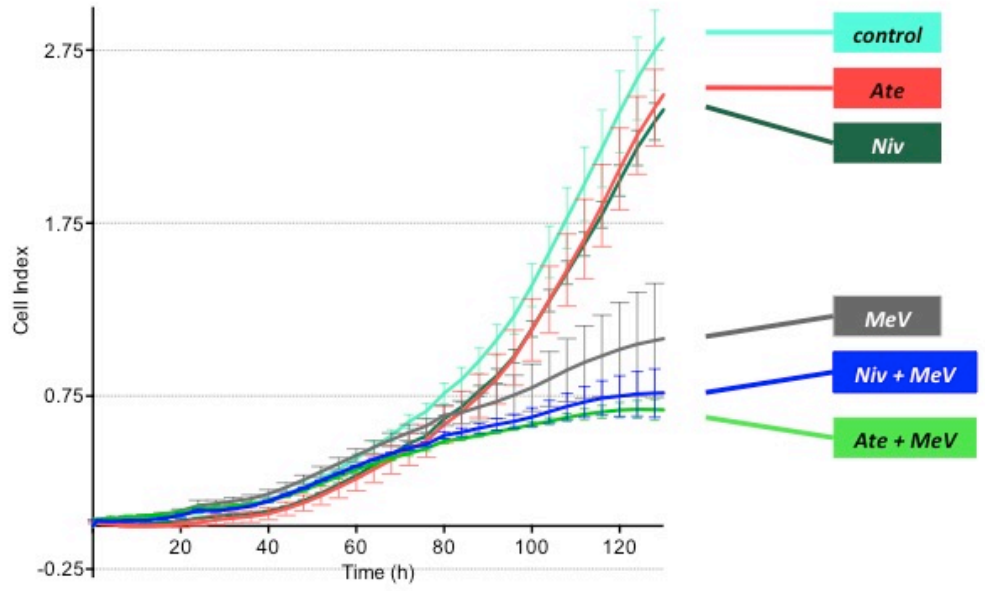

***B)** HCT-15 (2.500 cells / well), infected with MeV-GFP (MOI 10) or MOCK-infected, together with ICI atezolizumab or nivolumab*

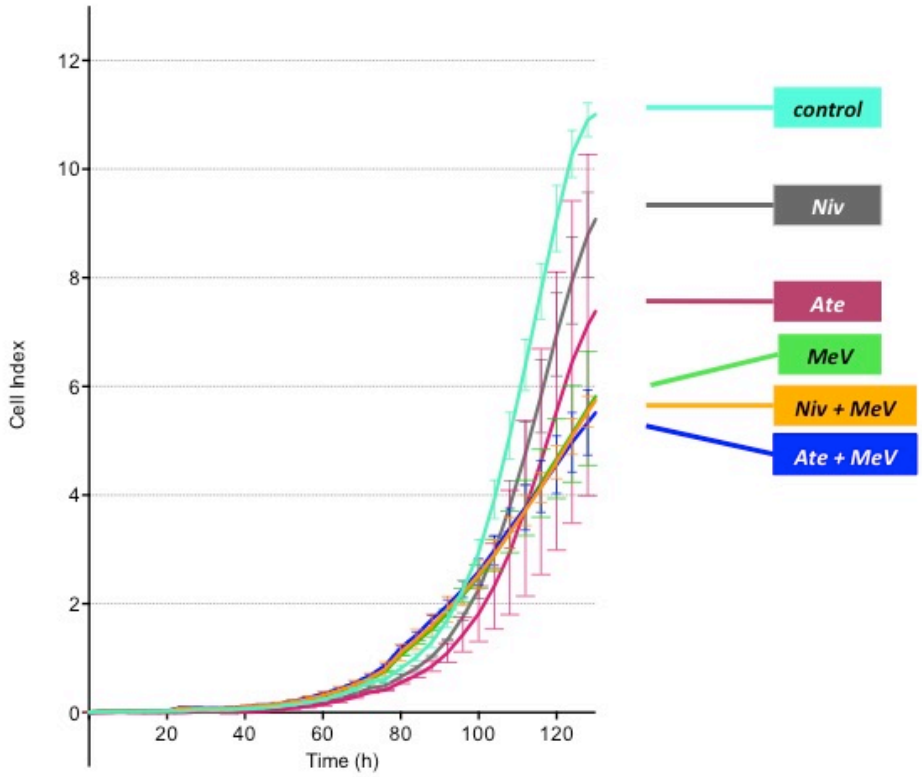

Figure 22 A - B: xCELLigence real-time assay of HT29 and HCT-15 growth and viability under treatment with MeV-GFP and / or immune checkpoint inhibitors
xCELLigence real-time cell monitoring assay was used to investigate growth and viability of CRC cells over a period of 130 hours under the influence of treatment with MeV-GFP, ICI, or a combination of both. 21 hours after plating of tumor cells, infection with MeV-GFP at the respective MOI (MOI 2.5 for HT29 and MOI 10 for HCT-15) or MOCK infection took place. 51 hpi, nivolumab or atezolizumab were added in a concentration of 5 µg / ml each.
The cell index (CI) is shown as a function of time. Measurement took place in triplets; means and SD are shown. For each tumor cell line, one representative experiment is shown.
Niv = nivolumab, Ate = atezolizumab, MeV = MeV-GFP.

In HT29, treatment with the measles virotherapeutic MeV-GFP more than halved the colorectal tumor cell growth and viability in comparison to controls after 130 hours.

Relating to the addition of ICI to uninfected tumor cells, curves of *atezolizumab* and *nivolumab* were almost identical. A slight trend towards CI decrease compared to the control curve could be observed. The same applied for ICI addition to MeV-GFP-infected HT29 tumor cells, where only a trend of CI decrease could be recorded by both *atezolizumab* and *nivolumab*.

To recapitulate, neither *atezolizumab* nor *nivolumab* could achieve a significant impairment of HT29 tumor growth and viability in a model without immune cells, as expected.

In HCT-15, similar results could be observed. Addition of MeV seemed to change growth kinetics throughout measurement: Between 21 hours and about 80 hours after start of xCELLigence recording, the MeV curve rose earlier than the MOCK curve, whereas in the period between 80 hours and 130 hours, the steepness of the MeV curve clearly decreased in comparison to MOCK control. Thus, after 130 hours of measurement, the CI of infected tumor cells was almost halved in comparison to control, although HCT-15 had been considered highly resistant to MeV-GFP-mediated oncolysis in SRB assays (displayed in 3.1.1).

In uninfected HCT-15, addition of each *nivolumab* and *atezolizumab* lead to a decrease of CIs, but in both cases less than the CI reduction achieved through measles infection. Results of uninfected HCT-15 tumor cells treated with *atezolizumab* should be regarded under reserve, referring to the range of SD. In MeV-GFP-infected tumor cells, no impairment of growth and viability by ICI could be recorded, as the two curves of ICI-treated HCT-15 cells (*yellow* for *nivolumab* and *dark blue* for *atezolizumab*) were equal to that of the infected control (*light green* for MeV-GFP only).

To put it into a nutshell, xCELLigence analysis of HCT-15 could show a CI decrease through MeV treatment and a trend of CI reduction through ICI treatment in uninfected tumor cells, but no consistent CI decrease through ICI in MeV-GFP-infected tumor cells.

3.4.2. xCELLigence real-time cell proliferation assay for analysis of HT29 / HCT-15 growth and viability under the influence of MeV-GFP-infection, treatment with nivolumab and / or atezolizumab and PBMC or NK cell coculture

As previously performed without immune cells, the anti-tumor effects of our treatment approach with MeV and / or ICI were now investigated in human CRC cells under the influence of cocultivation with PBMC or NK cells. Thus, a PD-1 / PD-L1 interaction between tumor and immune cell was permitted, depicting a therapeutic possibility for ICI intervention.

A) *HT29 (5.000 cells / well), infected with MeV-GFP (MOI 2.5) or MOCK-infected, together with ICI atezolizumab and PBMC (E : T = 20 : 1)*

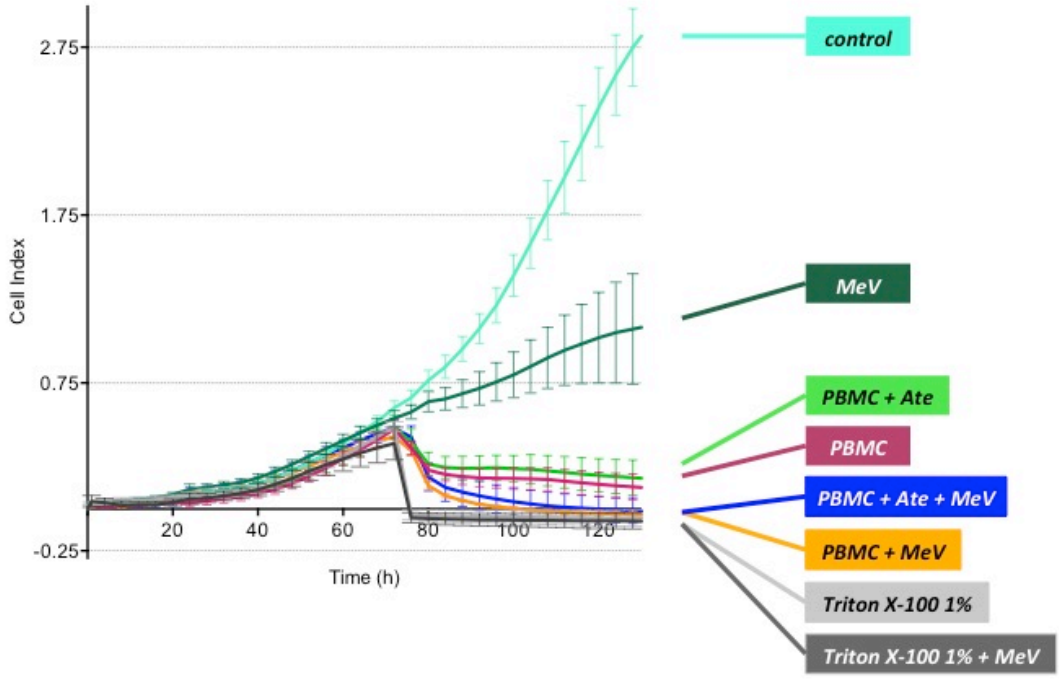

B) *HT29 (5.000 cells / well), infected with MeV-GFP (MOI 2.5) or MOCK-infected, together with ICI nivolumab and PBMC (E : T = 20 : 1)*

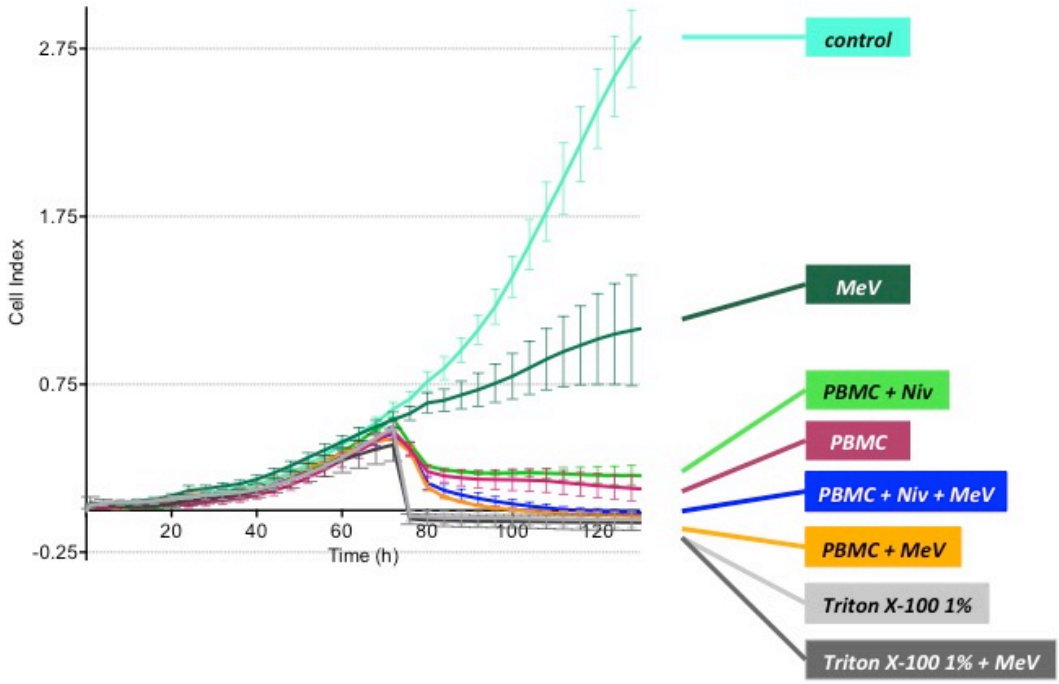

C) *HT29 (5.000 cells / well), infected with MeV-GFP (MOI 2.5) or MOCK-infected, together with ICI atezolizumab and nivolumab and PBMC (E : T = 20 : 1)*

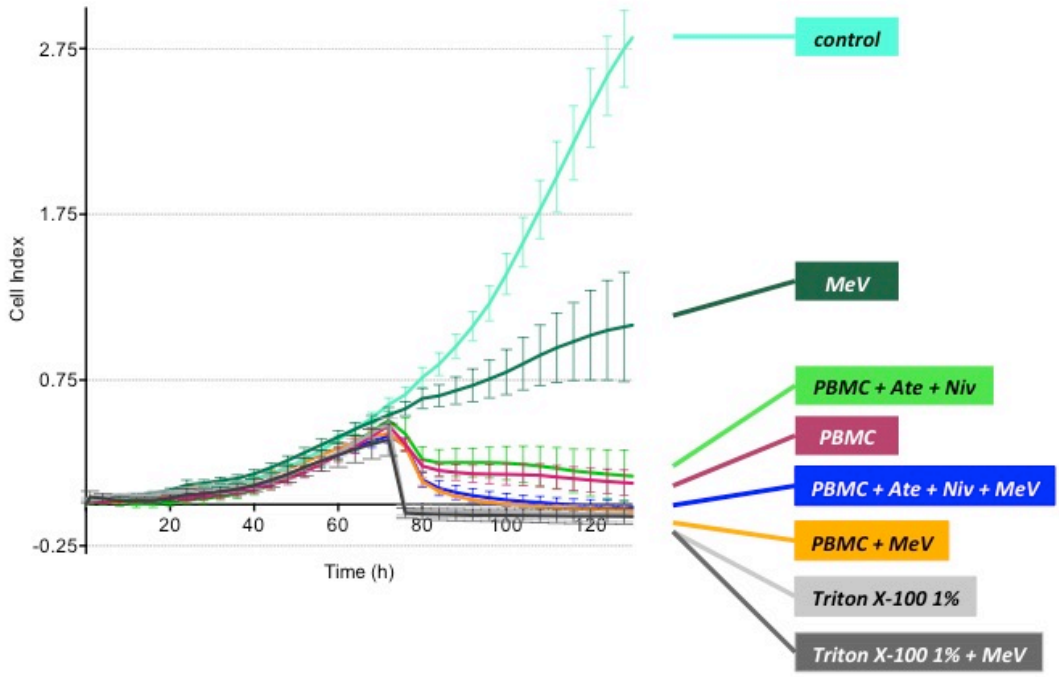

D) *HT29 (5.000 cells / well), infected with MeV-GFP (MOI 2.5) or MOCK-infected, together with ICI atezolizumab and NK cells (E : T = 2.5 : 1)*

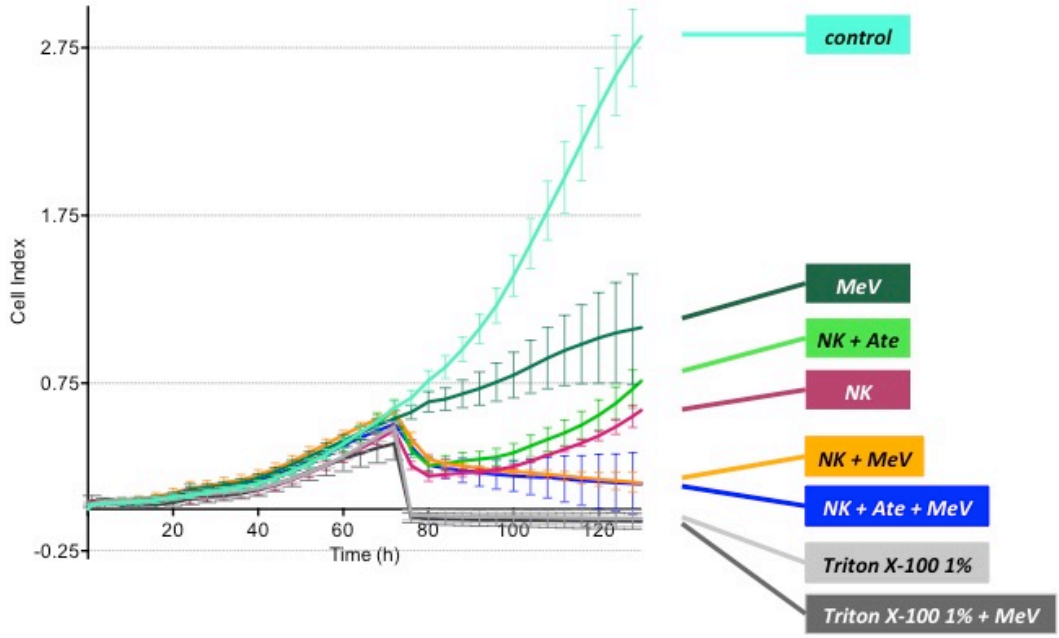

E) *HT29 (5.000 cells / well), infected with MeV-GFP (MOI 2.5) or MOCK-infected, together with ICI nivolumab and NK cells (E : T = 2.5 : 1)*

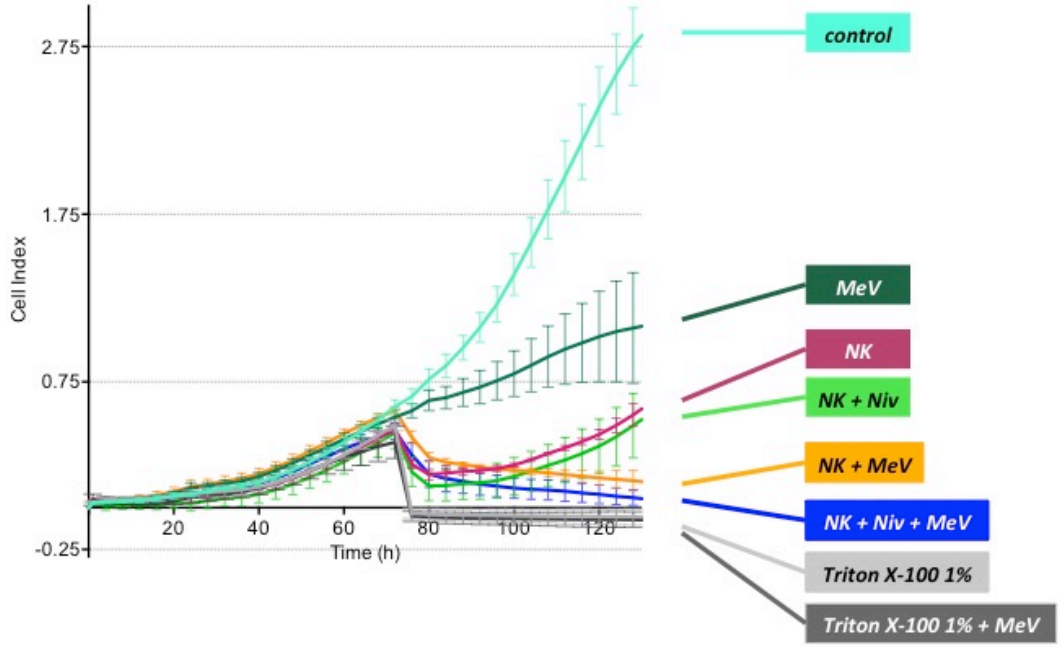

F) *HT29 (5.000 cells / well), infected with MeV-GFP (MOI 2.5) or MOCK-infected, together with ICI atezolizumab and NK cells (E : T = 1 : 1)*

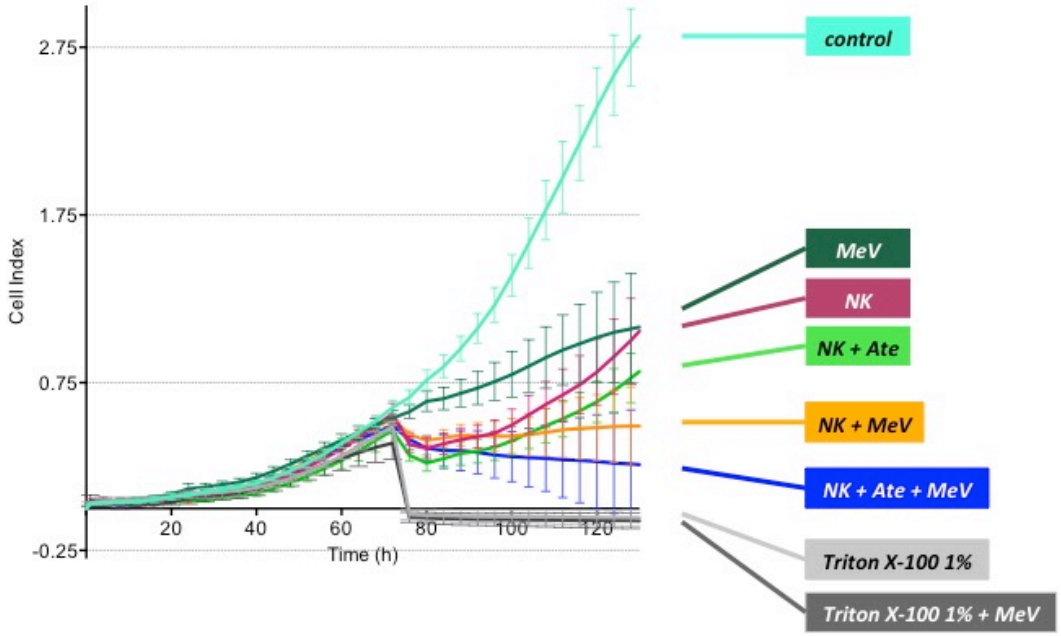

G) *HT29 (5.000 cells / well), infected with MeV-GFP (MOI 2.5) or MOCK-infected, together with ICI nivolumab and NK cells (E : T = 1 : 1)*

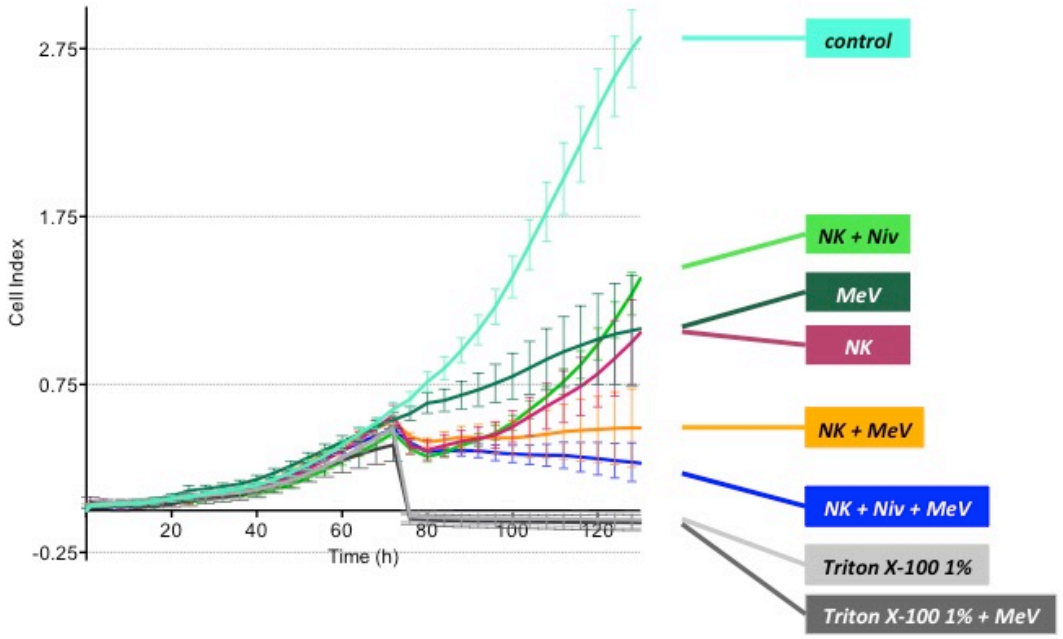

Figure 23, A - G: xCELLigence real-time assay of HT29 growth and viability under treatment with MeV-GFP, immune checkpoint inhibitors and PBMC / NK cells
xCELLigence real-time assay was used to investigate growth and viability of human CRC cells over a period of 130 hours under influence of a combination of MeV-GFP, treatment with ICI and PBMC or NK cell coculture.
21 hours after plating of 5.000 HT29 tumor cells per well, infection with MeV-GFP at MOI 2.5 or MOCK infection took place. 51 hpi, NK cells or PBMC, which both had optionally been incubated with 5 µg / ml of nivolumab and / or atezolizumab one hour before, were added at an E : T ratio of 20 : 1 for PBMC and 2.5 : 1 and 1 : 1 for NK cells. For control, 5 µg / ml atezolizumab or nivolumab were added without immune cell coincubation. PBMC and NK cells, as described in 2.3, had been purified from different healthy donors before and were a kind gift of AG Salih.
Triton X-100 1 % was used as a positive control for maximal tumor cell lysis.
The cell index (CI) is shown as a function of time. Measurement took place in triplets; means and SD are shown. For each tumor cell line, one representative experiment is shown.
Niv = nivolumab, Ate = atezolizumab, MeV = MeV-GFP, NK = NK cells.

In comparison to anti-tumor effects of measles virotherapeutic, the addition of PBMC at 51 hpi to uninfected HT29 CRC cells at an E : T ratio of 20 : 1 achieved an even higher grade of tumor cell mass and viability reduction in the respective xCELLigence run (see Fig. 23, A). Furthermore, PBMC together with MeV-GFP treatment even reached CI levels of the Triton X-100 1 % curve at about 100 hours after start of measurement, which displayed the control for maximal tumor cell killing.

Nevertheless, the further addition of the ICI *atezolizumab* under PBMC coincubation could improve tumor cell killing neither in uninfected, nor in MeV-infected HT29 colorectal tumor cells (see Fig. 23, A).

The same observations were made for *nivolumab*, the antibody targeted against PD-1, where ICI addition could again not further diminish HT29 tumor cell proliferation in comparison to treatment approaches with PBMC only, or PBMC together with oncolytic MeV-GFP (see Fig. 23, B).

Finally, referring to a combination therapy of *atezolizumab* and *nivolumab*, thus targeting both, immune checkpoint ligand as well as receptor, ICI addition was again comparable in its therapeutic effects to treatment with PBMC only or PBMC plus measles OV-infection (see Fig. 23, C).

Still, it should be considered that in the case of PBMC, possible therapeutic effects were rather exhausted, as the combination therapy consisting of immune cell coincubation together with MeV-GFP-treatment already achieved HT29 tumor cell reduction to a level of Triton X-100 1% control.

NK cell coincubation at an E : T ratio of 2.5 : 1 was examined next (see Fig. 23, D). Here, in comparison to PBMC addition, NK cells also reduced HT29 tumor cell mass and viability, especially in a first period up to about 80 hours after start of measurement (8 hours after addition of NK cells), whereas in a second period until the end of measurement after 130 hours, the CI increased again with prevailing HT29 tumor cell growth. Hence, in contrast to PBMC coincubation at E : T = 20 : 1, less HT29 tumor cell killing was observed through addition of NK cells at E : T = 2.5 : 1, keeping in mind the descent of different donors and, thus, diversity of MHC mismatch.

Similar to PBMC, NK cell coincubation of MeV-GFP-infected HT29 tumor cells even further decreased tumor cell mass over the whole measurement period. In contrast to NK cell coincubation only, this time no recrudescence of tumor growth did appear.

However, considering the additional treatment with an ICI, *atezolizumab* once more could not improve anti-tumor effects in uninfected or MeV-GFP-infected HT29 CRC cells under coculture with NK cells.

Nivolumab together with NK cell coincubation (E : T ratio 2.5 : 1) of uninfected HT29 tumor cells did not show a consistent, sustained increase of tumor cell killing compared to NK cells only, which also applied for measles-infected HT29 tumor cells (see Fig.

23, E). Yet, a tendency of additional therapeutic gain through *nivolumab* application could be described in both MOCK- and MeV-GFP-infected HT29 tumor cells under NK cell cocultivation.

As already found out for the higher E : T ratio, NK cell coincubation at an E : T ratio of 1 : 1 achieved an early tumor cell proliferation reduction until 80 hours after start of measurement, followed by a second phase of tumor cell proliferation increase, so that the NK cell curve finally met the end point of the MeV-GFP curve (see Fig. 23, F).

This time, addition of ICI, here *atezolizumab*, could attain a trend of tumor cell mass reduction in comparison to NK cells only, both in uninfected and MeV-GFP-infected HT29 tumor cells. Hence, the combination therapy of NK cells, measles virotherapeutic and anti-PD-L1 antibody was observed to reach best therapeutic results in this experiment. Still, the therapeutic effects could not accomplish those of using the higher E : T ratio of 2.5 : 1 in combination with ICI and measles OV.

The last experimental setting with HT29 tumor cells tested the combination of NK cells at the lower E : T ratio of 1 : 1, MeV-GFP and *nivolumab* (see Fig. 23, G). ICI addition could again achieve a trend of improved tumor cell killing in the context of a triple therapy. Results were approximately comparable with the therapeutic effects of the same combination, only with *atezolizumab* instead of *nivolumab*. However, this trend could not be observed in uninfected tumor cells, where *nivolumab* together with NK cells acted even worse than NK cells only, thus achieving a lower therapeutic effect than MeV in monotherapy.

***A)** HCT-15 (2.500 cells / well), infected with MeV-GFP (MOI 10) or MOCK-infected, together with ICI atezolizumab and PBMC (E : T = 10 : 1)*

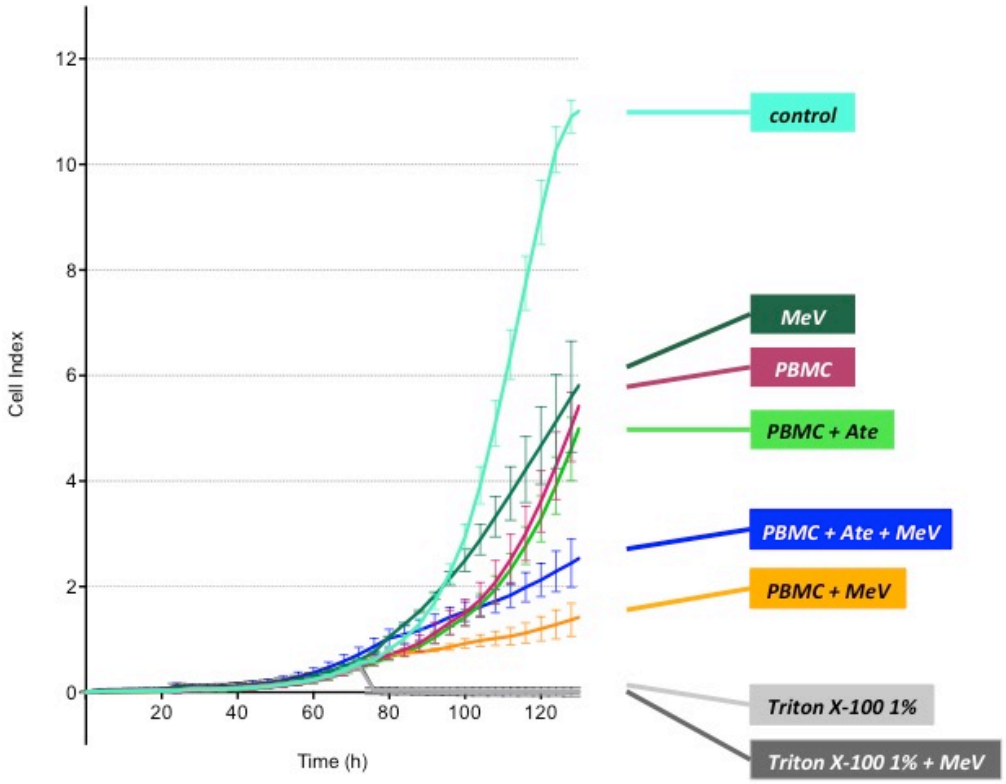

B) *HCT-15 (2.500 cells / well), infected with MeV-GFP (MOI 10) or MOCK-infected, together with ICI nivolumab and PBMC (E : T = 10 : 1)*

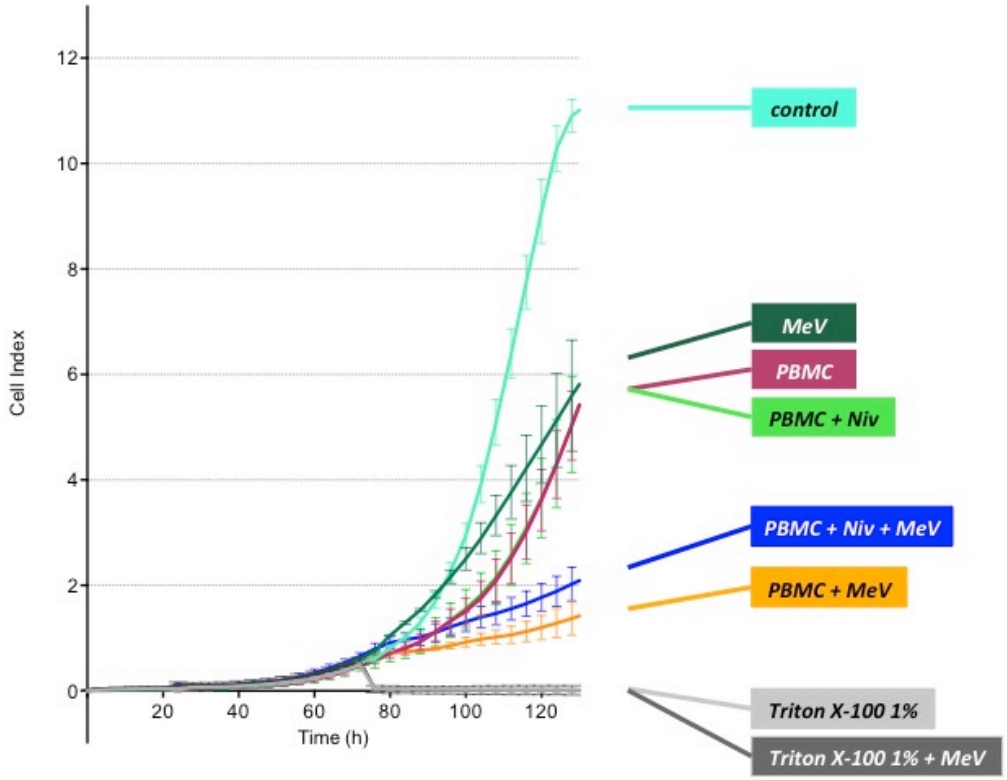

C) *HCT-15 (2.500 cells / well), infected with MeV-GFP (MOI 10) or MOCK-infected, together with ICI atezolizumab and NK cells (E : T = 1 : 1)*

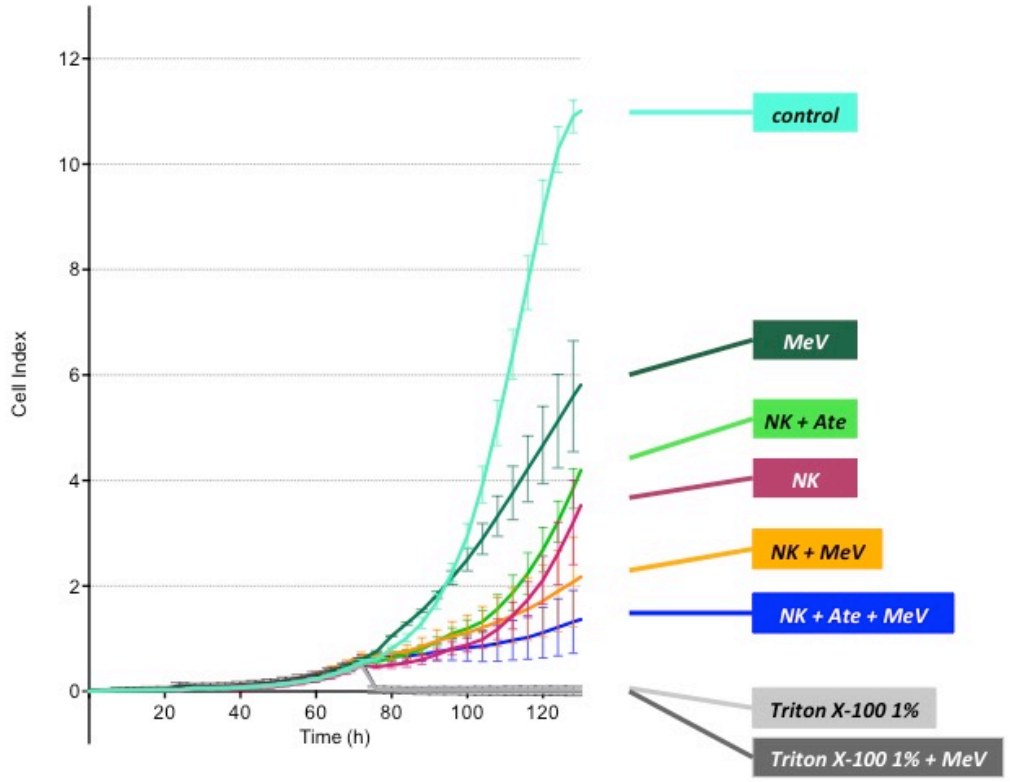

D) *HCT-15 (2.500 cells / well), infected with MeV-GFP (MOI 10) or MOCK-infected, together with ICI nivolumab and NK cells (E : T = 1 : 1)*

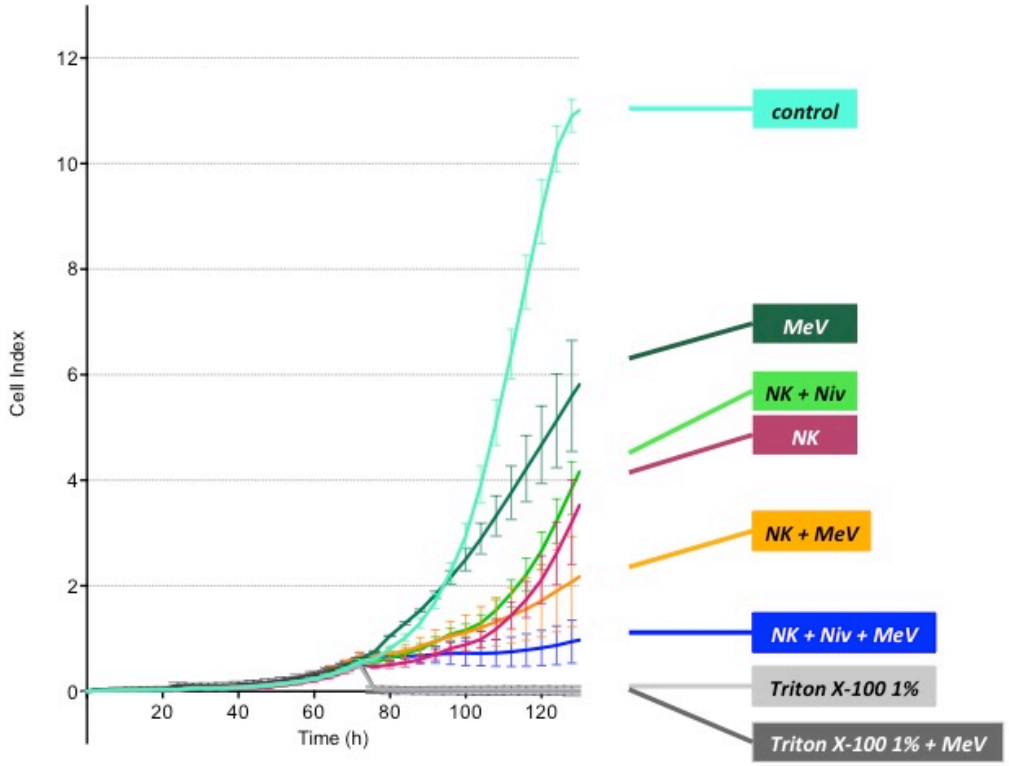

E) *HCT-15 (2.500 cells / well), infected with MeV-GFP (MOI 10) or MOCK-infected, together with ICI atezolizumab and nivolumab and NK cells (E : T = 1 : 1)*

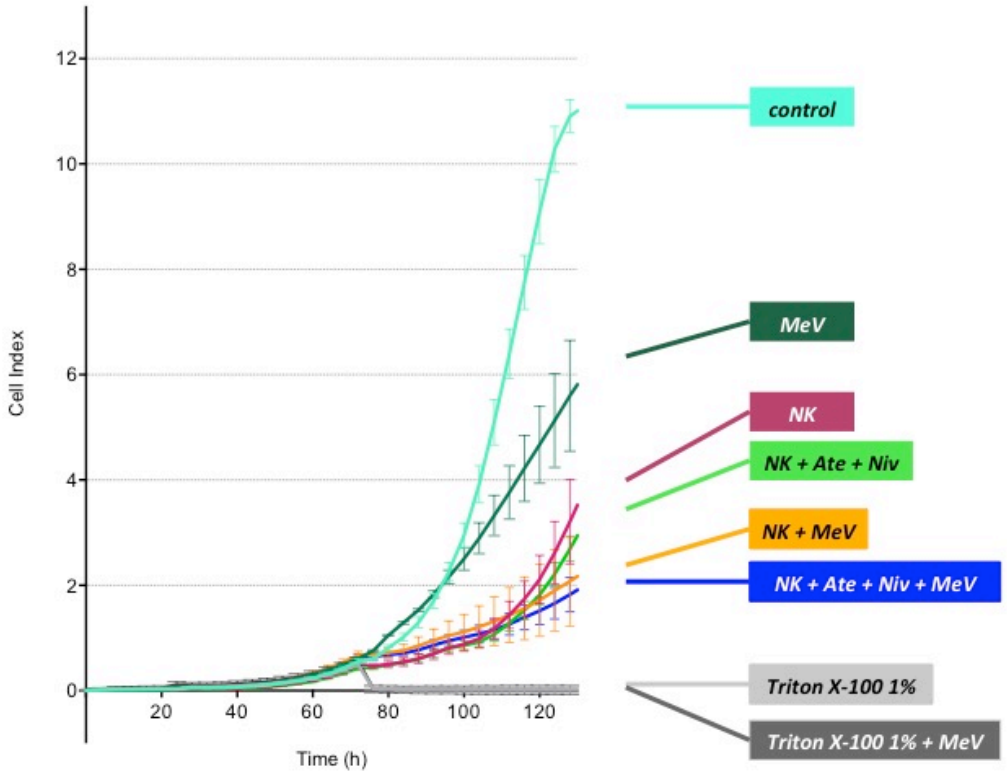

F) *HCT-15 (2.500 cells / well), infected with MeV-GFP (MOI 10) or MOCK-infected, together with ICI atezolizumab and NK cells (E : T = 0.5 : 1)*

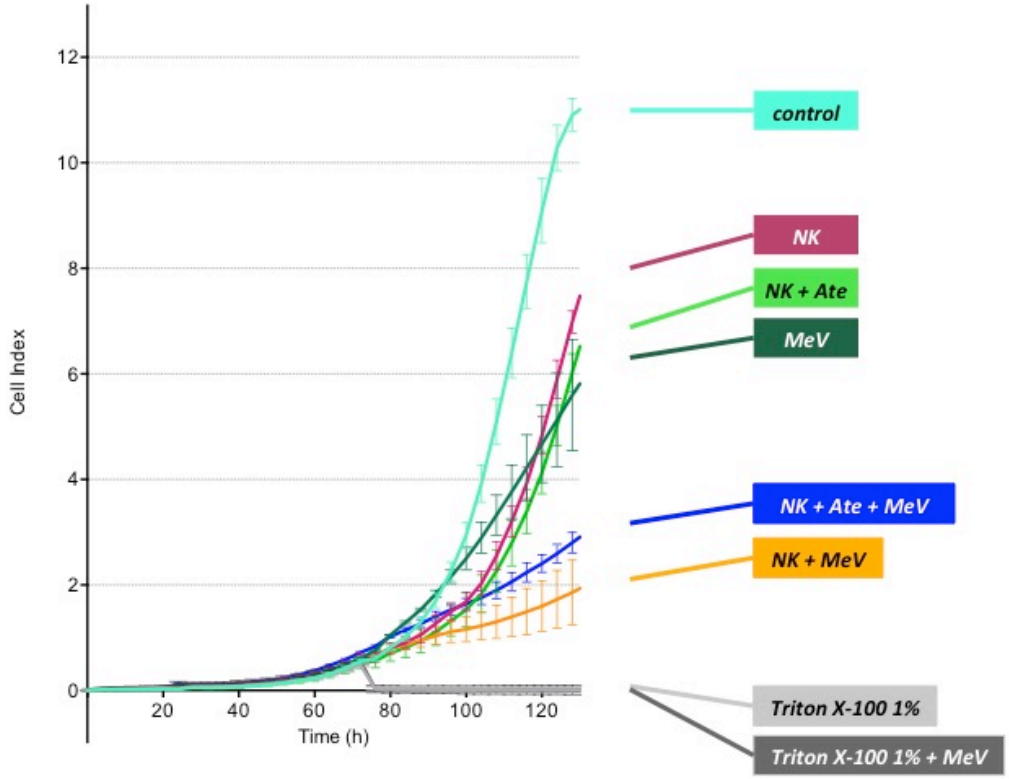

G) *HCT-15 (2.500 cells / well), infected with MeV-GFP (MOI 10) or MOCK-infected, together with ICI nivolumab and NK cells (E : T = 0.5 : 1)*

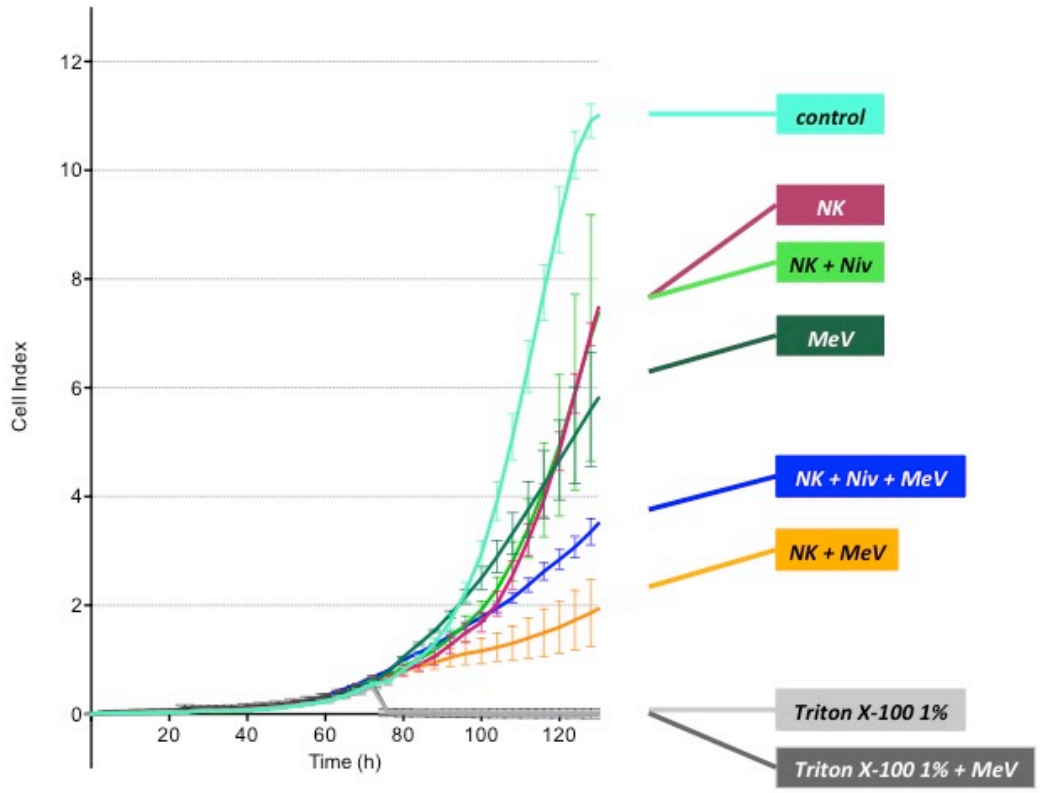

Figure 24, A - G: xCELLigence real-time cell proliferation assay of HCT-15 growth and viability under treatment with MeV-GFP, immune checkpoint inhibitors and PBMC / NK cell coculture

xCELLigence real-time cell monitoring assay was used to investigate growth and viability of human CRC cells over a period of 130 hours under influence of a combination of MeV-GFP, treatment with ICI and PBMC or NK cell coculture.
21 hours after plating of 2.500 HCT-15 tumor cells per well, infection with MeV-GFP at MOI 10 or MOCK infection took place. At 51 hpi, NK cells or PBMC, which both had optionally been incubated with 5 µg / ml of nivolumab and / or atezolizumab one hour before, were added at an E : T ratio of 10 : 1 for PBMC and 1 : 1 or 0.5 : 1 for NK cells. As a control, atezolizumab or nivolumab were added without immune cell coincubation. PBMC and NK cells, as described in 2.3, had been purified from different healthy donors before and were a kind gift of AG Salih.
The cell index (CI) is shown as a function of time. Measurement took place in triplets; means and SD are shown. For each tumor cell line, one representative experiment is shown.
Niv = nivolumab, Ate = atezolizumab, MeV = MeV-GFP, NK = NK cells.

The second CRC cell line tested in xCELLigence together with immune cell coincubation, measles virotherapeutic and ICI was HCT-15.

PBMC at an E : T ratio of 10 : 1 achieved tumor cell killing comparable to MeV-GFP-addition, referring to the end point of measurement (see Fig. 24, A). In this experimental subset, the treatment regimen of PBMC plus MeV-GFP-infection revealed

as the most efficient combination concerning oncolysis. Namely, after 130 hours of xCELLigence analysis, the analyzed CI of the double therapy amounted roughly $^1/_6$ of the CI of untreated control. Yet, the maximal tumor cell killing of Triton X-100 1 % could not be reached by any therapeutic regimen.

On the other hand, *atezolizumab* could not further strengthen tumor cell killing in uninfected tumor cells with the two curves for PBMC only and PBMC plus *atezolizumab* running almost identically. In MeV-GFP-infected cells, *atezolizumab* even worsened the anti-tumor effect of PBMC coincubation (also see Fig. 24, A).

Results with PD-1-targeting *nivolumab* were comparable to those with *atezolizumab (see Fig. 24, B)*. Best effects in tumor cell killing were achieved with the combination PBMC plus MeV-GFP, whereas ICI addition accomplished less tumor reduction (PBMC plus MeV-GFP plus *nivolumab*) or showed no therapeutic difference (PBMC plus *nivolumab*).

The next step was to examine the influence of ICI addition on therapeutic effects of a combination of NK cells at E : T ratio 1 : 1 and MeV-GFP virotherapeutic (see Fig. 24, C). In this case, NK cell-induced decrease of CI was more distinct than the measles-induced reduction. Still, the double treatment MeV plus NK cells achieved less therapeutic benefit in comparison to the findings in PBMC. Again, the combination NK cells plus MeV outplayed the two monotherapies in its therapeutic effect.

After addition of *atezolizumab*, a trend of further CI reduction could be observed in comparison to NK cells plus MeV only; but in uninfected cells, this trend was not consistent. Maximum therapeutic effects, this time induced by triple therapy, again achieved CI reduction to about $^1/_6$ of CI of control after 130 hours of analysis (also see Fig. 24, C).

With *nivolumab*, observations in xCELLigence analysis were mostly the same: A trend of further CI reduction via PD-1-targeting ICI became only apparent in MeV-GFP-infected HCT-15 tumor cells, but not in uninfected, where *nivolumab* addition induced a tendency of less therapeutic effect than NK cell coincubation alone (see Fig. 24, D). Still, the trend towards additional therapeutic use of ICI application as part of a triple combination therapy together with MeV and NK cells was observed slightly more noticeable than with *atezolizumab*, referring to Fig. 24 C.

Interestingly, application of both *atezolizumab* and *nivolumab* (see Fig. 24, E) could in turn not affirm a consistent trend of additional therapeutic effect in comparison to a regimen with NK cells plus MeV or to a treatment with NK cells only, which contradicted the findings of single ICI addition in Fig. 24 C and D.
Besides, reduction of the NK cell E : T ratio from 1 : 1 to 0.5 : 1 could also not reveal an improved therapeutic benefit of ICI addition (see Fig. 24, F). This time, NK cells could not reach the amount of tumor cell killing of MeV-GFP-treatment. Nevertheless, the combination of NK cells plus MeV was still very successful in CI reduction, again reaching a CI of roughly $^{1}/_{6}$ of the CI of untreated control after 130 hours of xCELLigence real-time analysis. In other words, combination therapy with MeV and NK cells at an E : T ratio of 0.5 : 1 could attain results in HCT-15 CRC treatment comparable to the same regimen with a higher E : T ratio of 1 : 1. Nonetheless, triple therapy with *atezolizumab* showed less therapeutic effect than the combination of OV and NK cells.
The same lack of improved therapeutic effects was observed after addition of *nivolumab* to the combination of MeV plus NK cells (E : T = 0.5 : 1) (see Fig. 24, G). In this case, tendency towards less anti-tumor efficacy became even more striking than for *atezolizumab* in Fig. 24 F.

To put it into a nutshell and recapitulate the findings of several xCELLigence runs, it could be observed in real-time cell viability and proliferation analysis of HT29 as well as HCT-15 tumor cell lines that (i) a treatment with MeV-GFP or immune cells considerably decreased CIs of both tumor cell lines and that (ii) a combined treatment of MeV-GFP infection and immune cell coincubation even resulted in additional reduction of CIs; but on the other hand, (iii) a combination of ICI (*nivolumab* and / or *atezolizumab*) in a triple therapeutic regimen together with measles virotherapeutic and immune cells could not further reduce tumor cell mass and viability in a consistent or sustainable way.

3.5. Quantification of antiviral effects of immune checkpoint inhibitors on the replication of MeV-GFP in human colorectal carcinoma cell lines

The therapeutic principle behind immune checkpoint blockade with *nivolumab* or *atezolizumab* is the inhibition of PD-1 / PD-L1 interaction, which physiologically initiates a downregulation of anti-tumor immunity. But on the other hand, such an ICI-induced stimulation of the human immune system might not only cause an efficient anti-tumor immune response, but also lead to an activation of immunological processes inhibiting viral spread and replication.

Necessarily, this aspect has also to be taken into account referring to MeV-GFP-based virotherapy in combination with anti-cancer immunotherapy. Thus, the influence of ICI on MeV-GFP replication in human CRC cell lines became focus of our investigations.

3.5.1. Quantification of antiviral effects of immune checkpoint inhibitors in a viral growth curve model on MeV-GFP-infected HT29 and HCT-15 tumor cells

In a first step, viral growth curves were used to analyze the effect of immune checkpoint blockade on MeV-GFP replication in infected human CRC cell lines. Due to limited access to ICI, *pembrolizumab* was used for viral growth curves instead of *nivolumab*, both targeting the immune checkpoint receptor PD-1. The MOIs used for measles-infection were selected accordingly to the different resistance patterns towards MeV-induced oncolysis, which had been investigated with SRB assays before (see 3.1.1).

The two tumor cell lines HT29 and HCT-15 were analyzed, which had also been used for xCELLigence analysis.

A) *Viral growth curves on MeV-GFP-infected HT29 (MOI 5)*

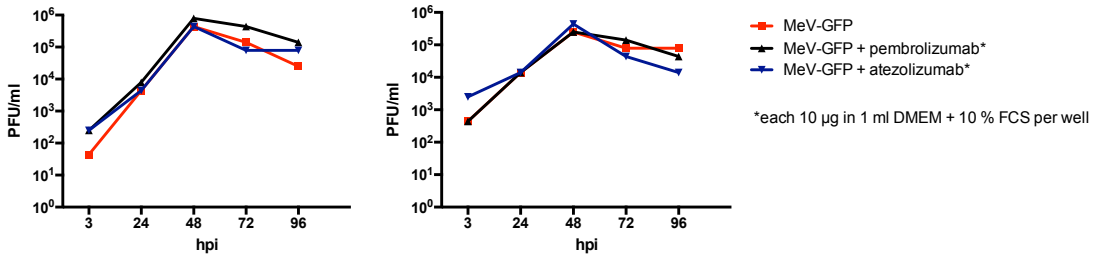

supernatants *lysates*

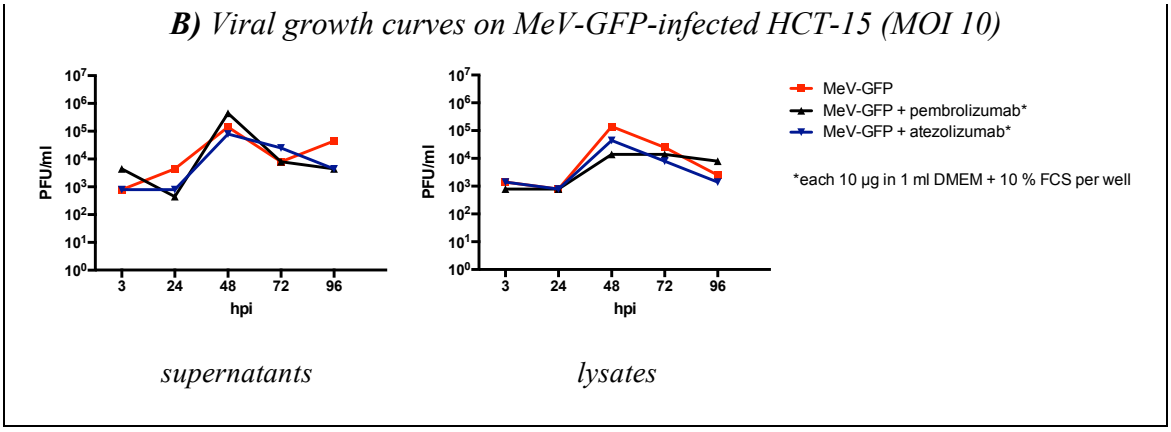

Figure 25, A - C: Quantification of antiviral effects of immune checkpoint inhibitors in a viral growth curve model on HT29 and HCT-15 tumor cells
For viral growth curves, supernatants as well as lysates of human CRC cells, which had been infected with MeV-GFP at MOIs of 5 or 10 before, were collected at 3, 24, 48, 72 and 96 hpi. ICIs pembrolizumab or atezolizumab (10 µg / ml) were added directly after infection. Titration was done on Vero cells.

First, kinetics of viral replication and virus release were examined in human colorectal cancer cells without further ICI treatment. Both colorectal tumor cell lines achieved a maximum of MeV-GFP-production and -release at 48 hpi. Amounts of virus detected in tumor cell lysates were approximately comparable to those in supernatants, referring to the samples taken at 3, 24, 48, 72 and 96 hpi. The decrease of titers at 72 and 96 hpi could be explained by reduction of tumor cell mass through oncolysis, hence equating to a diminished capacity of virus production machinery.

Virus titers reached 10^5 PFU / ml after infection at a MOI of 10 for HCT-15 and between 10^5 and 10^6 PFU / ml after infection at a MOI of 5 for HT29. These results could be expected, considering the different characteristics of resistance against MeV-induced oncolysis. Moreover, the findings were approximately comparable to results of viral growth curves of MeV-SCD in HCT-15, conducted in our working group by Noll et al. (Noll M., 2013).

Excluding the influence of NK cells or PBMC in this viral growth curve model, neither *pembrolizumab* nor *atezolizumab* influenced titers of MeV-GFP in supernatants or lysates of both tumor cell lines. These findings could exclude a direct influence of ICI on MeV-GFP replication kinetics or spread in the tested CRC cell lines.

3.5.2. Quantification of antiviral effects of immune checkpoint inhibitors in MeV-GFP-infected HT29 and HCT-15 tumor cells after immune cell cocultivation

In a next step, the influence of immune cell cocultivation was taken into account for analysis of the effects of ICI on viral replication and spread, so that the possibility of PD-1 / PD-L1 interaction between tumor cells and immune cells was given.

After MeV-GFP-infection of human CRC cells, viral titers were compared under different treatment conditions, including addition of ICI *nivolumab* and / or *atezolizumab*. For immune cell cocultivation, NK cells were used with an E : T ratio of 2.5 : 1; PBMC were applied with an E : T ratio of 10 : 1.

The two tumor cell lines HT29 and HCT-15 were analyzed, which had also been used for xCELLigence analysis.

HT29

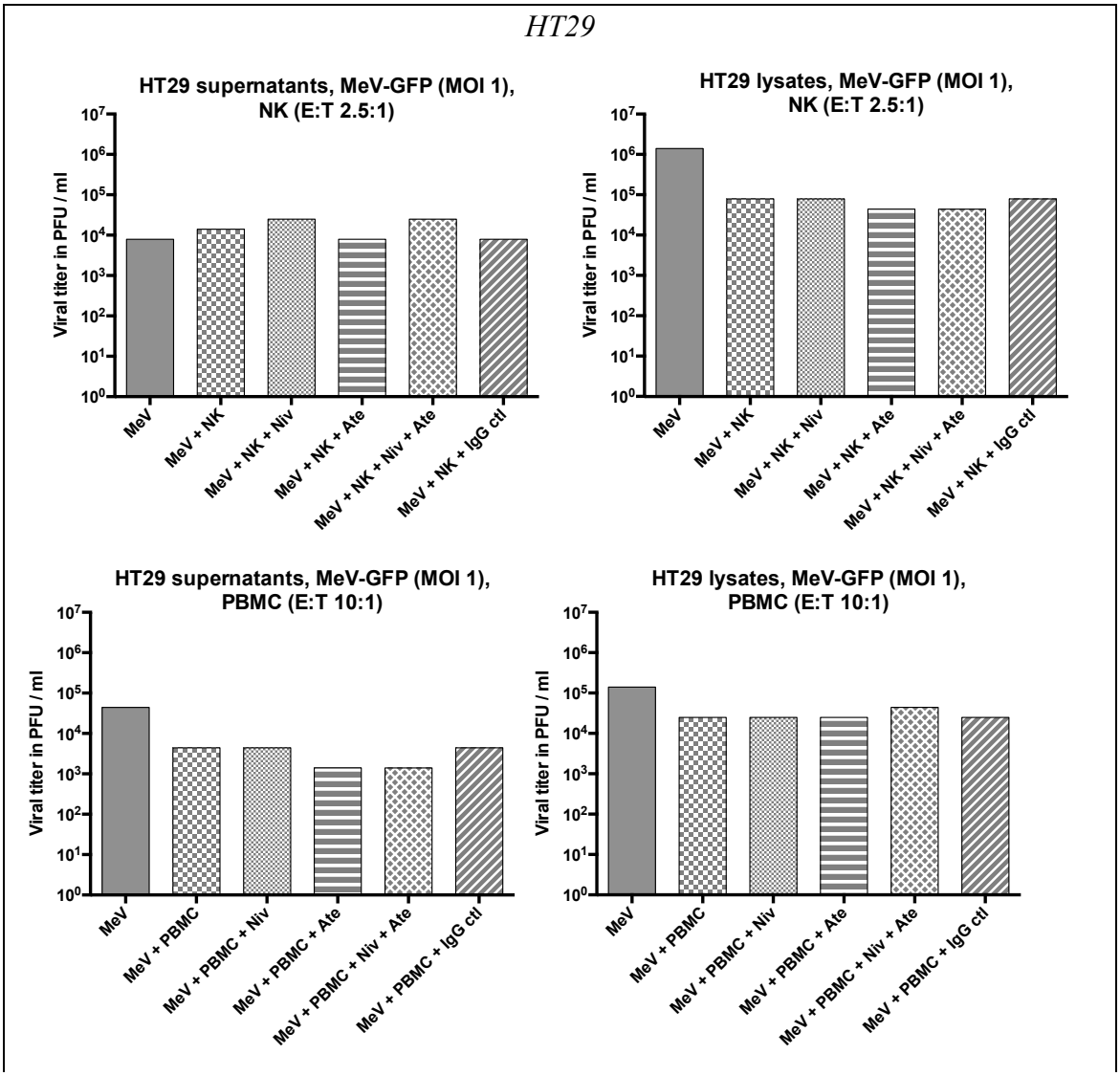

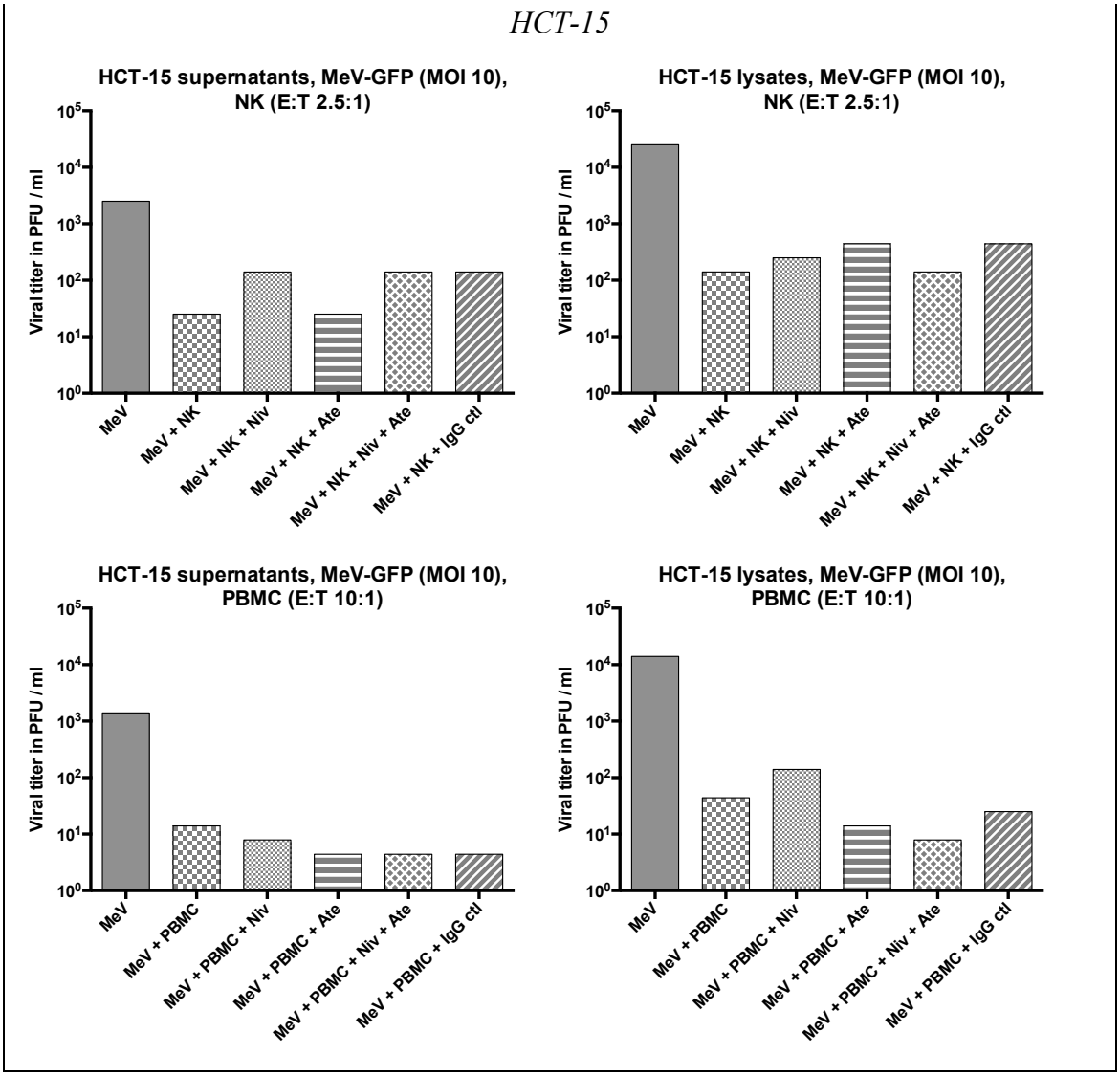

Figure 26: Quantification of antiviral effects of checkpoint inhibitors via virus titration on HT29 and HCT-15 tumor cells

In order to quantify conceivable effects of immune checkpoint blockade on viral replication in a model of human CRC cell / immune cell cocultivation, viral titers of each supernatants and lysates were determined after infection with MeV-GFP (MOI 1 for HT29 or MOI 10 for HCT-15), treatment with nivolumab or atezolizumab and cocultivation with NK cells (E : T = 2.5 : 1) or PBMC (E : T = 10 : 1).

Six treatment groups were differentiated: MeV-GFP-infected cells (i) without further treatment, (ii) with PBMC cocultivation alone, with PBMC cocultivation and additional (iii) nivolumab or (iv) atezolizumab incubation, with (v) PBMC cocultivation together with combined application of both nivolumab and atezolizumab or (vi) with PBMC cocultivation and IgG control. For ICI or human IgG control incubation, concentrations of each 5 µg / ml were used.

Supernatants as well as lysates of the different treatment regimes were collected at 48 hours after cocultivation with immune cells. Titration was done on Vero cells.

One out of two independent experiments is shown each.

In a model of coculture of NK cells / PBMC with MeV-GFP-infected HT29 tumor cells, treatment with *nivolumab* and / or *atezolizumab* showed no consistent impairment of

viral replication in comparison to controls without ICI treatment or to controls with human IgG treatment instead. This seemed to be consistent with results observed in viral growth curve models on HT29 CRC cells (Fig. 25, A). Addition of immune cells alone did not reduce viral titers by more than a factor of 10. Application of IgG control together with NK cells / PBMC resulted in viral titers comparable to those after immune cell coculture.

In a second experiment of NK cell / PBMC cocultivation, this time with MeV-GFP-infected HCT-15 tumor cells, viral titers were again impaired by immune cell coculture, ranging between a factor of 100 to 1.000. As HCT-15 cells had proven to be MeV-GFP-resistant in cytotoxicity assays (Fig. 14), supernatants as well as lysates generally contained a lower amount of viral particles than HT29, thus resulting in lower viral titers on average. Furthermore, it should be taken into account that a difference in immune cell-induced reduction of virus proliferation between the two CRC cell lines could also be due to various extents of MHC mismatch effects, relating to separate donors of immune cells and the different NCI-60 human tumor cell lines.

Apart from that, treatment with *nivolumab* and / or *atezolizumab* showed no interference with viral replication in HCT-15 tumor cells as well. Referring to NK cells, no homogeneous reduction of viral titers by adding ICI could be observed in supernatants or lysates. Only in comparison to human IgG control, *atezolizumab* achieved a titer reduction of about factor 10 in supernatants. Referring to PBMC, ICI-induced decrease of viral titers of more than factor 10 could be observed neither in supernatants nor in lysates. These findings also seemed to be consistent with the results of viral growth curves on HCT-15 tumor cells (Fig. 25 B).

In conclusion, ICI alone without immune cell coculture did not have any influence on replication in a viral growth curve model. Moreover, viral titrations under PBMC or NK cell coculture could not show a consistent influence of ICI on viral spread either.

This correlated with the observations in *in vitro* xCELLigence real-time tumor cell growth and viability analysis, where ICI were found to have no additional anti-tumor effects in comparison to measles virotherapeutic and immune cells only.

4. Discussion

The history of virotherapy can be dated back to the discovery of viruses over 100 years ago. In this context, the presumption that both naturally acquired viral infections and vaccinations with attenuated virus strains could induce regression of malignant tumors was reinforced by numerous clinical case reports (Bierman et al., 1953; Bluming, 1971; Hansen and Libnoch, 1978). The height of virotherapy was heralded with the possibility of genetic engineering of the viral genome, thus further improving tumor specificity (Hammond et al., 2001; Bucheit et al., 2003), implementing a non-invasive reconstruction of viral replication kinetics in the human organism (Peng et al., 2002a; Dingli et al., 2004) or realizing a supplemental activation of the host immune system against mutated tumor cells (Grossardt et al., 2013).

With the genetically modified herpes simplex virus *Talimogene laherparepvec* (*Imlygic*®, Amgen), a first virotherapeutic was FDA- as well as EMA-approved for treatment of advanced melanoma in 2015 (Andtbacka, 2015; FDA, 2015). Beyond, MeV also became subject of clinical case reports and early clinical trials in cancer patients (Msaouel et al., 2009; Russell et al., 2014; Robinson and Galanis, 2017). But nonetheless, virotherapy still implicates serious obstacles for research, as monotherapy with OVs already encountered *in vitro* resistances in several tumor entities, including human CRC cell lines (Noll M., 2013), hence making new multimodal treatment strategies inevitable.

A combined therapeutic regimen with ICI, for example mAbs against PD-1 and PD-L1, was chosen to overcome preexisting resistances by strengthening and consolidating the oncolysis-induced anti-tumor immune response (Dias JD, 2012; Engeland CE, 2014; Quetglas JI, 2015; Rojas et al., 2015; Woller N, 2015; Cockle et al., 2016; Rajani K, 2016; Shen et al., 2016). In terms of partly ineffective monotherapeutic treatment of CRC with ICI (Jager et al., 2016), this multimodal approach seems particularly interesting to uncover the power of immunotherapy.

In view of high prevalence and, on the other hand, still poor OS rates for metastatic disease in CRC (Gustavsson et al., 2015), our focus was set on three human CRC cell lines: HT29, HCT-15 and SW-620.

In vitro mono-treatment of human CRC with MeV virotherapeutic or ICI was not efficient enough to fully eradicate all tumor cell lines, partly facing preexisting resistances.

In a first phase, monotherapeutic approaches for treatment of CRC were tested for their cytotoxic potential via Sulforhodamine B viability assay.

For the measles virotherapeutic MeV-GFP, different patterns of resistance were found for the three human CRC cell lines. In detail, HT29 were found to be susceptible towards MeV-induced oncolysis, whereas SW-620 and HCT-15 showed preexisting resistance at 72 and 96 hpi, displaying remaining cell masses of almost 100 % at MOI 1. For SW-620, this resistance could be overcome by raising the MOI to 5 and 10. In contrast, not even an increase of the MOI up to 10 was able to overcome the resistance in HCT-15 tumor cells. These results complement findings of our laboratory, described by Noll et al. (Noll M., 2013), where SRB analysis was done for our suicide-gene enhanced virotherapeutic MeV-SCD at 96 hpi, using a MOI of 1. Here, HCT-15 belonged to those NCI-60 tumor cell lines revealing the highest grade of resistance towards MeV-SCD-induced oncolysis. Noll and colleagues considered differences in antiviral interferon (IFN) response to depict a possible explanation for variations in MeV-resistance, referring to the innate immunity of tumor cells. Thereby, expression of a protein called IFIT (interferon-induced protein with tetratricopeptide repeats) could be demonstrated in the MeV-GFP- and MeV-SCD-resistant HCT-15 tumor cells, thus indicating an active IFN pathway (Noll M., 2013). By the way, a residual activity of IFN signaling in tumor cells does not dissent with the principle of tumor-specific oncolysis via IFN pathway deficiency, as explained in 1.2.1: Some tumor cells may still dispose of a remaining innate immunity, but mostly decreased in comparison to healthy tissue (Haralambieva et al., 2007).

Appraising SRB results, MeV virotherapeutic as mono-treatment was found to be not able to eradicate all three human CRC cell lines, hence highlighting the urgency to enable multimodal virotherapeutic approaches.

In a next step, SRB cytotoxicity assays proved that *nivolumab* and *atezolizumab* both did not possess any innate anti-tumor traits, which could be explained by lack of an immune cell / tumor cell interaction to interfere with.

Expression of the immune checkpoint ligand PD-L1, representing a predictive as well as prognostic factor for ICI therapy, could be increased by MeV-infection in all three human CRC cell lines.

We set a focus on the question whether infection with an oncolytic measles virus could have impact on expression rates of the immune checkpoint ligand PD-L1 in the different human colorectal tumor cells.

First of all, basal PD-L1 expression on the different tumor cell lines was examined and compared with regard to different culturing conditions concerning used media and time of culturing.

Expectedly, the three human CRC cell lines differed in their basal PD-L1 expression: HT29 appeared to be the cell line with the highest percentage of PD-L1 expressing cells, namely 14.8 %, followed by HCT-15 with 2.8 % and SW-620 with 2.6 %. These observations fit into the pattern of earlier experiments from Llosa et al., where basal PD-L1 expression on human CRC was examined in relation to MSI status (Llosa et al., 2015). Interestingly, HCT-15, which belongs to the MSI fraction of CRC (Abaan et al., 2013; Ahmed et al., 2013), was a tumor cell line with low basal PD-L1 expression rates. In comparison to that, HT29 with MSS status (Abaan et al., 2013; Ahmed et al., 2013) expressed higher rates of PD-L1. This counteracts the hypothesis that the expression of immune checkpoint ligands in highly immunogenic MSI cancer, based on the high mutational load, represents an important immune escape mechanism. But actually, Llosa and colleagues could also not find high rates of PD-L1 expression on CRC tumor cells with MSI status in immunohistochemistry. In fact, PD-L1 expression was found on myeloid cells as well as TILs in tumor nests, tumor stroma and the lamina propria invasion front (Llosa et al., 2015), creating an immunosuppressive microenvironment. In regard to these findings, an interesting question, which could be followed in an appropriate mouse model of CRC, would be how tumor-infiltrating immune cells react in their PD-L1 expression in case of infection with a MeV virotherapeutic. To anticipate this idea, Woller et al. could prove that adenovirus-induced oncolysis was able to induce PD-L1 expression on tumor-infiltrating APCs in murine CMT64 lung tumors. Moreover, addition of anti-PD-1 to OV treatment further increased PD-L1 expression on APCs (Woller N, 2015).

In a next step, we examined the impact of different culturing conditions on PD-L1 expression rates. Thereby, no consistent results for all three tumor cell lines were found. HT29 was the only tumor cell line to undergo consistent changes in PD-L1 expression after incubation with Opti-MEM for both times of measurement, hence an increase in PD-L1 expression was observed. In contrast to that, expression rates of PD-L1 in HT29 CRC cells were impaired by longer duration of cultivation. This did not apply for HCT-15 and SW-620, where PD-L1 expression rose with time of culturing. To put it into a nutshell, heterogeneous reactions to different culturing conditions rather negated a consistent mechanism of influence on PD-L1 expression, but might depict a possible impact of various factors of cell metabolism on PD-L1 expression.

Finally, tumor cells were infected with the virotherapeutics MeV-GFP and MeV-SCD to analyze the consequences of MeV-OV treatment on PD-L1 expression, and thus on a possible ICI application. FACS analysis of immune checkpoint ligand expression after MeV-SCD-infection was performed to avoid distracting interference of the GFP with isotype- and anti-PD-L1-PE staining, arising especially in MeV-GFP-susceptible HT29 tumor cells. In favor of a multimodal immunovirotherapeutic approach, measles infection induced a sustainable increase of PD-L1 expression in all three human CRC cell lines. Even in high-grade MeV-resistant HCT-15 tumor cells, MeV-SCD infection could increase PD-L1 expression from an original extent of 5.9 % for MOCK infected cells at 24 hpi to 35.6 % for infected cells at 48 hpi, using a MOI of 10. Moreover, PD-L1 upregulation through MeV-SCD-infection was found to be time- as well as MOI-dependent for the two CRC cell lines HCT-15 and HT29.

In contrast to these findings, PD-L1 expression in SW-620 cells correlated positively with MOI but not with time of culturing after MeV-SCD-infection, as expression rates were considerably impaired at 48 hpi in comparison to 24 hpi for MOCK, MOI 5 and MOI 10. However, this effect could not be reproduced by using MeV-GFP for OV-infection or by comparing different culturing media. Perhaps advanced MeV-SCD-induced tumor cell killing at 48 hpi led to reduction of OV-infected, PD-L1-expressing SW-620 cells, but this theory would not explain a difference of 26.4 percentage points between PD-L1 expression in MOCK infected SW-620 cells at 24 hpi vs. 48 hpi.

As it is commonly suggested that high PD-L1 expression rates on tumor targets correlate with a successful outcome for ICI treatment (Topalian et al., 2012; Taube et

al., 2014; Dunne et al., 2016), it seems to be worthy to take a step forward to investigate therapeutic effects of ICI combined with MeV virotherapeutic in a murine CRC model. To give an example, combination treatment with the virotherapeutic MeV-EGFR (targeting epidermal growth factor receptor for host cell entry) and anti-PD-1 mAb could achieve prolonged survival in a syngeneic murine glioblastoma (GBM) model (Hardcastle et al., 2016). Moreover, Hardcastle and colleagues investigated the influence of MeV-NIS-infection of human GBM39 and GBM12 tumor cells on the expression of PD-L1. Furthermore, the impact of MeV-NIS-infection was compared with IFN-γ treatment. Untreated, the two human GBM cell lines barely expressed PD-L1 after 24 hours, but IFN-γ could achieve a significant increase in PD-L1 expression on both cell lines, in contrast to MeV-NIS. After 36 hours, MeV-NIS was also able to induce a significant increase of PD-L1 expression, compared to untreated cells or to controls treated with UV-inactivated MeV-NIS. Interestingly, the percentage of PD-L1 expressing GBM tumor cells 36 hours after IFN-γ treatment was again higher than after OV-infection (Hardcastle et al., 2016). These findings of Hardcastle et al. in an *in vitro* model of human GBM were consistent to our investigations in PD-L1 expression on human CRC cell lines, and could maintain the hypothesis that oncolysis through MeV virotherapy induces an immunological stimulus, which can be consolidated in a second step by antibodies targeted to PD-1 or PD-L1. The ICI-favorable tumor micro-environment due to the PD-L1 upregulation by MeV virotherapeutic strongly endorsed our approach to combine MeV-GFP with ICI for treatment of human CRC.

The important role of IFN-γ in upregulation of PD-L1 expression on tumor cells was also shown by Dong et al. (Dong H., 2002). It is hypothesized that tumor infiltrating $CD8^+$ T-cells are activated by contact to tumor specific antigens, thus secreting IFN-γ, which in turn upregulates PD-L1 expression on TILs and tumor cells, leading to an equilibrium of controlling anti-tumor immune response (Kim and Chen, 2016). On the other hand, activation of immune checkpoint receptor PD-1 diminishes the induction of IFN-γ secretion (Keir et al., 2008). Moreover, PD-L1 upregulation on monocytes is described as a consequence of IFN-γ and IFN-β signaling, referring to an approach of restraining autoreactive processes in the context of multiple sclerosis via interferon (Schreiner et al., 2004). In the special case of multimodal immunovirotherapy, virus-induced oncolysis would activate $CD8^+$ T-cells, which produce IFN-γ, leading to an

ICI-favorable PD-L1 upregulation (Rajani and Vile, 2015). Finally, to support this hypothesis, type I IFN receptor knockout mice with B16-F10 melanoma tumors were found to be resistant to a combination therapy out of Newcastle disease virus (NDV) and CTLA-4 blockade, whereas the combination treatment in C57Bl/6 mice could induce long-term survival (Zamarin D, 2014).

In contrast to our findings and to those of Hardcastle et al., Rajani et al. appraised that reovirus infection of murine B16 melanoma cells at a MOI of 0.1 did not lead to a PD-L1 upregulation in FACS analysis at 4 dpi. Interestingly, in further analysis of PD-L1 expression on B16 tumor cells after additional coincubation with NK cells from tumor naïve mice, reovirus infection could slightly increase PD-L1 expression in comparison to B16 cells only treated with NK cell coincubation (Rajani K, 2016). Considering prolonged survival through combination therapy of B16 melanoma with reovirus and anti-PD-1 in C57Bl/6 mice, Rajani et al. concluded that *in vivo* therapeutic effects were not moderated by direct influence of reovirus-infection on PD-L1 expression. Rather, an indirect way via increased NK cell activation against reovirus-infected B16 tumor cells was discussed.

On the one hand, differences between varying OVs and between *in vitro* mice and human tumor models should be taken into account. On the other hand, successful implementation of an OV / ICI combination therapy in a B16 melanoma mouse model, despite the background of lacking reovirus-induced PD-L1 upregulation (Rajani K, 2016), points out that our multimodal immunovirotherapeutic approach should be transferred to a suitable immunocompetent CRC mouse model, even now that MeV infection seems to pave the way for successful ICI application.

Taking the latest findings into account, first clinical trials support the hypothesis of improved efficacy in combining OVs with ICI: *Talimogene laherparepvec* and *pembrolizumab* were tested in patients with advanced melanoma, resulting in an ORR of 62 % and an acceptable toxicity profile in comparison to the respective monotherapies (NCT02263508) (Ribas et al., 2017). Remarkably, by adding the OV to the PD-1 inhibitor, therapeutic response was found to become independent from individual baseline levels of PD-L1 and IFN-γ expression or $CD8^+$ T-cell infiltration. These results, even though referring to a phase I clinical trial with limited patient

numbers and a focus on safety, strongly underline our hypothesis of viral oncolysis overcoming preexisting resistances against immune checkpoint blockade.

Poor PD-1 expression on NK cell populations from four different healthy donors could impair preconditions for achieving in vitro therapeutic effects with ICI treatment.

In a next step, we examined whether CD56 positive NK cell subsets from healthy donors could express the immune checkpoint receptor PD-1, inevitable as a target for immune checkpoint blockade. The focus was set on NK cell populations, as they represent a part of the early, innate anti-cancer immune response (Waldhauer and Steinle, 2008), reproduced in the rather short measurement period of subsequent xCELLigence experiments.

Our FACS analysis showed that the CD56 positive NK cells did not express PD-1 in a sustainable way: Neither in PBMC cultures (donor #1 and #2), nor in expanded NK cells (donor #3 and #4), more than 0.8 % of cells expressed PD-1, referring to CD56 positive cell populations. Interestingly, there was a PD-1 positive, CD56 negative cell subset among expanded NK cells, namely 1.9 % of cells from donor #3 and 2.8 % of cells from donor #4.

The result that almost no PD-1 expression could be found on CD56 positive NK cells seems to coincide with the experiments of Pesce et al. Here, PD-1 expression was investigated with the finding that NK cells of only about one fourth of overall 200 healthy donors were able to express PD-1 in high levels. Furthermore, this PD-1 positive population of NK cells was described as a $CD56^{dim}$ NK cell subset (Pesce et al., 2016), referring to a differentiation between $CD56^{dim}$ $CD16^{bright}$ NK cells, which make up about 90 % of the human NK cells and hold a cytotoxic function, and $CD56^{bright}$ $CD16^{dim}$ NK cells, which were found to play an immunoregulatory role (Cooper et al., 2001).

Referring to investigations of a reovirus / ICI combination therapy from Rajani and colleagues in an *in vitro* model of murine B16 melanoma, the NK cells used for cocultivation, which had been purified from spleen or lymph nodes of tumor naïve C57Bl/6 mice beforehand, barely expressed PD-1. Hence, it was suggested that the process of ICI-induced NK cell activation did not happen in the direct way of blocking

PD-1 receptors located on NK cells, but via cytokine production by PD-1 positive mediator cells, which were found in the NK cell-enriched cultures, and which were further described as CD3 positive (Rajani K, 2016).
To reconsider our findings, the low PD-1 expression rates on the tested NK cell sub-populations could provide a possible explanation for the lack of additional therapeutic effects of ICI treatment in xCELLigence analysis.

xCELLigence real-time tumor cell growth and viability analysis revealed outstanding therapeutic effects for a combination of MeV virotherapeutic and immune cell coincubation, but no additional tumor cell killing through ICI addition.

For *in vitro* investigation of our immunovirotherapeutic approach in CRC, xCELLigence analysis of tumor cell proliferation and viability was chosen with the advantage of real-time measurement over a period of 130 hours. Notwithstanding, this *in vitro* model of tumor cell / immune cell coculturing could only depict a very simplified model of the complex human immune system, including limited possibilities concerning duration of measurement.
In a first step, it was examined whether the addition of ICI alone could achieve therapeutic effects in uninfected as well as MeV-GFP-infected CRC cells without the influence of immune cell coculture. As expected, MeV alone already led to considerable tumor cell killing in HT29 cells. But neither *atezolizumab* nor *nivolumab* could sustainably diminish tumor cell growth and viability in comparison to controls, albeit surprisingly, a slight trend towards an increased tumor cell killing could be appraised in case of ICI addition to both infected and uninfected HT29 cells. Referring to HCT-15 tumor cells, treatment with MeV-GFP at the high MOI of 10 could considerably reduce tumor cell mass, although this cell line was found to be resistant to a great extent towards MeV-induced oncolysis in end point SRB assays. Maybe, this effect could be partly traced back to the extremely low CRC cell counts seeded on xCELLigence E-plates. Moreover, ICI addition led to a trend of decrease of CIs in uninfected, but not in infected HCT-15 tumor cells. Hence again, no consistent ICI-induced impairment of tumor cell growth and viability could be observed without a possible immune cell interaction.

To take a step forward, we hereupon cocultured CRC cells with NK cells or PBMC, respectively, and repeated the additional MeV-GFP-infection. Monotreatment with immune cells also attained good results in tumor cell killing compared to single MeV-infection, comprehensibly dependent on E : T ratios and further uncontrollable influencing factors, such as degree of MHC mismatch between tumor and immune cells. On average, immune cells plus MeV in combination achieved best therapeutic results in our xCELLigence setting. This phenomenon supported the hypothesis of MeV-induced oncolysis setting an immunogenic stimulus, thus enhancing tumor cell killing by NK cells or PBMC.

Donnelly et al. could prove this phenomenon for the human melanoma cell line Mel888, where MeV-infection lead to an increase of CD107 expression on $CD3^-$ $CD56^+$ NK cells, with CD107 being a marker for NK cell activation and degranulation (Alter, 2004; Donnelly et al., 2013). Additionally to the described activation of innate immunity by MeV-induced oncolysis, Donnelly and colleagues could also find a DC-mediated activation of PBMC against Mel888 tumor cells, displaying mechanisms of an adaptive anti-tumor immune response induced by the OV. Summing up, these findings perfectly correlated with the increased killing of CRC cells in our xCELLigence analysis, when cells were MeV-infected and cocultured with immune cells. Nonetheless, it should be considered that effects of an adaptive immune response, as Donnelly et al. could show after one and two weeks of coculture, were rather questionable in our experimental setting, referring to a much shorter time of coculture.

In a next step, the influence of immune checkpoint blockade in a triple therapeutic regimen together with MeV-GFP and immune cells was tested. Summing up results of overall xCELLigence runs with HT29 and HCT-15 cells, unfortunately, neither *atezolizumab* nor *nivolumab* application could homogeneously lead to an additional therapeutic gain. When addressing this lack of desirable ICI-induced improvement of tumor cell killing, several aspects should be considered.

Firstly, a preexisting anti-tumor immunity, represented by tumor-infiltrating lymphocytes such as $CD8^+$ T-cells, and the thereby induced PD-L1 upregulation, functioning as an immune escape answer of the tumor, were found to build the basement of a successful ICI interaction (Herbst et al., 2014; Tumeh et al., 2014). In case of our *in vitro* xCELLigence model, no preexisting tumor immunity could be expected, as the

immune cells had been isolated from healthy donors, and as no coincubation with CRC cells had taken place prior to xCELLigence analysis. Moreover, the already mentioned limited period of measurement, and therefore also of coculture, could implicate a lack of proper interaction between tumor cells, immune cells and immune checkpoint blockade. Adding another point, the FACS analysis of PD-1 expression on CD56 positive NK cell populations revealed rather low expression rates as a precondition to take place in a PD-1 / PD-L1 interaction, which could be inhibited by ICI. According to those findings, PD-1 expression rates irrespective of CD56 status were not higher than 3.5 % of overall cells in enriched NK cell cultures, and not higher than 15.1 % of PBMC cultures.

Interestingly, a further mechanism of NK cell-induced tumor cell killing could include antibody-dependent cellular cytotoxicity (ADCC), which is mediated by interaction between an IgG_1 mAb, such as *atezolizumab*, and CD16, which displays a Fc receptor on NK cells (Cooper et al., 2001; Veluchamy et al., 2016). In contrast to *nivolumab*, namely an IgG_4 mAb, CRC cell-opsonizing *atezolizumab* could therefore activate ADCC as an anti-tumor machinery independent from PD-1 / PD-L1 interaction. However, no consistent therapeutic difference could be found between treatment with NK cells plus *atezolizumab* and NK cells plus *nivolumab* in xCELLigence analysis.

In contrast to the lack of an additional therapeutic effect of our triple therapy *in vitro*, Rajani et al. could show a significant increase in TNF-α release by tumor-naïve NK cells cocultured with murine B16 melanoma cells, which had been treated with a combination of reovirus and anti-PD-1 or anti-PD-L1 beforehand (Rajani K, 2016). Measurement took place in supernatants collected two days after coincubation and four days after reovirus infection, thus in a time period captured by our xCELLigence measurement. Moreover, Rajani and colleagues could prove that this multimodal immunovirotherapeutic treatment of B16 cells together with NK cell coculture significantly decreased tumor cell mass in the case of reovirus / anti-PD-1 treatment. Interestingly, this measurement was executed seven days after reovirus infection, thus not any longer in the time period of our xCELLigence analysis. It stayed unclear whether an analysis of residual tumor cells was also conducted at an earlier point of time together with TNF-α measurement. Apart from the fact that those experiments took place in a murine, and not human, *in vitro* model, a discrepancy between the two experimental settings could again be attributed to the different chronology of

measurement in investigations of Rajani et al. and our investigations. Hence, maybe a longer measurement period for xCELLigence analysis should have been chosen, which in turn would lead to the question whether our real-time setting could really afford measurement durations lasting longer than a week.

To give a résumé over testing of an immunovirotherapeutic approach beyond *in vitro* tumor cell models, many favorable results could be depicted in animal models (Gao Y, 2009; Dias JD, 2012; Engeland CE, 2014; Zamarin D, 2014; Quetglas JI, 2015; Rojas et al., 2015; Woller N, 2015; Cockle et al., 2016; Hardcastle et al., 2016; Shen et al., 2016) and in patients (NCT01740297 (Puzanov et al., 2016), NCT02263508, NCT03069378, NCT02626000, NCT02965716). Referring to patients with advanced melanoma, the immunovirotherapeutic combination of *Talimogene laherparepvec* and *pembrolizumab* was lately tested in a phase 1b clinical trial by Ribas and colleagues (NCT02263508), whereby the OV prepared the ground for improved efficacy of the ICI, resulting in a 62 % ORR (Ribas et al., 2017). The difficulties to display such a complex context of interaction between tumor, immune system, virus and ICI *in vitro* and the prospects of success with those previous preclinical and clinical trials *in vivo* propose further analysis of our multimodal therapy in an appropriate immunocompetent CRC mouse model.

As a result for in vitro analysis of conceivable ICI-induced antiviral immune effects, we appraised a lack of influence on viral replication and spread.

One major challenge in the field of immunovirotherapy emerges to be the timing of virus and ICI application (Rajani and Vile, 2015; Rojas et al., 2015; Marchini et al., 2016). By exploiting the ICI-consolidated anti-tumor immune response, a likewise induced antiviral immune response belongs to the other side of the coin. This, on the one hand, could impair viral replication and spread, leading to faster clearance of the OV, and thus diminishing the effects of direct tumor oncolysis. On the other hand, such an immune response directed towards foreign viral antigens could also improve virus-induced tumor cell killing, if the host tumor cell expressed those viral proteins on its surface.

Albeit in a different context, both sides of the coin should be illuminated in discussing antiviral immune responses: Facing the different aspects of already preexisting antiviral

antibodies, which neutralize the virotherapeutic in case of systemic delivery, several approaches were considered to circumvent an immunological clearance of OV (see 1.2.1). But interestingly, the - at first glance undesirable - preexisting antiviral immune response could not simply be equated with a reduction of OV-induced anti-tumor immune response, as Bridle and colleagues showed: They proved that a sustainable anti-tumor immune response can be induced by application of oncolytic VSV together with a boosting anti-adenoviral vaccination beforehand, with both vaccine and oncolytic virus expressing specific tumor antigens (Bridle et al., 2010).

In either case, an immunovirotherapeutic regimen requires perfect timing, which seems to be indispensable for orchestrating a maximum effective tumor cell killing as well as long-lasting anti-tumor immune response.

As a logical next step, we tried to quantify antiviral effects of immune checkpoint blockade in MeV-infected human CRC cells, both in viral growth curves and in titrations of lysates and supernatants of tumor cells infected and cocultured with PBMC or NK cells. Referring to the viral growth curve model, we could not find any influence of ICI on viral replication and spread, as it had been expected without the possibility of ICI interfering with a tumor cell / immune cell interaction. In the second case of virus titrations under immune cell influence, an indirect mechanism of ICI impairing viral replication could be anticipated, namely the mechanism of ICI reducing the tumor cell mass and thereby the capacity of virus production. But nonetheless, virus titrations did also not show a homogeneous interference of ICI with viral replication in CRC cells. This could correlate with the lack of additional anti-tumor effects in xCELLigence analysis through ICI application, together with MeV and immune cell treatment.

In contrast to our findings, Rajani et al. described an anti-PD-1 antibody-induced decrease of reovirus titers in murine B16 melanoma cells cocultured with tumor-naïve NK cells (Rajani K, 2016). This decline in viral titers went along with a significant reduction of tumor cell mass after treatment with reovirus, anti-PD-1 and NK cells. In an *in vivo* syngeneic model of murine renal adenocarcinoma (Renca cells) or colorectal adenocarcinoma (MC38), Rojas et al. could prove via bioluminescence imaging that addition of anti-CTLA-4 antibody significantly impaired replication of an oncolytic vaccinia virus expressing a luciferase transgene, when ICI was administered as early as 0, 3 and 6 days post infection (dpi) (Rojas et al., 2015). Furthermore, Rojas and

colleagues investigated the effects of different time schedules for an immunoviro-therapeutic treatment approach, resulting in the finding that in contrast to the described early treatment regimen, which could not show a significant tumor mass reduction, a second treatment regimen with ICI application at 4, 7 and 10 dpi led to a considerable tumor cell mass decrease and improved overall survival. To summarize, those investigations suggest an advantage of delayed ICI administration, leaving enough time for the OV to replicate and to set an immunogenic stimulus via oncolysis.

Moreover, these considerations should be also taken into account when discussing the application of OVs coding for anti-PD-1 or anti-PD-L1 with the advantage of local ICI delivery, thereby indicating that immune checkpoint blockade takes effects shortly after begin of viral replication. However, in a B16-CD20 murine melanoma model, Engeland et al. could show that intratumorous treatment with MeV on four consecutive days, combined with intraperitoneal injections of anti-PD-L1 antibody at 6, 9, 12 and 15 days after tumor implantation, was comparable to treatment with MeV encoding anti-PD-L1, referring to overall survival (Engeland CE, 2014). Interestingly, the same did not apply for anti-CTLA-4, where systemic application in combination with MeV virotherapeutic led to improved survival in comparison to MeV expressing anti-CTLA-4. Again, an attempt to explain these differences relates to aspects of timing: CTLA-4 is described to play an important role in early implementation of anti-tumor immunity, in contrast to PD-L1, showing effects in later stages of activation of the immune system against malignant cells (Pardoll, 2012; Engeland CE, 2014). Therefore, systemic application of anti-CTLA-4 could display an advantage at the early time of maximum effect in comparison to probably slower delivery of locally MeV-produced ICI, so Engeland and colleagues. Apart from that, it would display an interesting question whether the usage of anti-CTLA-4 antibodies such as *ipilimumab* would have been beneficial for our xCELLigence *in vitro* testing with a limited time of measurement, as they implement early interference with the anti-tumor immune response.

Giving a résumé of the overall investigations of ICI-induced antiviral effects, our findings were not in accordance with those described in literature for other tumor models. Considering the individual experimental settings, differences between tumor models, various OVs, time of application and local or systemic administration of ICI should not be neglected. Still, the results of virus titrations in a CRC cell / immune cell

cocultivation model under ICI influence were rather unexpected, probably correspondingly to the missing anti-tumor effects of ICI in xCELLigence.

A multimodal immunovirotherapeutic approach of MeV and immune checkpoint blockade emerged to be worthy further testing in an immunocompetent CRC mouse model.

A successful immunovirotherapeutic treatment of CRC has to be evolved from an *in vitro* model, with testing in animal experiments as a second step, followed by clinical trials in patients. As argued above, MeV-induced PD-L1 upregulation in CRC cells turned out to be auspicious for such a combined treatment regimen, providing an ICI-favorable immunological tumor microenvironment. Therefore, albeit xCELLigence analysis could not reveal an additional therapeutic gain of ICI application to MeV-infected, immune cell-coincubated CRC cells *in vitro*, such a treatment regimen could be worthy to be tested in an immunocompetent mouse model.

A major impediment of establishing an immunovirotherapeutic approach with MeV is displayed by the measles tropism to human cells, which requires CD46 as a surface protein for measles infection of the host cell (Naniche et al., 1993). Moreover, a human tumor model expressing CD46 could only be adopted in immunodeficient mice, for example NOD / SCID (non-obese diabetic / severe combined immunodeficiency) mice. This again would conflict with the fact that a successful immune checkpoint blockade is in need of an intact immune system with all its various players, and that it cannot be tested in immunodeficient animals in a way that is transferable to the human organism.

Then why not use another virus for virotherapy, which is not dependent on the human cell tropism? Measles vaccine virus depicts several advantages in comparison to other OVs developed over the last years. First of all, measles vaccine virus was proved to be safe in clinical usage (Buijs et al., 2015) with long-time experience in terms of vaccination. Secondly, successful attempts to cure patients consolidated the application of measles OV as anti-cancer therapeutic (Russell et al., 2014), which was further pursued in several clinical trials (Msaouel et al., 2009; Robinson and Galanis, 2017). Last but not least, investigations in our working group concerning MeV virotherapy could show enhancement of therapeutic efficacy by arming the OV with suicide genes such as SCD, transforming the harmless prodrug 5-FC into the chemotherapeutic 5-FU

(Graepler F., 2005; Lampe J, 2013; Lange S, 2013; Noll M., 2013; Yurttas C, 2014). To cut short a long story of success in measles virotherapy, it was finally worthy to redirect measles tropism to other targets than CD46 (Schneider et al., 2000; Bucheit et al., 2003) and to overcome the problems of transducing measles OV into an immunocompetent mouse model (Engeland CE, 2014; Hardcastle et al., 2016). Furthermore, an immunocompetent CRC model was introduced in C57BL/6 mice, combining murine MC38 colon adenocarcinoma cells expressing CEA with a MeV virotherapeutic, which was redirected to this surface marker and additionally coded for another prodrug convertase, purine nucleoside phosphorylase (PNP), to make oncolysis more efficient (Ungerechts et al., 2007). In conclusion, a logical next step would be to further evaluate our immunovirotherapeutic approach in such a mouse model of CRC *in vivo*.
Finally, the idea of exploiting the immunogenic stimulus of measles oncolytic virotherapy with new immunoenhancing therapies such as immune checkpoint blockade will soon accomplish the phase of clinical trials, for example combining MeV with anti-PD-1 antibody in advanced pancreatic cancer (Engeland and colleagues, not yet recruiting). Moreover, new immunotherapeutics such as the so-called bispecific T-cell engagers (BiTE) arrived in clinical usage, which are able to recognize a tumor-specific antigen on the one hand, and a T-cell-specific surface marker on the other hand, thereby merging the T-cell directly with the tumor target (Huehls et al., 2015). Combined with measles OV, these BiTEs are tested for consolidating a long-lasting anti-tumor T-cell immunity (Speck et al., 2018).

To sum up our findings, which comprise a new multimodal treatment strategy for CRC based on a combination of MeV virotherapeutic with immune checkpoint blockade targeting PD-1 or PD-L1, *in vitro* investigations could reveal that MeV-infection clears the way for ICI treatment by upregulation of immune checkpoint ligand PD-L1 on CRC tumor cells. For the discussed reasons and for the previously presented promising results of further preclinical trials in the field of immunovirotherapy, the missing additional therapeutic effect in xCELLigence analysis of combining ICI with MeV virotherapeutic under immune cell cocultivation should not lead to rejection of this immunovirotherapeutic approach in CRC, but - quite the contrary - to further testing in early clinical trials, i.e. phase I/II studies.

5. Summary

In the recent past of virotherapy, the characteristic trait of virus-induced oncolysis to trigger an immunogenic stimulus against malignant cells was utilized for new immuno-virotherapeutic combination approaches, thereby overcoming preexisting resistances. Aim of this dissertation thesis was to investigate such a novel multimodal therapeutic strategy for treatment of colorectal carcinoma (CRC). In an *in vitro* model of human CRC cell lines from the NCI-60 tumor cell panel, it was tested whether immune check-point inhibitors (ICI) could achieve a therapeutic gain, combined with an oncolytic measles vaccine virus expressing green fluorescent protein (MeV-GFP) and with NK cells or peripheral blood mononuclear cells (PBMC).

Sulforhodamine B (SRB) cytotoxicity assays were performed to uncover preexisting resistances of the respective monotherapies in the different tumor cell lines. In two human CRC cell lines, HT29 (susceptible to measles-induced oncolysis) and SW-620 (exhibiting an intermediate resistance to measles-induced oncolysis), infection with MeV-GFP achieved a multiplicity of infection (MOI)- and time-dependent reduction of tumor cell mass, whereas HCT-15 tumor cells were observed to be highly resistant to MeV-GFP-induced oncolysis. Moreover, monotherapeutic treatment of HT29 and HCT-15 with *nivolumab* (targeting PD-1) or *atezolizumab* (targeting PD-L1) did not reduce tumor cell viability in the absence of immune cells.

FACS analysis of PD-L1 expression on CRC cell lines was conducted to firstly estimate the basal expression of this immune checkpoint ligand, whereupon tumor cells were measles-infected and, in a second step, the influence of infection on PD-L1 expression was investigated. Showing different degrees of basal PD-L1 expression, infection with both MeV-GFP and MeV-SCD, a suicide gene-enhanced measles virotherapeutic coding for Super-cytosine deaminase (SCD), increased PD-L1 expression in all three human CRC cell lines. In terms of MeV-SCD-infection, expression of PD-L1 further rose with augmentation of MOI for all three tested CRC cell lines and also with time of culture after infection for two out of three tested tumor cell lines. Furthermore, expression rates of the immune checkpoint receptor PD-1 on CD56 positive NK cell populations from four different healthy donors were investigated, resulting in less than

1 % of PD-1 positive cells. This result can be assessed as a poor precondition to take place in a direct PD-1 / PD-L1 interaction.

In a next step, we tested for augmented anti-tumor efficacy under the influence of our combination treatment and immune cell coculture, using the real-time tumor cell growth and viability xCELLigence analysis. Thereby, the combination of immune cell co-culture with measles infection could already show increased therapeutic effects in comparison to the respective monotreatments, albeit unfortunately, this effect could not be further strengthened by additional application of ICI (*nivolumab* and / or *atezolizumab*).

Finally, antiviral effects of immune checkpoint blockade were examined: Neither in a viral growth curve model, nor in viral titrations after immune cell coincubation, an influence of ICI on replication and spread of MeV-GFP in CRC cell lines could be found.

To summarize, the upregulation of PD-L1 on human CRC cells via MeV-infection correlates with a promising therapeutic setting for combining ICI with measles-based virotherapy. However, *in vitro* xCELLigence analysis under immune cell coculture could not reveal a therapeutic gain of our immunovirotherapeutic approach. Nonetheless, considering the limited possibilities of an *in vitro* model of the complex human immune system, our therapeutic regimen should be further investigated in an immunocompetent mouse model of CRC and, even more, in the context of early clinical trials (i.e. phase I/II studies).

Zusammenfassung

In der jüngsten Vergangenheit der Virotherapie wurde die spezielle Eigenschaft der virusinduzierten Onkolyse, einen immunogenen Stimulus gegen bösartige Zellen zu triggern, ausgenutzt, um mit neuen immunovirotherapeutischen Kombinationsansätzen vorbestehende Tumor-Resistenzen zu überwinden.

Ziel dieser Dissertationsschrift war es, einen solchen neuen multimodalen Therapieansatz für das kolorektale Karzinom (CRC) zu untersuchen. In einem *in vitro* Modell humaner kolorektaler Karzinomzelllinien aus dem NCI-60 Tumorzellverzeichnis wurde getestet, ob Immun-Checkpoint-Inhibitoren (ICI) einen solchen therapeutischen Zusatznutzen erbringen können, wenn sie mit onkolytischen Masernimpfviren, welche grün fluoreszierendes Protein exprimieren (MeV-GFP), und mit NK Zellen oder peripheren mononukleären Blutzellen (PBMC) kombiniert werden.

Um vorbestehende Resistenzen der jeweiligen Monotherapien in den unterschiedlichen Tumorzelllinien zu testen, wurden zunächst Sulforhodamine B (SRB) Zytotoxizitätsassays durchgeführt. In zwei humanen kolorektalen Karzinomzelllinien, HT29 (suszeptibel gegenüber Masern-induzierter Onkolyse) und SW-620 (intermediär resistent gegenüber Masern-induzierter Onkolyse), konnte eine Infektion mit MeV-GFP eine konzentrations- und zeitabhängige Tumorzellmassenreduktion erreichen, wohingegen sich HCT-15 Tumorzellen als hoch resistent gegenüber MeV-GFP-induzierter Onkolyse erwiesen. Außerdem konnte gezeigt werden, dass die Monotherapie von HT29 und HCT-15 mit *Nivolumab* (gerichtet gegen PD-1) oder *Atezolizumab* (gerichtet gegen PD-L1) die Tumorzellviabilität in Abwesenheit von Immunzellen nicht reduziert.

In einem weiteren Schritt wurden FACS Messungen der PD-L1 Expression auf den genannten Darmkrebszelllinien durchgeführt, um zunächst die basale Expression dieses Immuncheckpoint-Liganden zu beurteilen, woraufhin die Tumorzellen mit Masern infiziert wurden und in einem zweiten Schritt der Einfluss einer Infektion auf die PD-L1 Expression untersucht wurde. Ausgehend von unterschiedlichen basalen PD-L1 Expressionsraten konnte eine Infektion sowohl mit MeV-GFP als auch mit MeV-SCD, einem Suizidgen-verstärkten Masernvirotherapeutikum, das für eine Supercytosin

Deaminase (SCD) kodiert, die PD-L1 Expression in allen drei huamanen Darmkrebszelllinien steigern. Bezüglich der Infektion mit MeV-SCD stieg die Expression in allen drei getesteten Darmkrebszelllinien mit der Viruskonzentration und in zwei von drei getesteten Tumorzelllinien auch mit der Kultivierungszeit nach der Infektion.

Zudem wurden auch die Expressionsraten des Immuncheckpoint-Rezeptors PD-1 auf CD56 positiven NK Zell-Populationen von vier unterschiedlichen, gesunden Spendern untersucht, wobei sich weniger als 1 % PD-1 positive Zellen ergaben. Dieses Ergebnis kann bewertet werden als eine ausgangsmäßig schlechte Voraussetzung dafür, an einer direkten PD-1 / PD-L1 Interaktion teilzunehmen.

In einer Echtzeitmessung von Tumorzellwachstum und -viabilität im xCELLigence Assay wurde in einem weiteren Schritt unter Einfluss von unserer Kombinationstherapie und von Immunzellkokultur auf eine erhöhte Anti-Tumor-Effektivität getestet. Dabei konnte bereits durch die Kombination von Immunzellkokultur mit Maserninfektion ein gesteigerter therapeutischer Effekt im Vergleich zu beiden Monotherapien gezeigt werden, der sich jedoch leider durch zusätzliche Behandlung mit ICI (*Nivolumab* und / oder *Atezolizumab*) nicht weiter steigern ließ.

Schließlich wurden antivirale Effekte einer Immuncheckpointblockade untersucht: Weder in einem Viruswachstumskurvenmodell, noch bei Virustitrierungen nach Immunzellkoinkubation konnte eine Beeinflussung der Replikation und Ausbreitung von MeV-GFP in CRC Zelllinien durch ICI gefunden werden.

Zusammenfassend kann man davon ausgehen, dass die Hochregulierung von PD-L1 auf humanen Darmkrebszellen durch eine Infektion mit MeV einem vielversprechenden therapeutischen Ansatz entspricht, um ICI und Masern-basierte Virotherapie zu kombinieren. Allerdings konnten *in vitro* xCELLigence Analysen unter Immunzellkokultur zunächst keinen therapeutischen Zugewinn durch unseren immunovirotherapeutischen Ansatz erkennen lassen. In Anbetracht der limitierten Möglichkeiten eines *in vitro* Modells des komplexen menschlichen Immunsystems sollte unser therapeutisches Regime allerdings dennoch in einem immunkompetenten Darmkrebs-Mausmodell und besser noch im Rahmen früher klinischer Studien (Phase I/II) genauer untersucht werden.

6. References

ABAAN, O. D., POLLEY, E. C., DAVIS, S. R., ZHU, Y. J., BILKE, S., WALKER, R. L., PINEDA, M., GINDIN, Y., JIANG, Y., REINHOLD, W. C., HOLBECK, S. L., SIMON, R. M., DOROSHOW, J. H., POMMIER, Y. & MELTZER, P. S. 2013. The exomes of the NCI-60 panel: a genomic resource for cancer biology and systems pharmacology. *Cancer Res,* 73**,** 4372-82.

AHMED, D., EIDE, P. W., EILERTSEN, I. A., DANIELSEN, S. A., EKNAES, M., HEKTOEN, M., LIND, G. E. & LOTHE, R. A. 2013. Epigenetic and genetic features of 24 colon cancer cell lines. *Oncogenesis,* 2**,** e71.

AIT OUAKRIM, D., PIZOT, C., BONIOL, M., MALVEZZI, M., BONIOL, M., NEGRI, E., BOTA, M., JENKINS, M. A., BLEIBERG, H. & AUTIER, P. 2015. Trends in colorectal cancer mortality in Europe: retrospective analysis of the WHO mortality database. *Bmj,* 351**,** h4970.

ALTER, G., MALENFANT, J.M., ALTFELD M. 2004. CD107a as a functional marker for the identification of natural killer cell activity. *Journal of Immunological Methods,* 294**,** 15-22.

ANDERSON, B. D., NAKAMURA, T., RUSSELL, S. J. & PENG, K. W. 2004. High CD46 receptor density determines preferential killing of tumor cells by oncolytic measles virus. *Cancer Res,* 64**,** 4919-26.

ANDTBACKA, R. H. I., KAUFMAN, H. L., COLLICHIO, F., AMATRUDA, T., SENZER, N., CHESNEY, J., DELMAN, K. A., SPITLER, L. E., PUZANOV, I., AGARWALA, S. S., MILHEM, M., CRANMER, L., CURTI, B., LEWIS, K., ROSS, M., GUTHRIE, T., GERALD P. LINETTE, G. P., DANIELS, G. A., HARRINGTON, K., MIDDLETON, M. R., MILLER JR, W. H., ZAGER, J. S., YE, Y., YAO, B., LI, A., DOLEMAN, S., VANDERWALDE, A., GANSERT, J. AND COFFIN, R. S. 2015. Talimogene Laherparepvec Improves Durable Response Rate in Patients With Advanced Melanoma. *Journal of Clinical Oncology*.

AREF, S., BAILEY, K. & FIELDING, A. 2016. Measles to the Rescue: A Review of Oncolytic Measles Virus. *Viruses,* 8.

BAUZON M, H. T. 2014. Armed therapeutic viruses - a disruptive therapy on the horizon of cancer immunotherapy. *Frontiers in Immunology,* 5.

BIERMAN, H. R., CRILE, D. M., DOD, K. S., KELLY, K. H., PETRAKIS, N. L., WHITE, L. P. & SHIMKIN, M. B. 1953. Remissions in leukemia of childhood following acute infectious disease: staphylococcus and streptococcus, varicella, and feline panleukopenia. *Cancer,* 6**,** 591-605.

BLECHACZ, B., SPLINTER, PL, GREINER, S, MYERS, R, PENG, KW, FEDERSPIEL, MJ, RUSSELL, SJ & LARUSSO, NF 2006. Engineered measles virus as a novel oncolytic viral therapy system for hepatocellular carcinoma. *Hepatology,* 44**,** 1465-1477.

BLUMING, A. Z., ZIEGLER, J. L. 1971. Regression of Burkitt's Lymphoma in Association with Measles Infection *The Lancet,* 298**,** 105-106.

BODMER, W. F., BAILEY, C. J., BODMER, J., BUSSEY, H. J., ELLIS, A., GORMAN, P., LUCIBELLO, F. C., MURDAY, V. A., RIDER, S. H., SCAMBLER, P. & ET AL. 1987.

Localization of the gene for familial adenomatous polyposis on chromosome 5. *Nature,* 328**,** 614-6.

BOLAND, C. R. & GOEL, A. 2010. Microsatellite instability in colorectal cancer. *Gastroenterology,* 138**,** 2073-2087.e3.

BRAHMER, J. R., DRAKE, C. G., WOLLNER, I., POWDERLY, J. D., PICUS, J., SHARFMAN, W. H., STANKEVICH, E., PONS, A., SALAY, T. M., MCMILLER, T. L., GILSON, M. M., WANG, C., SELBY, M., TAUBE, J. M., ANDERS, R., CHEN, L., KORMAN, A. J., PARDOLL, D. M., LOWY, I. & TOPALIAN, S. L. 2010. Phase I study of single-agent anti-programmed death-1 (MDX-1106) in refractory solid tumors: safety, clinical activity, pharmacodynamics, and immunologic correlates. *J Clin Oncol,* 28**,** 3167-75.

BREITBACH, C. J., ARULANANDAM, R., DE SILVA, N., THORNE, S. H., PATT, R., DANESHMAND, M., MOON, A., ILKOW, C., BURKE, J., HWANG, T. H., HEO, J., CHO, M., CHEN, H., ANGARITA, F. A., ADDISON, C., MCCART, J. A., BELL, J. C. & KIRN, D. H. 2013. Oncolytic vaccinia virus disrupts tumor-associated vasculature in humans. *Cancer Res,* 73**,** 1265-75.

BRIDLE, B. W., STEPHENSON, K. B., BOUDREAU, J. E., KOSHY, S., KAZDHAN, N., PULLENAYEGUM, E., BRUNELLIERE, J., BRAMSON, J. L., LICHTY, B. D. & WAN, Y. 2010. Potentiating cancer immunotherapy using an oncolytic virus. *Mol Ther,* 18**,** 1430-9.

BUCHEIT, A. D., KUMAR, S., GROTE, D. M., LIN, Y., VON MESSLING, V., CATTANEO, R. B. & FIELDING, A. K. 2003. An oncolytic measles virus engineered to enter cells through the CD20 antigen. *Mol Ther,* 7**,** 62-72.

BUIJS, P. R., VERHAGEN, J. H., VAN EIJCK, C. H. & VAN DEN HOOGEN, B. G. 2015. Oncolytic viruses: From bench to bedside with a focus on safety. *Hum Vaccin Immunother,* 11**,** 1573-84.

CAI, S., LI, Y., DING, Y., CHEN, K. & JIN, M. 2014. Alcohol drinking and the risk of colorectal cancer death: a meta-analysis. *Eur J Cancer Prev,* 23**,** 532-9.

CARETHERS, J. M. & STOFFEL, E. M. 2015. Lynch syndrome and Lynch syndrome mimics: The growing complex landscape of hereditary colon cancer. *World J Gastroenterol,* 21**,** 9253-61.

CATTANEO, R., MIEST, T., SHASHKOVA, E. V. & BARRY, M. A. 2008. Reprogrammed viruses as cancer therapeutics: targeted, armed and shielded. *Nat Rev Microbiol,* 6**,** 529-40.

CHEN, L. & FLIES, D. B. 2013. Molecular mechanisms of T cell co-stimulation and co-inhibition. *Nat Rev Immunol,* 13**,** 227-42.

COCKLE, J. V., RAJANI, K., ZAIDI, S., KOTTKE, T., THOMPSON, J., DIAZ, R. M., SHIM, K., PETERSON, T., PARNEY, I. F., SHORT, S., SELBY, P., ILETT, E., MELCHER, A. & VILE, R. 2016. Combination viroimmunotherapy with checkpoint inhibition to treat glioma, based on location-specific tumor profiling. *Neuro Oncol,* 18**,** 518-27.

COOPER, M. A., FEHNIGER, T. A. & CALIGIURI, M. A. 2001. The biology of human natural killer-cell subsets. *Trends Immunol,* 22**,** 633-40.

DANENBERG, P. V. 1977. Thymidylate synthetase - a target enzyme in cancer chemotherapy. *Biochim Biophys Acta,* 473**,** 73-92.

DE VRIES, R. D. & DE SWART, R. L. 2014. Measles immune suppression: functional impairment or numbers game? *PLoS Pathog,* 10**,** e1004482.

DIAS JD, H. O., DIACONU I, HIRVINEN M, BONETTI A, GUSE K, ESCUTENAIRE S, KANERVA A, PESONEN S, LÖSKOG A, CERULLO V, HEMMINKI A 2012. Targeted cancer immunotherapy with oncolytic adenovirus coding for a fully human monoclonal antibody specific for CTLA-4. *Gene Therapy,* 19**,** 988-98.

DINGLI, D., PENG, K. W., HARVEY, M. E., GREIPP, P. R., O'CONNOR, M. K., CATTANEO, R., MORRIS, J. C. & RUSSELL, S. J. 2004. Image-guided radiovirotherapy for multiple myeloma using a recombinant measles virus expressing the thyroidal sodium iodide symporter. *Blood,* 103**,** 1641-6.

DONG H., S. S. E., SALOMAO D. R., TAMURA H., HIRANO F., FLIES D. B., ROCHE P. C., LU J., ZHU G., TAMADA K., LENNON V. A., CELIS E., CHEN L. 2002. Tumor-associated B7-H1 promotes T-cell apoptosis: A potential mechanism of immune evasion. *Nature Medicine* 8**,** 793 - 800.

DONNELLY, O. G., ERRINGTON-MAIS, F., STEELE, L., HADAC, E., JENNINGS, V., SCOTT, K., PEACH, H., PHILLIPS, R. M., BOND, J., PANDHA, H., HARRINGTON, K., VILE, R., RUSSELL, S., SELBY, P. & MELCHER, A. A. 2013. Measles virus causes immunogenic cell death in human melanoma. *Gene Ther,* 20**,** 7-15.

DORIG, R. E., MARCIL, A., CHOPRA, A. & RICHARDSON, C. D. 1993. The human CD46 molecule is a receptor for measles virus (Edmonston strain). *Cell,* 75**,** 295-305.

DUKE, T. & MGONE, C. S. 2003. Measles: not just another viral exanthem. *Lancet,* 361**,** 763-73.

DUNNE, P. D., MCART, D. G., O'REILLY, P. G., COLEMAN, H. G., ALLEN, W. L., LOUGHREY, M., VAN SCHAEYBROECK, S., MCDADE, S., SALTO-TELLEZ, M., LONGLEY, D. B., LAWLER, M. & JOHNSTON, P. G. 2016. Immune-derived PD-L1 gene expression defines a subgroup of stage II/III colorectal cancer patients with favorable prognosis that may be harmed by adjuvant chemotherapy. *Cancer Immunol Res*.

ENGELAND CE, G. C., VEINALDE R, BOSSOW S, LUTZ D, KAUFMANN JK, SHEVCHENKO I, UMANSKY V, NETTELBECK DM, WEICHERT W, JÄGER D, VON KALLE C, UNGERECHTS G 2014. CTLA-4 and PD-L1 checkpoint blockade enhances oncolytic measles virus therapy. *Molecular Therapy,* 22**,** 1149-1159.

ENGSTROM, P. F., ARNOLETTI, J. P., BENSON, A. B., 3RD, CHEN, Y. J., CHOTI, M. A., COOPER, H. S., COVEY, A., DILAWARI, R. A., EARLY, D. S., ENZINGER, P. C., FAKIH, M. G., FLESHMAN, J., JR., FUCHS, C., GREM, J. L., KIEL, K., KNOL, J. A., LEONG, L. A., LIN, E., MULCAHY, M. F., RAO, S., RYAN, D. P., SALTZ, L., SHIBATA, D., SKIBBER, J. M., SOFOCLEOUS, C., THOMAS, J., VENOOK, A. P. & WILLETT, C. 2009. NCCN Clinical Practice Guidelines in Oncology: colon cancer. *J Natl Compr Canc Netw,* 7**,** 778-831.

ESENSTEN, J. H., HELOU, Y. A., CHOPRA, G., WEISS, A. & BLUESTONE, J. A. 2016. CD28 Costimulation: From Mechanism to Therapy. *Immunity,* 44**,** 973-88.

FDA 2015. FDA approves first-of-its-kind product for the treatment of melanoma. *In FDA News Release; FDA: Silver Spring, MD, USA*.

FEHRENBACHER, L., SPIRA, A., BALLINGER, M., KOWANETZ, M., VANSTEENKISTE, J., MAZIERES, J., PARK, K., SMITH, D., ARTAL-CORTES, A., LEWANSKI, C., BRAITEH, F., WATERKAMP, D., HE, P., ZOU, W., CHEN, D. S., YI, J., SANDLER,

A. & RITTMEYER, A. 2016. Atezolizumab versus docetaxel for patients with previously treated non-small-cell lung cancer (POPLAR): a multicentre, open-label, phase 2 randomised controlled trial. *Lancet,* 387**,** 1837-46.

FERLAY, J., SOERJOMATARAM, I., DIKSHIT, R., ESER, S., MATHERS, C., REBELO, M., PARKIN, D. M., FORMAN, D. & BRAY, F. 2015. Cancer incidence and mortality worldwide: sources, methods and major patterns in GLOBOCAN 2012. *Int J Cancer,* 136**,** E359-86.

FISHER, K. 2006. Striking out at disseminated metastases: the systemic delivery of oncolytic viruses. *Curr Opin Mol Ther,* 8**,** 301-13.

FISHER, K. D., STALLWOOD, Y., GREEN, N. K., ULBRICH, K., MAUTNER, V. & SEYMOUR, L. W. 2001. Polymer-coated adenovirus permits efficient retargeting and evades neutralising antibodies. *Gene Ther,* 8**,** 341-8.

GALANIS, E., HARTMANN, L. C., CLIBY, W. A., LONG, H. J., PEETHAMBARAM, P. P., BARRETTE, B. A., KAUR, J. S., HALUSKA, P. J., JR., ADERCA, I., ZOLLMAN, P. J., SLOAN, J. A., KEENEY, G., ATHERTON, P. J., PODRATZ, K. C., DOWDY, S. C., STANHOPE, C. R., WILSON, T. O., FEDERSPIEL, M. J., PENG, K. W. & RUSSELL, S. J. 2010. Phase I trial of intraperitoneal administration of an oncolytic measles virus strain engineered to express carcinoembryonic antigen for recurrent ovarian cancer. *Cancer Res,* 70**,** 875-82.

GALON, J., COSTES, A., SANCHEZ-CABO, F., KIRILOVSKY, A., MLECNIK, B., LAGORCE-PAGES, C., TOSOLINI, M., CAMUS, M., BERGER, A., WIND, P., ZINZINDOHOUE, F., BRUNEVAL, P., CUGNENC, P. H., TRAJANOSKI, Z., FRIDMAN, W. H. & PAGES, F. 2006. Type, density, and location of immune cells within human colorectal tumors predict clinical outcome. *Science,* 313**,** 1960-4.

GAO Y, W.-D. P., GRIFFIN JA, BARMADA MA, BERGMAN I 2009. Recombinant vesicular stomatitis virus targeted to Her2/neu combined with anti-CTLA4 antibody eliminates implanted mammary tumors. *Cancer Gene Therapy*.

GEEVARGHESE, S. K., GELLER, D. A., DE HAAN, H. A., HORER, M., KNOLL, A. E., MESCHEDER, A., NEMUNAITIS, J., REID, T. R., SZE, D. Y., TANABE, K. K. & TAWFIK, H. 2010. Phase I/II study of oncolytic herpes simplex virus NV1020 in patients with extensively pretreated refractory colorectal cancer metastatic to the liver. *Hum Gene Ther,* 21**,** 1119-28.

GILL, S., THOMAS, R. R. & GOLDBERG, R. M. 2003. Review article: colorectal cancer chemotherapy. *Aliment Pharmacol Ther,* 18**,** 683-92.

GRAEPLER F., L. M.-L., WYBRANIETZ W. A., SCHMIDT U., SMIRNOW I., GROS C. D., SPIEGEL M., SCHENK A., GRAF H., LAUER U. A., VONTHEIN R., GREGOR M., ARMEANU S., BITZER M., LAUER U. M. 2005. Bifunctional chimeric SuperCD suicide gene -YCD: YUPRT fusion is highly effective in a rat hepatoma model. *World Journal of Gastroenterology,* 11**,** 6910-6919.

GREENTREE, L. B. 1983. Hodgkin's disease: therapeutic role of measles vaccine. *Am J Med,* 75**,** 928.

GRODEN, J., THLIVERIS, A., SAMOWITZ, W., CARLSON, M., GELBERT, L., ALBERTSEN, H., JOSLYN, G., STEVENS, J., SPIRIO, L., ROBERTSON, M. & ET AL. 1991. Identification and characterization of the familial adenomatous polyposis coli gene. *Cell,* 66**,** 589-600.

GROSSARDT, C., ENGELAND, C. E., BOSSOW, S., HALAMA, N., ZAOUI, K., LEBER, M. F., SPRINGFELD, C., JAEGER, D., VON KALLE, C. & UNGERECHTS, G. 2013. Granulocyte-macrophage colony-stimulating factor-armed oncolytic measles virus is an effective therapeutic cancer vaccine. *Hum Gene Ther,* 24**,** 644-54.

GROTE, D., RUSSELL, S. J., CORNU, T. I., CATTANEO, R., VILE, R., POLAND, G. A. & FIELDING, A. K. 2001. Live attenuated measles virus induces regression of human lymphoma xenografts in immunodeficient mice. *Blood,* 97**,** 3746-54.

GUR, C., IBRAHIM, Y., ISAACSON, B., YAMIN, R., ABED, J., GAMLIEL, M., ENK, J., BAR-ON, Y., STANIETSKY-KAYNAN, N., COPPENHAGEN-GLAZER, S., SHUSSMAN, N., ALMOGY, G., CUAPIO, A., HOFER, E., MEVORACH, D., TABIB, A., ORTENBERG, R., MARKEL, G., MIKLIC, K., JONJIC, S., BRENNAN, C. A., GARRETT, W. S., BACHRACH, G. & MANDELBOIM, O. 2015. Binding of the Fap2 protein of Fusobacterium nucleatum to human inhibitory receptor TIGIT protects tumors from immune cell attack. *Immunity,* 42**,** 344-55.

GUSTAVSSON, B., CARLSSON, G., MACHOVER, D., PETRELLI, N., ROTH, A., SCHMOLL, H. J., TVEIT, K. M. & GIBSON, F. 2015. A review of the evolution of systemic chemotherapy in the management of colorectal cancer. *Clin Colorectal Cancer,* 14**,** 1-10.

HAMMOND, A. L., PLEMPER, R. K., ZHANG, J., SCHNEIDER, U., RUSSELL, S. J. & CATTANEO, R. 2001. Single-chain antibody displayed on a recombinant measles virus confers entry through the tumor-associated carcinoembryonic antigen. *J Virol,* 75**,** 2087-96.

HANSEN, R. M. & LIBNOCH, J. A. 1978. Remission of chronic lymphocytic leukemia after smallpox vaccination. *Arch Intern Med,* 138**,** 1137-8.

HARALAMBIEVA, I., IANKOV, I., HASEGAWA, K., HARVEY, M., RUSSELL, S. J. & PENG, K. W. 2007. Engineering Oncolytic Measles Virus to Circumvent the Intracellular Innate Immune Response. *Mol Ther,* 15.

HARDCASTLE, J., MILLS, L., MALO, C. S., JIN, F., KUROKAWA, C., GEEKIYANAGE, H., SCHROEDER, M., SARKARIA, J., JOHNSON, A. J. & GALANIS, E. 2016. Immunovirotherapy with measles virus strains in combination with anti-PD-1 antibody blockade enhances antitumor activity in glioblastoma treatment. *Neuro Oncol*.

HARRINGTON, K. J., HINGORANI, M., TANAY, M. A., HICKEY, J., BHIDE, S. A., CLARKE, P. M., RENOUF, L. C., THWAY, K., SIBTAIN, A., MCNEISH, I. A., NEWBOLD, K. L., GOLDSWEIG, H., COFFIN, R. & NUTTING, C. M. 2010. Phase I/II study of oncolytic HSV GM-CSF in combination with radiotherapy and cisplatin in untreated stage III/IV squamous cell cancer of the head and neck. *Clin Cancer Res,* 16**,** 4005-15.

HASEGAWA, K., PHAM, L., O'CONNOR, M. K., FEDERSPIEL, M. J., RUSSELL, S. J. & PENG, K. W. 2006. Dual therapy of ovarian cancer using measles viruses expressing carcinoembryonic antigen and sodium iodide symporter. *Clin Cancer Res,* 12**,** 1868-75.

HEINZERLING, L., KUNZI, V., OBERHOLZER, P. A., KUNDIG, T., NAIM, H. & DUMMER, R. 2005. Oncolytic measles virus in cutaneous T-cell lymphomas mounts antitumor immune responses in vivo and targets interferon-resistant tumor cells. *Blood,* 106**,** 2287-94.

HERBST, R. S., SORIA, J. C., KOWANETZ, M., FINE, G. D., HAMID, O., GORDON, M. S., SOSMAN, J. A., MCDERMOTT, D. F., POWDERLY, J. D., GETTINGER, S. N., KOHRT, H. E., HORN, L., LAWRENCE, D. P., ROST, S., LEABMAN, M., XIAO, Y., MOKATRIN, A., KOEPPEN, H., HEGDE, P. S., MELLMAN, I., CHEN, D. S. & HODI, F. S. 2014. Predictive correlates of response to the anti-PD-L1 antibody MPDL3280A in cancer patients. *Nature,* 515**,** 563-7.

HEROLD, G. 2015. *Innere Medizin : eine vorlesungsorientierte Darstellung; unter Berücksichtigung des Gegenstandskataloges für die Ärztliche Prüfung; mit ICD 10-Schlüssel im Text und Stichwortverzeichnis,* Köln, Herold.

HUEHLS, A. M., COUPET, T. A. & SENTMAN, C. L. 2015. Bispecific T-cell engagers for cancer immunotherapy. *Immunol Cell Biol,* 93**,** 290-6.

HUTZEN, B., RAFFEL, C. & STUDEBAKER, A. W. 2015. Advances in the design and development of oncolytic measles viruses. *Oncolytic Virother,* 4**,** 109-18.

IANKOV, I. D., BLECHACZ, B., LIU, C., SCHMECKPEPER, J. D., TARARA, J. E., FEDERSPIEL, M. J., CAPLICE, N. & RUSSELL, S. J. 2007. Infected cell carriers: a new strategy for systemic delivery of oncolytic measles viruses in cancer virotherapy. *Mol Ther,* 15**,** 114-22.

JAGER, D., HALAMA, N., ZORNIG, I., KLUG, P., KRAUSS, J. & HAAG, G. M. 2016. Immunotherapy of Colorectal Cancer. *Oncol Res Treat,* 39**,** 346-50.

JOHNSON, D. B., PUZANOV, I. & KELLEY, M. C. 2015. Talimogene laherparepvec (T-VEC) for the treatment of advanced melanoma. *Immunotherapy,* 7**,** 611-9.

JUAN J. ROJAS, P. S., WEIZHOU HOU, AND STEVE H. THORNE 2015. Defining Effective Combinations of Immune Checkpoint Blockade and Oncolytic Virotherapy. *Clinical Cancer Research***,** 5543-51.

KÄRBER, G. 1931. Beitrag zur kollektiven Behandlung pharmakologischer Reihenversuche. *Archiv f experiment Pathol u Pharmakol* 162**,** 480-483

KAUFMAN, H. L., KIM, D. W., DERAFFELE, G., MITCHAM, J., COFFIN, R. S. & KIM-SCHULZE, S. 2010. Local and distant immunity induced by intralesional vaccination with an oncolytic herpes virus encoding GM-CSF in patients with stage IIIc and IV melanoma. *Ann Surg Oncol,* 17**,** 718-30.

KAUFMANN, J. K., BOSSOW, S., GROSSARDT, C., SAWALL, S., KUPSCH, J., ERBS, P., HASSEL, J. C., VON KALLE, C., ENK, A. H., NETTELBECK, D. M. & UNGERECHTS, G. 2013. Chemovirotherapy of malignant melanoma with a targeted and armed oncolytic measles virus. *J Invest Dermatol,* 133**,** 1034-42.

KEIR, M. E., BUTTE, M. J., FREEMAN, G. J. & SHARPE, A. H. 2008. PD-1 and its ligands in tolerance and immunity. *Annu Rev Immunol,* 26**,** 677-704.

KELLY, E., RUSSELL, S. J. 2007. History of Oncolytic Viruses: Genesis to Genetic Engineering. *Molecular Therapy,* 15**,** 651-659.

KEMPER, C., LEUNG, M., STEPHENSEN, C. B., PINKERT, C. A., LISZEWSKI, M. K., CATTANEO, R. & ATKINSON, J. P. 2001. Membrane cofactor protein (MCP; CD46) expression in transgenic mice. *Clin Exp Immunol,* 124**,** 180-9.

KIM, J. M. & CHEN, D. S. 2016. Immune escape to PD-L1/PD-1 blockade: seven steps to success (or failure). *Ann Oncol,* 27**,** 1492-504.

KNIPE, D. M. (ed.) 2013. *Fields virology. - 1,* Philadelphia [u.a.]: Wolters Kluwer/Lippincott Williams & Wilkins Health.

KUNZI, V., OBERHOLZER, P. A., HEINZERLING, L., DUMMER, R. & NAIM, H. Y. 2006. Recombinant measles virus induces cytolysis of cutaneous T-cell lymphoma in vitro and in vivo. *J Invest Dermatol,* 126**,** 2525-32.

LAMPE J, B. S., WEILAND T, SMIRNOW I, LEHMANN R, NEUBERT W, BITZER M, LAUER UM 2013. An armed oncolytic measles vaccine virus eliminates human hepatoma cells independently of apoptosis. *Gene Therapy,* 20**,** 1033-1041.

LANDREAU, P., DROUILLARD, A., LAUNOY, G., ORTEGA-DEBALLON, P., JOOSTE, V., LEPAGE, C., FAIVRE, J., FACY, O. & BOUVIER, A. M. 2015. Incidence and survival in late liver metastases of colorectal cancer. *J Gastroenterol Hepatol,* 30**,** 82-5.

LANGE S, L. J., BOSSOW S, ZIMMERMANN M, NEUBERT W, BITZER M, LAUER UM 2013 A novel armed oncolytic measles vaccine virus for the treatment of cholangiocarcinoma. *Human Gene Therapy,* 24**,** 554-564.

LASRY, A., ZINGER, A. & BEN-NERIAH, Y. 2016. Inflammatory networks underlying colorectal cancer. *Nat Immunol,* 17**,** 230-40.

LE, D. T., URAM, J. N., WANG, H., BARTLETT, B. R., KEMBERLING, H., EYRING, A. D., SKORA, A. D., LUBER, B. S., AZAD, N. S., LAHERU, D., BIEDRZYCKI, B., DONEHOWER, R. C., ZAHEER, A., FISHER, G. A., CROCENZI, T. S., LEE, J. J., DUFFY, S. M., GOLDBERG, R. M., DE LA CHAPELLE, A., KOSHIJI, M., BHAIJEE, F., HUEBNER, T., HRUBAN, R. H., WOOD, L. D., CUKA, N., PARDOLL, D. M., PAPADOPOULOS, N., KINZLER, K. W., ZHOU, S., CORNISH, T. C., TAUBE, J. M., ANDERS, R. A., ESHLEMAN, J. R., VOGELSTEIN, B. & DIAZ, L. A., JR. 2015. PD-1 Blockade in Tumors with Mismatch-Repair Deficiency. *N Engl J Med,* 372**,** 2509-20.

LEACH, D. R., KRUMMEL, M. F. & ALLISON, J. P. 1996. Enhancement of antitumor immunity by CTLA-4 blockade. *Science,* 271**,** 1734-6.

LIU, C., RUSSELL, S. J. & PENG, K. W. 2010. Systemic therapy of disseminated myeloma in passively immunized mice using measles virus-infected cell carriers. *Mol Ther,* 18**,** 1155-64.

LIU T.C., G. E., KIRN D. 2007. Clinical trial results with oncolytic virotherapy: a century of promise, a decade of progress. *Nature Clinical Practice Oncology* 4**,** 101-117.

LLOSA, N. J., CRUISE, M., TAM, A., WICKS, E. C., HECHENBLEIKNER, E. M., TAUBE, J. M., BLOSSER, R. L., FAN, H., WANG, H., LUBER, B. S., ZHANG, M., PAPADOPOULOS, N., KINZLER, K. W., VOGELSTEIN, B., SEARS, C. L., ANDERS, R. A., PARDOLL, D. M. & HOUSSEAU, F. 2015. The vigorous immune microenvironment of microsatellite instable colon cancer is balanced by multiple counter-inhibitory checkpoints. *Cancer Discov,* 5**,** 43-51.

LOMBARDI, L., MORELLI, F., CINIERI, S., SANTINI, D., SILVESTRIS, N., FAZIO, N., ORLANDO, L., TONINI, G., COLUCCI, G. & MAIELLO, E. 2010. Adjuvant colon cancer chemotherapy: where we are and where we'll go. *Cancer Treat Rev,* 36 Suppl 3**,** S34-41.

LUNG, M. S., TRAINER, A. H., CAMPBELL, I. & LIPTON, L. 2015. Familial colorectal cancer. *Intern Med J,* 45**,** 482-91.

MARCHINI, A., SCOTT, E. M. & ROMMELAERE, J. 2016. Overcoming Barriers in Oncolytic Virotherapy with HDAC Inhibitors and Immune Checkpoint Blockade. *Viruses,* 8.

MARKHAM, A. 2016. Atezolizumab: First Global Approval. *Drugs,* 76**,** 1227-32.

MARTIN-LIBERAL, J., OCHOA DE OLZA, M., HIERRO, C., GROS, A., RODON, J. & TABERNERO, J. 2017. The expanding role of immunotherapy. *Cancer Treat Rev,* 54**,** 74-86.

MCDERMOTT, D. F., SOSMAN, J. A., SZNOL, M., MASSARD, C., GORDON, M. S., HAMID, O., POWDERLY, J. D., INFANTE, J. R., FASSO, M., WANG, Y. V., ZOU, W., HEGDE, P. S., FINE, G. D. & POWLES, T. 2016. Atezolizumab, an Anti-Programmed Death-Ligand 1 Antibody, in Metastatic Renal Cell Carcinoma: Long-Term Safety, Clinical Activity, and Immune Correlates From a Phase Ia Study. *J Clin Oncol,* 34**,** 833-42.

MELCHER, A., PARATO, K., ROONEY, C. M. & BELL, J. C. 2011. Thunder and lightning: immunotherapy and oncolytic viruses collide. *Mol Ther,* 19**,** 1008-16.

MINTON, J. P. 1973. Mumps virus and BCG vaccine in metastatic melanoma. *Arch Surg,* 106**,** 503-6.

MOORE, A. E. 1952. Viruses with oncolytic properties and their adaptation to tumors. *Ann N Y Acad Sci,* 54**,** 945-52.

MRKIC, B., PAVLOVIC, J., RULICKE, T., VOLPE, P., BUCHHOLZ, C. J., HOURCADE, D., ATKINSON, J. P., AGUZZI, A. & CATTANEO, R. 1998. Measles virus spread and pathogenesis in genetically modified mice. *J Virol,* 72**,** 7420-7.

MSAOUEL, P., DISPENZIERI, A. & GALANIS, E. 2009. Clinical testing of engineered oncolytic measles virus strains in the treatment of cancer: an overview. *Curr Opin Mol Ther,* 11**,** 43-53.

MSAOUEL, P., IANKOV, I. D., DISPENZIERI, A. & GALANIS, E. 2012. Attenuated oncolytic measles virus strains as cancer therapeutics. *Curr Pharm Biotechnol,* 13**,** 1732-41.

MSAOUEL, P., OPYRCHAL, M., DOMINGO MUSIBAY, E. & GALANIS, E. 2013. Oncolytic measles virus strains as novel anticancer agents. *Expert Opin Biol Ther,* 13**,** 483-502.

MÜHLEBACH M. D., M. M., SINN P. L., PRÜFER S., UHLIG K. M., LEONARD V. H. J., NAVARATNARAJAH C. K., FRENZKE M., WONG X. X., SAWATSKY B., RAMACHANDRAN S., MCCRAY P. B., CICHUTEK K., VON MESSLING V., LOPEZ M. & CATTANEO R. 2011. Adherens junction protein nectin-4 is the epithelial receptor for measles virus. *Nature***,** 530-533.

NAHAPETIAN, A. T., THOMAS, J. N. & THILLY, W. G. 1986. Optimization of environment for high density Vero cell culture: effect of dissolved oxygen and nutrient supply on cell growth and changes in metabolites. *J Cell Sci,* 81**,** 65-103.

NAIK, J. D., TWELVES, C. J., SELBY, P. J., VILE, R. G. & CHESTER, J. D. 2011. Immune recruitment and therapeutic synergy: keys to optimizing oncolytic viral therapy? *Clin Cancer Res,* 17**,** 4214-24.

NAKAI, M. & IMAGAWA, D. T. 1969. Electron microscopy of measles virus replication. *J Virol,* 3**,** 187-97.

NAKAMURA, Y., LATHROP, M., LEPPERT, M., DOBBS, M., WASMUTH, J., WOLFF, E., CARLSON, M., FUJIMOTO, E., KRAPCHO, K., SEARS, T. & ET AL. 1988. Localization of the genetic defect in familial adenomatous polyposis within a small region of chromosome 5. *Am J Hum Genet,* 43**,** 638-44.

NANICHE, D., VARIOR-KRISHNAN, G., CERVONI, F., WILD, T. F., ROSSI, B., RABOURDIN-COMBE, C. & GERLIER, D. 1993. Human membrane cofactor protein (CD46) acts as a cellular receptor for measles virus. *J Virol,* 67**,** 6025-32.

NAVARATNARAJAH, C. K., OEZGUEN, N., RUPP, L., KAY, L., LEONARD, V. H., BRAUN, W. & CATTANEO, R. 2011. The heads of the measles virus attachment protein move to transmit the fusion-triggering signal. *Nat Struct Mol Biol,* 18**,** 128-34.

NCI-WEBPAGE Accessed April 23, 2017. National Cancer Institute: Surveillance, Epidemiology, and End Results Program. SEER Stat Fact Sheets: Colon and Rectum Cancer. *Available from:* http://seer.cancer.gov/statfacts/html/colorect.html.

NCI-WEBPAGE Accessed August 17, 2016. National Canster Institute: Developmental Therapeutics Program, Cell Lines in the In Vitro Screen. *Available from:* https://dtp.cancer.gov/discovery_development/nci-60/cell_list.htm.

NOLL M., B. S., LAMPE J., MALEK N. P., BITZER M., LAUER U. M. 2013. Primary resistance phenomena to oncolytic measles vaccine viruses. *International Journal of Oncology,* 43**,** 103-12.

OLUYEMI, A. O., WELCH, A. R., YOO, L. J., LEHMAN, E. B., MCGARRITY, T. J. & CHUANG, C. H. 2014. Colorectal cancer screening in high-risk groups is increasing, although current smokers fall behind. *Cancer,* 120**,** 2106-13.

OSTAFF, M. J., STANGE, E. F. & WEHKAMP, J. 2013. Antimicrobial peptides and gut microbiota in homeostasis and pathology. *EMBO Mol Med,* 5**,** 1465-83.

PARDOLL, D. M. 2012. The blockade of immune checkpoints in cancer immunotherapy. *Nat Rev Cancer,* 12**,** 252-64.

PARK, B. H., HWANG, T., LIU, T. C., SZE, D. Y., KIM, J. S., KWON, H. C., OH, S. Y., HAN, S. Y., YOON, J. H., HONG, S. H., MOON, A., SPETH, K., PARK, C., AHN, Y. J., DANESHMAND, M., RHEE, B. G., PINEDO, H. M., BELL, J. C. & KIRN, D. H. 2008. Use of a targeted oncolytic poxvirus, JX-594, in patients with refractory primary or metastatic liver cancer: a phase I trial. *Lancet Oncol,* 9**,** 533-42.

PARK, S. H., BREITBACH, C. J., LEE, J., PARK, J. O., LIM, H. Y., KANG, W. K., MOON, A., MUN, J. H., SOMMERMANN, E. M., MARURI AVIDAL, L., PATT, R., PELUSIO, A., BURKE, J., HWANG, T. H., KIRN, D. & PARK, Y. S. 2015. Phase 1b Trial of Biweekly Intravenous Pexa-Vec (JX-594), an Oncolytic and Immunotherapeutic Vaccinia Virus in Colorectal Cancer. *Mol Ther,* 23**,** 1532-40.

PENG, K. W., AHMANN, G. J., PHAM, L., GREIPP, P. R., CATTANEO, R. & RUSSELL, S. J. 2001. Systemic therapy of myeloma xenografts by an attenuated measles virus. *Blood,* 98**,** 2002-7.

PENG, K. W., FACTEAU, S., WEGMAN, T., O'KANE, D. & RUSSELL, S. J. 2002a. Non-invasive in vivo monitoring of trackable viruses expressing soluble marker peptides. *Nat Med,* 8**,** 527-31.

PENG, K. W., MYERS, R., GREENSLADE, A., MADER, E., GREINER, S., FEDERSPIEL, M. J., DISPENZIERI, A. & RUSSELL, S. J. 2013. Using clinically approved cyclophosphamide regimens to control the humoral immune response to oncolytic viruses. *Gene Ther,* 20**,** 255-61.

PENG, K. W., TENEYCK, C. J., GALANIS, E., KALLI, K. R., HARTMANN, L. C. & RUSSELL, S. J. 2002b. Intraperitoneal therapy of ovarian cancer using an engineered measles virus. *Cancer Res,* 62**,** 4656-62.

PENHEITER, A. R., WEGMAN, T. R., CLASSIC, K. L., DINGLI, D., BENDER, C. E., RUSSELL, S. J. & CARLSON, S. K. 2010. Sodium iodide symporter (NIS)-mediated radiovirotherapy for pancreatic cancer. *AJR Am J Roentgenol,* 195**,** 341-9.

PESCE, S., GREPPI, M., TABELLINI, G., RAMPINELLI, F., PAROLINI, S., OLIVE, D., MORETTA, L., MORETTA, A. & MARCENARO, E. 2016. Identification of a subset of human natural killer cells expressing high levels of programmed death 1: A phenotypic and functional characterization. *J Allergy Clin Immunol*.

PHUONG, L. K., ALLEN, C., PENG, K. W., GIANNINI, C., GREINER, S., TENEYCK, C. J., MISHRA, P. K., MACURA, S. I., RUSSELL, S. J. & GALANIS, E. C. 2003. Use of a vaccine strain of measles virus genetically engineered to produce carcinoembryonic antigen as a novel therapeutic agent against glioblastoma multiforme. *Cancer Res,* 63**,** 2462-9.

POON, M. A., O'CONNELL, M. J., MOERTEL, C. G., WIEAND, H. S., CULLINAN, S. A., EVERSON, L. K., KROOK, J. E., MAILLIARD, J. A., LAURIE, J. A., TSCHETTER, L. K. & ET AL. 1989. Biochemical modulation of fluorouracil: evidence of significant improvement of survival and quality of life in patients with advanced colorectal carcinoma. *J Clin Oncol,* 7**,** 1407-18.

POSTOW, M. A., CALLAHAN, M. K. & WOLCHOK, J. D. 2015. Immune Checkpoint Blockade in Cancer Therapy. *J Clin Oncol,* 33**,** 1974-82.

PRESTWICH, R. J., ERRINGTON, F., DIAZ, R. M., PANDHA, H. S., HARRINGTON, K. J., MELCHER, A. A. & VILE, R. G. 2009. The case of oncolytic viruses versus the immune system: waiting on the judgment of Solomon. *Hum Gene Ther,* 20**,** 1119-32.

PUZANOV, I., MILHEM, M. M., MINOR, D., HAMID, O., LI, A., CHEN, L., CHASTAIN, M., GORSKI, K. S., ANDERSON, A., CHOU, J., KAUFMAN, H. L. & ANDTBACKA, R. H. 2016. Talimogene Laherparepvec in Combination With Ipilimumab in Previously Untreated, Unresectable Stage IIIB-IV Melanoma. *J Clin Oncol,* 34**,** 2619-26.

QUETGLAS JI, L. S., AZNAR MÁ, BOLAÑOS E, AZPILIKUETA A, RODRIGUEZ I, CASALES E, SÁNCHEZ-PAULETE AR, SEGURA V, SMERDOU C, MELERO I 2015. Virotherapy with a Semliki Forest Virus-Based Vector Encoding IL12 Synergizes with PD-1/PD-L1 Blockade. *Cancer Immunology Research,* 3**,** 449-54.

RAJANI K, P. C., KOTTKE T, THOMPSON J, ZAIDI S, ILETT L, SHIM KG, DIAZ RM, PANDHA H, HARRINGTON K, COFFEY M, MELCHER A, VILE R 2016.

Combination Therapy With Reovirus and Anti-PD-1 Blockade Controls Tumor Growth Through Innate and Adaptive Immune Responses. *Molecular Therapy,* 24**,** 166-174.

RAJANI, K. R. & VILE, R. G. 2015. Harnessing the Power of Onco-Immunotherapy with Checkpoint Inhibitors. *Viruses,* 7**,** 5889-901.

REID, T., GALANIS, E., ABBRUZZESE, J., SZE, D., WEIN, L. M., ANDREWS, J., RANDLEV, B., HEISE, C., UPRICHARD, M., HATFIELD, M., ROME, L., RUBIN, J. & KIRN, D. 2002. Hepatic arterial infusion of a replication-selective oncolytic adenovirus (dl1520): phase II viral, immunologic, and clinical endpoints. *Cancer Res,* 62**,** 6070-9.

RIBAS, A., DUMMER, R., PUZANOV, I., VANDERWALDE, A., ANDTBACKA, R. H. I., MICHIELIN, O., OLSZANSKI, A. J., MALVEHY, J., CEBON, J., FERNANDEZ, E., KIRKWOOD, J. M., GAJEWSKI, T. F., CHEN, L., GORSKI, K. S., ANDERSON, A. A., DIEDE, S. J., LASSMAN, M. E., GANSERT, J., HODI, F. S. & LONG, G. V. 2017. Oncolytic Virotherapy Promotes Intratumoral T Cell Infiltration and Improves Anti-PD-1 Immunotherapy. *Cell,* 170**,** 1109-1119.e10.

ROBERT-KOCH-INSTITUT 2016. Infektionsepidemiologisches Jahrbuch meldepflichtiger Krankheiten für 2015.

ROBINSON, S. & GALANIS, E. 2017. Potential and clinical translation of oncolytic measles viruses. *Expert Opin Biol Ther,* 17**,** 353-363.

ROJAS, J. J., SAMPATH, P., HOU, W. & THORNE, S. H. 2015. Defining Effective Combinations of Immune Checkpoint Blockade and Oncolytic Virotherapy. *Clin Cancer Res,* 21**,** 5543-51.

ROSENBERG, J. E., HOFFMAN-CENSITS, J., POWLES, T., VAN DER HEIJDEN, M. S., BALAR, A. V., NECCHI, A., DAWSON, N., O'DONNELL, P. H., BALMANOUKIAN, A., LORIOT, Y., SRINIVAS, S., RETZ, M. M., GRIVAS, P., JOSEPH, R. W., GALSKY, M. D., FLEMING, M. T., PETRYLAK, D. P., PEREZ-GRACIA, J. L., BURRIS, H. A., CASTELLANO, D., CANIL, C., BELLMUNT, J., BAJORIN, D., NICKLES, D., BOURGON, R., FRAMPTON, G. M., CUI, N., MARIATHASAN, S., ABIDOYE, O., FINE, G. D. & DREICER, R. 2016. Atezolizumab in patients with locally advanced and metastatic urothelial carcinoma who have progressed following treatment with platinum-based chemotherapy: a single-arm, multicentre, phase 2 trial. *Lancet,* 387**,** 1909-20.

ROWAN, A. J., LAMLUM, H., ILYAS, M., WHEELER, J., STRAUB, J., PAPADOPOULOU, A., BICKNELL, D., BODMER, W. F. & TOMLINSON, I. P. 2000. APC mutations in sporadic colorectal tumors: A mutational "hotspot" and interdependence of the "two hits". *Proc Natl Acad Sci U S A,* 97**,** 3352-7.

RUSSELL, S. J., FEDERSPIEL, M. J., PENG, K. W., TONG, C., DINGLI, D., MORICE, W. G., LOWE, V., O'CONNOR, M. K., KYLE, R. A., LEUNG, N., BUADI, F. K., RAJKUMAR, S. V., GERTZ, M. A., LACY, M. Q. & DISPENZIERI, A. 2014. Remission of disseminated cancer after systemic oncolytic virotherapy. *Mayo Clin Proc,* 89**,** 926-33.

RUSSELL, S. J. & PENG, K. W. 2009. Measles virus for cancer therapy. *Curr Top Microbiol Immunol,* 330**,** 213-41.

RUSSELL, S. J., PENG, K. W. & BELL, J. C. 2012. Oncolytic virotherapy. *Nat Biotechnol,* 30**,** 658-70.

SALEH, M. & TRINCHIERI, G. 2011. Innate immune mechanisms of colitis and colitis-associated colorectal cancer. *Nat Rev Immunol,* 11**,** 9-20.

SCHATTNER, A. 1984. Therapeutic role of measles vaccine in Hodgkin's disease. *Lancet,* 1**,** 171.

SCHNEIDER, U., BULLOUGH, F., VONGPUNSAWAD, S., RUSSELL, S. J. & CATTANEO, R. 2000. Recombinant measles viruses efficiently entering cells through targeted receptors. *J Virol,* 74**,** 9928-36.

SCHREINER, B., MITSDOERFFER, M., KIESEIER, B. C., CHEN, L., HARTUNG, H. P., WELLER, M. & WIENDL, H. 2004. Interferon-beta enhances monocyte and dendritic cell expression of B7-H1 (PD-L1), a strong inhibitor of autologous T-cell activation: relevance for the immune modulatory effect in multiple sclerosis. *J Neuroimmunol,* 155**,** 172-82.

SEARS, C. L. 2009. Enterotoxigenic Bacteroides fragilis: a rogue among symbiotes. *Clin Microbiol Rev,* 22**,** 349-69, Table of Contents.

SHEN, W., PATNAIK, M. M., RUIZ, A., RUSSELL, S. J. & PENG, K. W. 2016. Immunovirotherapy with vesicular stomatitis virus and PD-L1 blockade enhances therapeutic outcome in murine acute myeloid leukemia. *Blood,* 127**,** 1449-58.

SHIN, D. S. & RIBAS, A. 2015. The evolution of checkpoint blockade as a cancer therapy: what's here, what's next? *Curr Opin Immunol,* 33**,** 23-35.

SIMON, K. 2016. Colorectal cancer development and advances in screening. *Clin Interv Aging,* 11**,** 967-76.

SKEHAN, P., STORENG, R., SCUDIERO, D., MONKS, A., MCMAHON, J., VISTICA, D., WARREN, J. T., BOKESCH, H., KENNEY, S., BOYD, M. R. 1990. New colorimetric cytotoxicity assay for anticancer-drug screening. *J Natl Cancer Inst,* 82**,** 1107-12.

SMITH, T. T., ROTH, J. C., FRIEDMAN, G. K. & GILLESPIE, G. Y. 2014. Oncolytic viral therapy: targeting cancer stem cells. *Oncolytic Virother,* 2014**,** 21-33.

SPEARMAN, C. 1908. The Method of “Right and Wrong Cases” (Constant Stimuli) without Gauss’s Formula. . *Br J Psychol* 2**,** 227-242.

SPECK, T., HEIDBUECHEL, J. P. W., VEINALDE, R., JAEGER, D., VON KALLE, C., BALL, C. R., UNGERECHTS, G. & ENGELAND, C. E. 2018. Targeted BiTE Expression by an Oncolytic Vector Augments Therapeutic Efficacy Against Solid Tumors. *Clin Cancer Res,* 24**,** 2128-2137.

STOJDL, D. F., LICHTY, B., KNOWLES, S., MARIUS, R., ATKINS, H., SONENBERG, N. & BELL, J. C. 2000. Exploiting tumor-specific defects in the interferon pathway with a previously unknown oncolytic virus. *Nat Med,* 6**,** 821-5.

TAQI, A. M., ABDURRAHMAN, M. B., YAKUBU, A. M. & FLEMING, A. F. 1981. Regression of Hodgkin's disease after measles. *Lancet,* 1**,** 1112.

TATSUO, H., ONO, N., TANAKA, K. & YANAGI, Y. 2000. SLAM (CDw150) is a cellular receptor for measles virus. *Nature,* 406**,** 893-7.

TAUBE, J. M., KLEIN, A., BRAHMER, J. R., XU, H., PAN, X., KIM, J. H., CHEN, L., PARDOLL, D. M., TOPALIAN, S. L. & ANDERS, R. A. 2014. Association of PD-1, PD-1 ligands, and other features of the tumor immune microenvironment with response to anti-PD-1 therapy. *Clin Cancer Res,* 20**,** 5064-74.

THORNE, S. H., HERMISTON, T. & KIRN, D. 2005. Oncolytic virotherapy: approaches to tumor targeting and enhancing antitumor effects. *Semin Oncol,* 32**,** 537-48.

TOPALIAN, S. L., HODI, F. S., BRAHMER, J. R., GETTINGER, S. N., SMITH, D. C., MCDERMOTT, D. F., POWDERLY, J. D., CARVAJAL, R. D., SOSMAN, J. A., ATKINS, M. B., LEMING, P. D., SPIGEL, D. R., ANTONIA, S. J., HORN, L., DRAKE, C. G., PARDOLL, D. M., CHEN, L., SHARFMAN, W. H., ANDERS, R. A., TAUBE, J. M., MCMILLER, T. L., XU, H., KORMAN, A. J., JURE-KUNKEL, M., AGRAWAL, S., MCDONALD, D., KOLLIA, G. D., GUPTA, A., WIGGINTON, J. M. & SZNOL, M. 2012. Safety, activity, and immune correlates of anti-PD-1 antibody in cancer. *N Engl J Med,* 366**,** 2443-54.

TOPALIAN, S. L., WEINER, G. J. & PARDOLL, D. M. 2011. Cancer immunotherapy comes of age. *J Clin Oncol,* 29**,** 4828-36.

TUMEH, P. C., HARVIEW, C. L., YEARLEY, J. H., SHINTAKU, I. P., TAYLOR, E. J., ROBERT, L., CHMIELOWSKI, B., SPASIC, M., HENRY, G., CIOBANU, V., WEST, A. N., CARMONA, M., KIVORK, C., SEJA, E., CHERRY, G., GUTIERREZ, A. J., GROGAN, T. R., MATEUS, C., TOMASIC, G., GLASPY, J. A., EMERSON, R. O., ROBINS, H., PIERCE, R. H., ELASHOFF, D. A., ROBERT, C. & RIBAS, A. 2014. PD-1 blockade induces responses by inhibiting adaptive immune resistance. *Nature,* 515**,** 568-71.

TURNBULL S, W. E., SCOTT KJ, APPLETON E, MELCHER A, RALPH C 2015. Evidence for Oncolytic Virotherapy: Where Have We Got to and Where Are We Going? *Viruses,* 7**,** 6291-312.

UNGERECHTS, G., SPRINGFELD, C., FRENZKE, M. E., LAMPE, J., PARKER, W. B., SORSCHER, E. J. & CATTANEO, R. 2007. An immunocompetent murine model for oncolysis with an armed and targeted measles virus. *Mol Ther,* 15**,** 1991-7.

VELUCHAMY, J. P., SPANHOLTZ, J., TORDOIR, M., THIJSSEN, V. L., HEIDEMAN, D. A., VERHEUL, H. M., DE GRUIJL, T. D. & VAN DER VLIET, H. J. 2016. Combination of NK Cells and Cetuximab to Enhance Anti-Tumor Responses in RAS Mutant Metastatic Colorectal Cancer. *PLoS One,* 11**,** e0157830.

VILE, R. G. 2014. How To Train Your Oncolytic Virus: the Immunological Sequel. *Molecular Therapy,* 22**,** 1881-1884.

WALDHAUER, I. & STEINLE, A. 2008. NK cells and cancer immunosurveillance. *Oncogene,* 27**,** 5932-43.

WALDMANN, T. A. 2003. Immunotherapy: past, present and future. *Nature Medicine,* 9**,** 269 - 277.

WATERHOUSE, P., PENNINGER, J. M., TIMMS, E., WAKEHAM, A., SHAHINIAN, A., LEE, K. P., THOMPSON, C. B., GRIESSER, H. & MAK, T. W. 1995. Lymphoproliferative disorders with early lethality in mice deficient in Ctla-4. *Science,* 270**,** 985-8.

WEBER, J. S., D'ANGELO, S. P., MINOR, D., HODI, F. S., GUTZMER, R., NEYNS, B., HOELLER, C., KHUSHALANI, N. I., MILLER, W. H., JR., LAO, C. D., LINETTE, G. P., THOMAS, L., LORIGAN, P., GROSSMANN, K. F., HASSEL, J. C., MAIO, M., SZNOL, M., ASCIERTO, P. A., MOHR, P., CHMIELOWSKI, B., BRYCE, A., SVANE, I. M., GROB, J. J., KRACKHARDT, A. M., HORAK, C., LAMBERT, A., YANG, A. S. & LARKIN, J. 2015. Nivolumab versus chemotherapy in patients with

advanced melanoma who progressed after anti-CTLA-4 treatment (CheckMate 037): a randomised, controlled, open-label, phase 3 trial. *Lancet Oncol,* 16**,** 375-84.

WOLLER N, G. E., FLEISCHMANN-MUNDT B, SCHUMACHER A, KNOCKE S, KLOOS AM, SABOROWSKI M, GEFFERS R, MANNS MP, WIRTH TC, KUBICKA S, KÜHNEL F 2015. Viral Infection of Tumors Overcomes Resistance to PD-1-immunotherapy by Broadening Neoantigenome-directed T-cell Responses. *Molecular Therapy,* 23**,** 1630-40.

WOLLER N, G. E., URECHE CI, SCHUMACHER A, KÜHNEL F 2014. Oncolytic viruses as anticancer vaccines. *Frontiers in Oncology*.

XIAO, Y. & FREEMAN, G. J. 2015. The microsatellite instable subset of colorectal cancer is a particularly good candidate for checkpoint blockade immunotherapy. *Cancer Discov,* 5**,** 16-8.

YURTTAS C, B. S., MALEK NP, BITZER M, LAUER UM 2014. Pulsed versus continuous application of the prodrug 5-fluorocytosine to enhance the oncolytic effectiveness of a measles vaccine virus armed with a suicide gene. *Human Gene Therapy Clinical Development,* 25**,** 85-96.

ZAMARIN D, H. R., SUBUDHI SK, PARK JS, MANSOUR M, PALESE P, MERGHOUB T, WOLCHOK JD, ALLISON JP 2014. Localized oncolytic virotherapy overcomes systemic tumor resistance to immune checkpoint blockade immunotherapy. *Science Translational Medicine,* 6.

ZAMARIN D, P. M. 2015. Immune checkpoint modulation: rational design of combination strategies. *Pharmacology & Therapeutics,* 150**,** 23-32.

ZIMMERMANN, M., ARMEANU, S., SMIRNOW, I., KUPKA, S., WAGNER, S., WEHRMANN, M., ROTS, M. G., GROOTHUIS, G. M., WEISS, T. S., KONIGSRAINER, A., GREGOR, M., BITZER, M. & LAUER, U. M. 2009. Human precision-cut liver tumor slices as a tumor patient-individual predictive test system for oncolytic measles vaccine viruses. *Int J Oncol,* 34**,** 1247-56.

ZITVOGEL, L., TESNIERE, A. & KROEMER, G. 2006. Cancer despite immunosurveillance: immunoselection and immunosubversion. *Nat Rev Immunol,* 6**,** 715-27.

7. Erklärung zum Eigenanteil der Dissertationsschrift

Hiermit erkläre ich, Frau cand. med. Svenja Gehring, dass meine Arbeit zur Erlangung des Doktorgrades Dr. med. in der Medizinischen Klinik der Universität Tübingen, Abteilung Innere Medizin VIII, Arbeitsgruppe Virotherapie, unter Betreuung von Herrn Prof. Dr. med. Ulrich Lauer durchgeführt wurde.

Die Konzeption der Versuche erfolgte in Zusammenarbeit mit Herrn Prof. Dr. med. Ulrich Lauer und Frau Dr. med. Susanne Berchtold (Laborleiterin Arbeitsgruppe Virotherapie), sowie nach Beratung durch Herrn Dr. med. Dr. rer. nat. Sascha Venturelli (Arbeitsgruppe Tumor-Epigenetik), Herrn Dr. rer. nat. Markus Burkard (Arbeitsgruppe Tumor-Epigenetik) und Frau Dr. rer. nat. Stefanie Maurer (Arbeitsgruppe Molekulare Tumorimmunologie).

Sämtliche Versuche wurden (nach Einarbeitung durch Labormitglieder Frau Dr. med. Susanne Berchtold, Frau Irina Smirnow (MTA), Herrn Dr. rer. nat. Markus Burkard sowie durch Frau Dr. rer. nat. Stefanie Maurer, Arbeitsgruppe Molekulare Tumorimmunologie) von mir eigenständig durchgeführt.

Die statistische Auswertung erfolgte (nach Anleitung durch Frau Dr. med. Susanne Berchtold, Herrn Dr. med. Dr. rer. nat. Sascha Venturelli sowie Herrn Dr. rer. nat. Markus Burkard) durch mich.

Ich versichere, das Manuskript selbständig (nach Anleitung durch Frau Dr. med. Susanne Berchtold) verfasst zu haben und keine weiteren als die von mir angegebenen Quellen verwendet zu haben.

Svenja Gehring
Tübingen, den 03.06.2019

Danksagung

Mein außerordentlicher Dank gilt im besonderen Maße meinem Doktorvater, Professor Dr. med. Ulrich Lauer, der mein wissenschaftliches Arbeiten inspirierte und mich förderte, wo es nur möglich war.

Mein herzlichster Dank gilt vor allem auch Dr. Susanne Berchtold, die mir bei der Konzeption und Durchführung meiner Versuche eine wesentliche Unterstützung war und für Fragen stets ein offenes Ohr hatte.

Mein besonderer Dank gilt auch Irina Smirnow, die mich vor allem bei der Einarbeitung sowie bei technischen Fragen im Labor betreute. Ebenso gilt mein besonderer Dank Dr. Dr. Sascha Venturelli, Dr. Markus Burkard und Christian Leischner, welche mir vor allem bei Fragen zur Datenanalyse zur Hilfe standen. Vielen Dank auch Dr. Stefanie Maurer, die mir mit ihrem Rat bei der Konzeption und Umsetzung der Versuche mit Immunzell-Kokultur beiseite stand. Zudem danke ich Christine Geisler und Andrea Schenk, die mir ebenfalls bei Fragen zur praktischen Umsetzung meiner Versuche eine große Hilfe waren.

Für die freundliche Bereitstellung von Immunzellen danke ich Dr. Stefanie Maurer. Für die freundliche Bereitstellung der Immun-Checkpoint-Inhibitoren danke ich PD Dr. Marcus Schittenhelm.

Ebenso danke ich Meike Seidel, die viel Zeit und Geduld investierte, um meine Dissertationsschrift gegenzulesen. Zudem gilt der Dank meinen Eltern sowie Niklas Vogel, die mir über den Zeitraum meiner Promotion eine stetige Unterstützung waren.

Sicherlich wäre die intensive Forschungsarbeit ohne die ideelle sowie finanzielle Unterstützung durch das IZKF Promotionskolleg unter der Leitung von Prof. Dr. Marlies Knipper und Dr. Inka Montero so nicht möglich gewesen. Ich danke in diesem Rahmen für die Hilfe bei der Umsetzung meines Forschungsprojektes sowie für die Ratschläge zur schriftlichen Dissertationsabfassung.

Zudem danke ich der Studienstiftung des deutschen Volkes e.V. für die finanzielle Unterstützung.